TAL TECH

DOCTORAL THESIS

Equivalent Single Layer Approach for Ultimate Strength Assessment of Ship Structures

Teguh Putranto

Equivalent Single Layer Approach for Ultimate Strength Assessment of Ship Structures

TEGUH PUTRANTO

**TAL
TECH**
PRESS

TALLINN UNIVERSITY OF TECHNOLOGY
School of Engineering
Kuressaare College

The dissertation was accepted for the defense of the degree of Doctor of Philosophy (Ph.D.) on 07 February 2023

Supervisor: Professor Mihkel Kõrgesaar,
Kuressaare College, School of Engineering,
Tallinn University of Technology,
Kuressaare, Estonia

Opponents: Professor Joško Parunov,
Faculty of Mechanical Engineering and Naval Architecture,
University of Zagreb,
Zagreb, Croatia

Professor Adam Sobey,
Maritime Engineering Group,
University of Southampton,
Southampton, United Kingdom

Defense of the thesis: 16 March 2023, Tallinn

Declaration:
Hereby I declare that this doctoral thesis, my original investigation and achievement, submitted for the doctoral degree at Tallinn University of Technology, has not been submitted for any academic degree elsewhere.

Teguh Putranto

_____
signature

European Union
European Regional
Development Fund

Investing
in your future

Ekvivalentne koorikelement laeva konstruktsioonide piirtugevuse hindamiseks

TEGUH PUTRANTO

TAL
TECH
KIRJASTUS

Contents

Abstract
Equivalent Single Layer Approach for Ultimate Strength Assessment of Ship Structures

Ship structures are composed of assemblies made up of stiffened panels. This structure is designed to provide the strength required to withstand internal and external loads. To assess the ultimate strength of the ship structures, finite element analysis (FEA) is performed. Furthermore, FEA becomes increasingly necessary due to the requirement of the classification society to conduct global direct strength analyses. However, computational FEA can be highly time-consuming when the entire hull girder is modeled in detail. Therefore, this doctoral thesis proposes a homogenization method that can reduce the effort of the finite element method (FEM) to calculate the ultimate strength of the stiffened panel.

This method works by replacing the stiffened panel with an equivalent single layer (ESL) which has the same stiffness properties. The stiffness of the ESL is based on the constitutive relations that represent the deformation modes of the unit cell (UC), which is a repeating unit in the stiffened panel. Periodic boundary conditions are imposed in the UC analysis. The non-linear stiffness of the ESL is employed to consider the response of local buckling and material yielding. The applicability of the ESL approach for the ultimate limit state (ULS) analysis of the stiffened panel and hull girder is presented.

The results reveal that the ESL approach can successfully predict the ultimate strength of the stiffened panel. The ESL approach was tested for different stiffened panel configurations according to the slenderness of the plate and stiffener, revealing a wide range of applicability. Despite local buckling and material yielding, good accuracy was obtained in load-end shortening response.

In the global response analyses, the bending moment-curvature relation of the hull girder was accurately predicted until the ultimate strength was reached. Furthermore, the longitudinal stress distribution in a cross-section was captured with good accuracy. The ESL approach expedites the modeling of complicated thin-walled stiffened structures and reduces computational time while maintaining good accuracy compared to the full three-dimensional (3D) FEM.

Kokkuvõte
Ekvivalentne koorikelement laeva konstruktsioonide piirtugevuse hindamiseks

Laevakonstruktsioonides kannavad sise- ja väliskoormusi saledad jäigastatud plaadid, mille arvutamisel kontrollitakse paneeli piirkoormust erinevates koormusolukordades. Konstruktsiooni tugevus piirolukorras peab olema piisav, et laev oleks võimeline ilma suuremate vigastusteta kandma õnnetuslikke või ekstremaalseid koormusi. Tavapärane plaadi piirtugevuse analüüs viiakse läbi mittelineaarse lõplike elementide meetodi (LEM) abil ning kätkeb endas detailse mudeli koostamist. Kuna laeva tala mittelineaarne LEM analüüs on mudeli suuruse tõttu väga mahukas ja aeganõudev, arendati käesolevas doktoritöös välja ekvivalentne koorikelement, mis oluliselt lihtsustab LEM modelleerimist ja vähendab laeva tala piirtugevuse hindamisele kuluvat aega.

Arendatud metoodika (ESL) kätkeb endas jäigastatud plaadi asendamist ekvivalentse koorikelemendiga LEM tarkvaras, millel on vaadeldava plaadiga samad jäikusomadused. Koorikelemendi jäikusmaatriks on defineeritud jäigastatud plaadist eraldatud väikseima perioodiliselt korduva konstruktsioonielemendi (ühikelemendi) analüüsil erinevate koormusolukordade korral. Koorikelemendi jäikusomaduste määramiseks koormati ühikelementi survel nii piki kui põiki jäigastajat, paindel ümber mõlema plaadi tasapinnas oleva telje, tasapinnalisel lõikel risti jäigastajaga ja väändel. Ühikelemendi perioodiliste ääretingimuste modeldamine lõi eeldused, et ühikelement käitub samaväärselt konstruktsiooni vastava osaga ning seega kirjeldab ühikelemendi põhjal defineeritud jäikusmaatriks olukorda tegelikus konstruktsioonis. Kuna konstruktsiooni piirtugevus on määratud kas voolamise, stabiilsuse kao või kombinatsioonina nendest, siis olid need olukorrad esindatud ka ühikelemendi deformatsioonil. Seetõttu oli saadud jäikusmaatriks mittelineaarne võttes arvesse ühikelemendi plastseid deformatsioone ja võimalikku stabiilsuse kadu.

ESL koorikelementi valideeriti nii jäigastatud plaadi kui ka laeva tala piirtugevuse analüüsimiseks. Jäigastatud plaadi puhul analüüsiti erinevaid plaadi ja jäigastajate konfiguratsioone. Vaatamata lokaalsele läbinõtkumisele ja materjali voolamisele suutis meetod neid olukordi kirjeldada piisava täpsusega võrreldes detailsete LEM simulatsioonidega.

Laevatala analüüsimisel võrreldi talale rakendatud momendi ja tala kõveruse suhet ning laevakeres tekkivaid pikipingeid LEM meetodi tulemustega. Momendi hindamisel oli arendatud meetodi täpsus kuni piirtugevuse saavutamiseni võrreldav LEM meetodiga. Piirtugevuse ületamisel meetodi täpsus vähenes konstruktsiooni lokaalse stabiilsuse kao tõttu. Pikipingete ennustamisel plaadistuses saavutati samuti väga hea täpsus.

Kokkuvõtvalt, arendatud meetod kiirendab oluliselt õhukeseseinaliste jäigastatud konstruktsioonide mittelineaarset analüüsi ja vähendab arvutusaega, säilitades samas hea täpsuse võrreldes LEM meetodiga.

Acknowledgements

First, I am very grateful to my supervisor, Prof. Mihkel Kõrgesaar, for all his encouragement, guidance, support and excellent technical skills that made possible the successful completion of the thesis. The useful research and insightful discussions related to my thesis work are acknowledged. I would like to express my gratitude to Prof. Kristjan Tabri and DSc. Hendrik Naar for their contributions to the research. In addition, I am also grateful to Prof. Jasmin Jelovica from The University of British Columbia for providing his valuable advice to the research. Many thanks also to all my colleagues at Kuressaare College for their concern and support.

My dearest thanks go to my wife, Muniroh, and my sons, Rayhan and Hamzah, for being here and supporting me throughout the journey and encouraging me during my difficult and exhausting times. Without their support, this thesis could not have been completed. I would like to thank my mother Endah Joeniastoety and my sister Intan Permatasari for their support and prayers for my success. Last but not least, I would also like to thank Halja Peäske and Olev Peäske for thinking of us as family and for giving us such wonderful memories while we were here.

Kuressaare, 2022
Teguh Putranto

List of Publications

This present Ph.D. thesis consists of a summary and publications in the following peer-reviewed journals:

I T. Putranto, M. Kõrgesaar, J. Jelovica, K. Tabri, and H. Naar. Ultimate strength assessment of stiffened panel under uni-axial compression with non-linear equivalent single layer approach. *Marine Structures*, 78:103004, 2021

II T. Putranto, M. Kõrgesaar, and J. Jelovica. Ultimate strength assessment of stiffened panels using equivalent single layer approach under combined in-plane compression and shear. *Thin-Walled Structures*, 180:109943, 2022

III T. Putranto, M. Kõrgesaar, and K. Tabri. Application of equivalent single layer approach for ultimate strength analyses of ship hull girder. *Journal of Marine Science and Engineering*, 10(10):1–20, 2022

and the other relevant publications in the following peer-reviewed conference proceedings:

IV T. Putranto and M. Kõrgesaar. Numerical investigation on the buckling response of stiffened panel subjected to axial compression with non-linear equivalent single layer approach. In J.S. Chung, editor, *Proceedings of the 31st International Ocean and Polar Engineering Conference, ISOPE 2021*, volume 1, 2021

V T. Putranto and M. Kõrgesaar. Numerical study on the structural behavior of intact and damaged box beams under four-point bending load. In C.G. Soares, editor, *Proceedings of the 8th International Conference on Collision and Grounding of Ships and Offshore Structures (ICCGS 2019), 21-23 October, 2019, Lisbon, Portugal*, volume 1, 2019

Author's Contributions to the Publications

Contributions to the papers in this thesis are:

I In Publication I, the author performed unit cell analyses starting from model preparation to automatically extracting ABCD stiffness matrices using Python scripts. Additionally, the author simulated non-linear stiffness of ESL using the UGENS subroutine in the Abaqus software and compared the results with 3D FEM. M. Kõrgesaar and J. Jelovica provided information on the Abaqus user subroutine. K. Tabri provided the grillage finite element (FE) model. The manuscript was prepared by the author. M. Kõrgesaar, J. Jelovica, K. Tabri, and H. Naar made valuable comments, feedback, and improvements on the analysis and the manuscript.

II In Publication II, the author included the sub-matrix of A_{13} stiffness as a non-zero value in the ESL model of the stiffened panel under a combination of compression and shear. The author performed a validation of the ESL approach to 3D FEM and the experimental test from the literature. Additionally, the authors analyzed the accuracy of the ESL in the loading scenarios and several collapse modes. The manuscript was prepared by the author. M. Kõrgesaar and J. Jelovica made valuable comments, feedback and improvements on the analysis and the manuscript.

III In Publication III, the author conducted the FE analysis of models of a single compartment box girder and the entire hull girder of the ship. The author conducted ultimate strength predictions on both models using the ESL approach and 3D FEM. The author used the Abaqus VUGENS subroutine for the explicit analysis to simulate the non-linear stiffness of the ESL. Additionally, the author analyzed the accuracy of ESL in predicting the ultimate strength for ship grounding and collision cases. K. Tabri provided the tanker FE model. The manuscript was prepared by the author. M. Kõrgesaar, and K. Tabri made valuable comments and feedback on the analysis and the manuscript.

Original Features

The author believes that the following features in this thesis are original.

1. The influence of geometric and material non-linearities on the axial force response at the unit cell level is explained (Publication I). The initial imperfection shape composed of a sinusoidal waveform is obtained from the eigenmode analyses.

2. The application of periodic boundary conditions for the unit cell analyses is explained. The boundary conditions are determined based on the first-order shear deformation theory (FSDT). In addition to traditional displacement boundary conditions, equation constraints (Abaqus) are used to define the boundary conditions (Publication I).

3. The non-linear stiffness matrix of ESL is shown to depend on local buckling, material yielding, and imperfections (Publication I). The stiffness matrix of ESL is modified by taking into account the effect of A_{13} stiffness. This sub-matrix characterizes the axial force response during shear loading which is shown to develop during both uni-axial and shear loading (Publication II).

4. The ultimate strength analysis of the stiffened panel using the ESL approach is performed under pure compression (Publication I) and combined loading (Publication II). The validation of the ESL approach with experimental results is carried out in different panel configurations and loading scenarios. The influence of the collapse modes on the accuracy of ESL is explained (Publication II). The effect of ESL element sizes on ESL accuracy and computational time is discussed (Publication III).

5. The ESL methodology using the Abaqus VUGENS subroutine is implemented in the explicit FE code. The ESL is shown to be applicable for ultimate limit state (ULS) analyses of both intact and damaged ship (Publication III).

List of Abbreviations and Symbols

2D	Two-dimensional
3D	Three-dimensional
$[D]$	Bending stiffness
$\{\varepsilon^1\}$	Bending strain
$\{M\}$	Bending moment
$[C]$	Bending-membrane coupling stiffness
CSR	Common Structural Rules
DNV	Det Norske Veritas
ESL	Equivalent single layer
FEA	Finite element analysis
FEM	Finite element method
FE	Finite element
FSDT	First-order shear deformation theory
$\{\varepsilon^0\}$	In-plane membrane strain
IACS	International Association of Classification Societies
ISUM	Idealized Structural Unit Method
$\{N\}$	Membrane force
$[A]$	Membrane stiffness
$[B]$	Membrane-bending coupling stiffness
SP	Stiffened panel
β_p	Plate slenderness
β_s	Stiffener slenderness
$\{Q\}$	Transverse shear force
$[D_Q]$	Transverse shear stiffness
$\{\gamma^0\}$	Transverse shear strain
ULS	Ultimate limit state
UC	Unit cell

1 Introduction

1.1 Background

Design of ship structures is a time-consuming process that requires extensive analyses and iterations to achieve optimality, see Fig. 1. The structural analysis of the ship aims to determine the overall strength of the hull girder, including the global stresses and deformations of all primary members of the hull in the specified load cases [1]. To obtain a reliable structural design efficiently, a method with low computational effort and high precision is needed to perform the strength analysis of ship structures. The method should fit into an existing design framework that is largely driven by the requirements of classification societies, which currently rely heavily on direct assessment based on finite element analysis (FEA). Therefore, in this thesis, a method is proposed to reduce the modeling effort and analysis time.
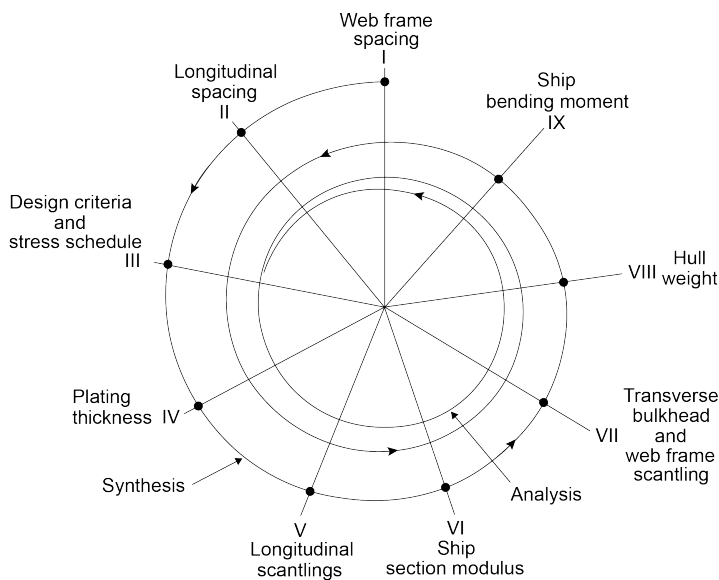

Figure 1: Structural design spiral [2].

As computer technology advances rapidly today, a numerical method is now widely used in structural engineering. A numerical method is a computer-based method for dealing with mathematical problems that are cumbersome to solve analytically. In engineering applications, a major advantage of the numerical method is the ability to provide a reliable solution related to design and optimization, since it saves both time and economic resources compared to experiments. Today, there are many numerical methods available to solve structural engineering problems.

The finite element method (FEM) is a numerical method for performing a finite element analysis (FEA) of any given physical phenomenon to predict structural behavior. In the FEM, physical structures are modeled by a series of finite elements interconnected with each other by specific points called nodes. The method was developed in the 1950s to solve complex problems of elasticity and structural analysis in civil and aircraft engineering [3, 4]. Today, the applications of this method are quite diverse.

Using FEM, structural analysis can be performed taking non-linear structural behavior into account. To capture the non-linear structural behavior, traditional 3D FEA relies on

detailed modeling of the structures. However, the number of degrees of freedom (DOF) in large-scale ship structural FEA model can reach more than a million making the analysis time-consuming. The most obvious solution to this problem is to reduce the use of elements, thus reducing computational time [5]. Therefore, the purpose of this thesis is to present a method that makes detailed 3D FE modeling and analysis of ship structures more efficient.

In addition to simplifying FE modeling of structures, the proposed method allows to capture the response of the panel considering buckling and yielding behavior. Both of these non-linearities contribute to the accuracy of the ultimate strength analysis. Under tension, the load-end shortening curve is linear until the onset of material yielding, see Fig. 2. Compression load leads to panel buckling, which is different depending on whether material non-linearities are accounted or not. The stiffness of the panel increases linearly until the buckling strength is reached. In the post-buckling stage, the compression force continues to increase, but the stiffness of the panel is reduced. The compression force continues to increase until the ultimate strength, often referred to as the maximum force, is reached.
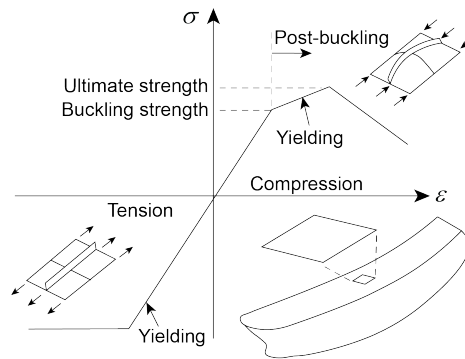

Figure 2: Idealized behavior of a panel under compression and tension loading [6].

1.2 State of the art

Stiffened panels are the main structural components of the ship hull that provide strength to withstand internal and external loads. These panels are made up of the plate and the attached stiffeners that provide the main load-bearing capacity to carry in-plane and out-of-plane loads. There are many benefits associated with stiffened panels, including excellent strength-to-weight ratios and ease of fabrication [7].

During ship operation, stiffened panels are subjected to different loading scenarios, such as in-plane, bending, torsion, and lateral pressure. In these scenarios, different types of collapse mode can occur, including local and global failures in the stiffened panel [8–10], see Figure 3 [11]. Each type of collapse mode has a different load-end shortening curve pattern, as shown in Fig. 4. This loading can have a deleterious effect if it exceeds the strength capacity of the ship structure. To prevent these potentially catastrophic events, classification societies require a demonstration of the ultimate strength of the hull girder and its components. Therefore, the design of ship structures involves multiple rounds of evaluation of possible collapse scenarios of all the stiffened panels. To remain competitive, these assessments must be performed efficiently.

The ultimate strength assessment of the hull girder has been thoroughly investigated
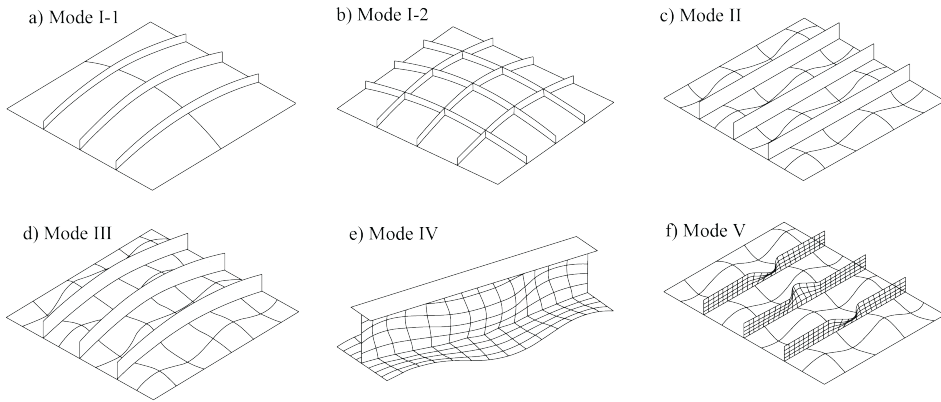
Figure 3: Collapse modes: (a) mode I-1: overall collapse of a uni-axially stiffened panel; (b) mode I-2: overall collapse of a cross-stiffened panel; (c) mode II: plate collapse without distinct failure of the stiffener; (d) mode III: beam-column collapse; (e) mode IV: collapse by local web buckling of the stiffener; (f) mode V: collapse by flexural-torsional buckling of the stiffener [11].

in the past few decades. The first attempt was made by Caldwell [12], who introduced an equivalent thickness approach to replace the stiffened panel to calculate the ultimate strength of the hull girder. The concept of the approach was further developed by Paik and Mansour [13] who assumed a stress distribution through the cross-section of a ship, however the strength reduction due to buckling was not considered. The strength reduction coefficient method was proposed by Smith [14]. Smith's method was applied to an incremental-iterative approach in which the load-end shortening curves of each structural element are used for the progressive collapse analysis. This approach has been developed in response to regulatory requirements and specific load scenarios. Additionally, classification societies commonly consider the two-dimensional (2D) cross-section of the hull girder for the ultimate strength assessment. Current methods for calculating the ultimate strength of the hull girder can be categorized into three groups:

- direct methods (linear method and empirical formula),
- progressive collapse analysis (Smith's method), and
- numerical methods such as the idealized structural unit method (ISUM) and the finite element method (FEM).

These methods are effective in progressive collapse analysis. Of these three methods, there are increasing numbers of studies that focus on the ISUM and FEM to determine the ultimate strength of the hull girder [15].

The ISUM is acknowledged as one of the most reliable methods to evaluate the progressive collapse of the hull girder. This method can include the buckling response caused by all possible loading components of the hull girder for ultimate strength analyses [5, 16–19]. The implementation of this method can be found in the ALPS/HULL program of the MAESTRO FEM analysis package. The ISUM can handle the interaction with local and global buckling [20] for a section between the webframes of the hull girder. However, longer models that extend over several webframes are needed for compartment level buckling analysis, allowing the inclusion of actual pressure distributions and the consideration of various loading scenarios [21]. The length of the model plays a role in the post-buckling behavior, which affects the capacity for bending moments [22]. Furthermore,
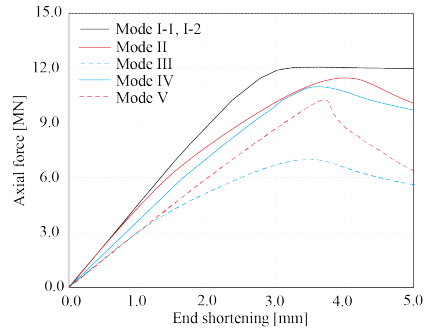
Figure 4: Load-end shortening curve for each collapse mode.

full-scale ship models are recommended to reduce boundary effects, which typically result in a more conservative response and more severe scantlings [23, 24].

In recent years, great attention has been paid to the analysis of the buckling and ultimate strength of the stiffened panel under compression [25–29]. However, the buckling mode is more complex under shear load than under compressive load due to the tension field, further affecting the ultimate strength of the stiffened panel. Some research has been conducted on the parametric study to investigate the buckling and ultimate strength of the stiffened panel under shear load. According to Loughlan and Hussain [30] and Pavlovčič et al. [31, 32], the buckling mode changed from global buckling to local buckling under shear load as the stiffener height increased. Su et al. [33] found that local buckling on the thin plate caused the final failure earlier than on the thick plate. Wang et al. [34] developed a formula to predict the ultimate shear strength of the stiffened panel considering the plate and stiffener slenderness parameters. Some of the studies above have been done on the ultimate shear strength characteristics of the stiffened panel, while studies on the effect of the combination of compression and shear on the ultimate strength analysis are still not enough. Compared to pure compression, the ultimate strength of the stiffened panel under a combination of compression and shear can be lower.

The finite element (FE) modeling of the full-scale hull girder allows progressive collapse analysis to consider interactions between structural elements at the local and global levels under combined loading. However, the FE simulation of the entire structure of the ship involves extremely large computational and modeling effort. To reduce this effort without compromising accuracy of the 3D FEM results, this thesis proposes the use of an equivalent single layer (ESL) approach.

The ESL approach is a combination of mathematical models developed from Kirchhoff-Love plate and Euler-Bernoulli beam theories. In the ESL approach, the shell kinematics of the deformation behavior is based on the first-order shear deformation theory (FSDT). Several books have been written on these topics; Reddy [35] presents the theoretical basis, extends them with respect to transverse shear deformation, and provides examples of applications to a variety of engineering issues. The concept of the ESL approach is to replace a discrete model of a complex system with a single plate with a homogenized continuum by modeling the stiffness equivalent to the original. The ESL approach has been used to model sandwich panels [36]. Using the ESL approach, the time required for the computation and analysis of sandwich panels can be reduced and effectively integrated with the optimization procedures [37, 38] to produce a complete design in the preliminary design stage.

The ESL approach can be defined by considering both linear and non-linear stiffness matrices. Based on the linear stiffness matrix, the shell elements of a hull girder were defined as orthotropic material properties [39], and the strength analysis can consider the response due to global bending moments [40]. ESL with a linear stiffness matrix was used to analyze the global elastic buckling response of corrugated panels [41] and the global vibration of sandwich panels [42]. Additionally, it was also implemented in sandwich panel modeling to study the effect of fabrication quality on elastic buckling characteristics and corrosion factors [43–45]. In those simulations, the non-linear stiffness matrix was not incorporated since the primary focus was on the analysis of elastic global response. The non-linear stiffness matrix of the ESL allows for consideration of the evolution of stiffness during the deformation process. The non-linearites can originate either from material or geometry. Goncalves et al. [46] included local buckling non-linearity in stiffness definition that improved ESL accuracy in predicting the buckling response of sandwich structures while Kõrgesaar et al. [47] included material non-linearity to capture the behavior of sandwich panels under tension. However, in buckling analysis, material non-linearity has not been considered. Consideration of non-linear material behavior is important in stiffened panels as they display excessive plasticity in the plate field and stiffeners at the point of ultimate strength [11, p.271]. Therefore, the review by Romanoff et al. [48] recommended a more comprehensive study of ESL to improve and develop the theory for its more widespread use.

The ESL approach has been well established for the analysis of sandwich and composite panels that are symmetric in the thickness direction, but applications to asymmetric stiffened panels in thickness directions are lacking. When stiffened panels are deformed out-of-plane, the asymmetry increases the interaction between the membrane-bending coupling response, which must be taken into account. The application of the ESL approach representing an asymmetric stiffened panel presents a challenge and a novel aspect of this thesis.

In this thesis, the ESL approach is proposed taking into account the advantages it provides. With the ESL approach, the computation time can be reduced and the accuracy can be maintained. The use of the number of elements and nodes can be minimized, thereby reducing the FE modeling effort and analysis time. To cover more complex response analyses, the non-linear stiffness of ESL is used since it can consider the response due to local buckling and material non-linearity.

1.3 Objective of the Thesis

The main goal of this thesis is to provide a framework for the ultimate strength analysis of the hull girders using the ESL approach. In the ESL methodology, the stiffened panel is replaced by a single plate where the stiffness is the same as the original panel, while the primary structural members, such as webframes, girders, and stringers, are modeled in detail. To achieve this, the implementation of the framework requires several key steps. Therefore, the thesis has the following objectives:

1. Reduce the number of elements and nodes used in hull girder modeling in the preprocessing stage using ESL;

2. Reduce the computational time required for the finite element analysis on the hull girder model;

3. Obtain the ultimate strength of hull girder using ESL;

4. Validate the ESL results with the 3D FEM and experiments.

1.4 Scope of work

The finite element analysis (FEA) is performed to predict the global response of the ship, ultimately ensuring that the design of the ship structure is reliable. Additionally, this analysis is necessary to comply with the requirements of the classification authorities on the assessment of the strength of a structural design of a ship. To ease the FE modeling effort and reduce the computational time, we propose an ESL approach. This approach is implemented into a commercial FE software Abaqus through user defined subroutine to predict the ultimate strength of the stiffened panel and the hull girder. The investigation is broken down into three publications, as shown in Fig. 5.

In Publication I, the ESL approach is implemented in the stiffened panel and grillage models to predict the ultimate strength under compression. In the ESL modeling, plates and stiffeners are replaced with an ESL plate, while girders and webframes are modeled in detail using shell elements with isotropic properties. The non-linear stiffness of ESL is used to capture the response of local buckling and material non-linearity during simulation. The accuracy of ESL simulations is quantified by comparisons with the 3D FEM results, and the actual topology represented with shell elements can show the progressive collapse behaviors.

In Publication II, the effect of combined loading on the ultimate strength of stiffened panel is examined. The ESL stiffness matrix is extended by including the A_{13} sub-matrix as non-zero. The ultimate strength analysis is conducted for several stiffened panel configurations based on the plate and stiffener slenderness. The inclusion of axial force caused by shear stiffness A_{13} is shown to improve ESL accuracy in the post-buckling stage of stiffened panels.

In Publication III, the ESL approach is used to assess the ultimate strength of the hull girder in intact and damaged condition. In explicit analysis, VUGENS subroutine is invoked to consider the non-linear stiffness of ESL. Computational efficiency and reduced modeling effort is achieved using the ESL approach. Additionally, ESL also enables to capture the progressive collapse response of hull girder.

1.5 Limitations

In this study, the analyses of the ESL approach are limited to the following cases.

1. Stiffened panels can be substituted with an ESL model if they are composed of flat plates and attached stiffeners where they are straight and parallel to each other.

2. The load applied to the stiffened panel continuously increases without reversing. Thus, the effect of residual stress and pre-load on the ultimate strength analysis is neglected.

3. The direction of compressive loading applied to the stiffened panel is parallel to the stiffener direction.

4. Geometric imperfections are defined as a linear superposition of the buckling eigenmode obtained from the eigenvalue buckling analysis.

5. Hydrodynamic characteristics, including added mass, damping, and restoring forces, are neglected in the ultimate strength analysis of the hull girder.
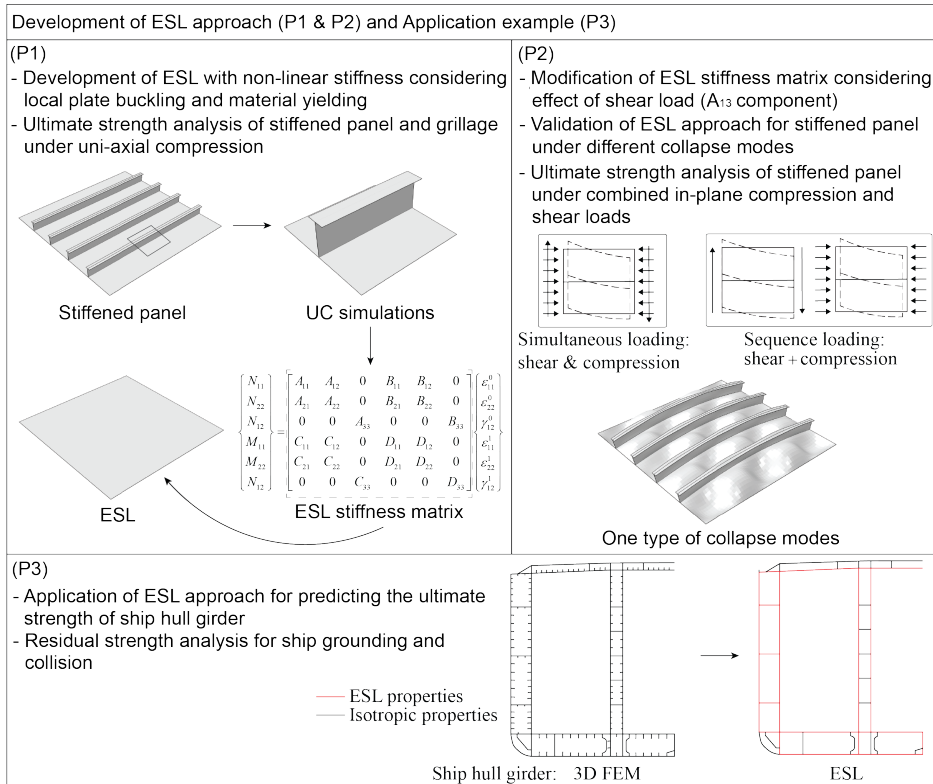
Development of ESL approach (P1 & P2) and Application example (P3)

(P1)
- Development of ESL with non-linear stiffness considering local plate buckling and material yielding
- Ultimate strength analysis of stiffened panel and grillage under uni-axial compression

Stiffened panel   UC simulations

$$\begin{Bmatrix} N_{11} \\ N_{22} \\ N_{12} \\ M_{11} \\ M_{22} \\ N_{12} \end{Bmatrix} = \begin{bmatrix} A_{11} & A_{12} & 0 & B_{11} & B_{12} & 0 \\ A_{21} & A_{22} & 0 & B_{21} & B_{22} & 0 \\ 0 & 0 & A_{33} & 0 & 0 & B_{33} \\ C_{11} & C_{12} & 0 & D_{11} & D_{12} & 0 \\ C_{21} & C_{22} & 0 & D_{21} & D_{22} & 0 \\ 0 & 0 & C_{33} & 0 & 0 & D_{33} \end{bmatrix} \begin{Bmatrix} \varepsilon_{11}^0 \\ \varepsilon_{22}^0 \\ \gamma_{12}^0 \\ \varepsilon_{11}^1 \\ \varepsilon_{22}^1 \\ \gamma_{12}^1 \end{Bmatrix}$$

ESL   ESL stiffness matrix

(P2)
- Modification of ESL stiffness matrix considering effect of shear load (A_{13} component)
- Validation of ESL approach for stiffened panel under different collapse modes
- Ultimate strength analysis of stiffened panel under combined in-plane compression and shear loads

Simultaneous loading: shear & compression   Sequence loading: shear + compression

One type of collapse modes

(P3)
- Application of ESL approach for predicting the ultimate strength of ship hull girder
- Residual strength analysis for ship grounding and collision

—— ESL properties
—— Isotropic properties

Ship hull girder: 3D FEM   ESL

Figure 5: Description of the investigation.

2 Equivalent single layer

2.1 Overview of the ESL approach

In the ESL approach, a three-dimensional (3D) stiffened panel is replaced with a two-dimensional (2D) single layer whose stiffness is the same as the original panel, see Fig. 6. The ESL stiffness matrix is composed of $[A]$ for the membrane, $[B]$ for the membrane-bending coupling, $[C]$ for the bending-membrane coupling, $[D]$ for the bending, and $[D_Q]$ for the transverse shear components based on the FSDT kinematics, as expressed in Eq. (1):

$$\left\{\begin{array}{c} \{N\} \\ \{M\} \\ \{Q\} \end{array}\right\} = \begin{bmatrix} [A] & [B] & 0 \\ [C] & [D] & 0 \\ 0 & 0 & [D_Q] \end{bmatrix} \left\{\begin{array}{c} \{\varepsilon^0\} \\ \{\varepsilon^1\} \\ \{\gamma^0\} \end{array}\right\}. \tag{1}$$

Here $\{N\}$ is the membrane force, $\{M\}$ is the bending moment, $\{Q\}$ is the transverse shear force, $\{\varepsilon^0\}$ is the membrane strain, $\{\varepsilon^1\}$ is the bending strain and $\{\gamma^0\}$ is the transverse shear strain.
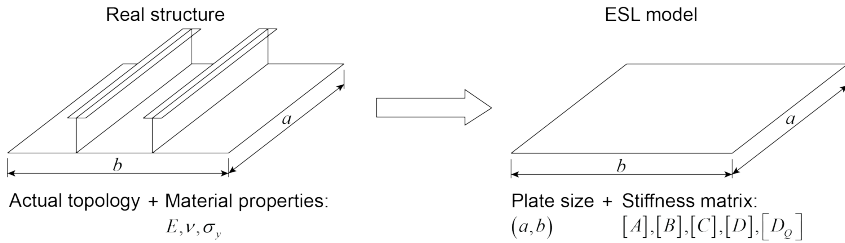
Figure 6: Differences in modeling a real stiffened panel compared to the ESL approach.

To analyze different types of stiffened panel, only ESL stiffness matrices need to be changed without re-meshing the model. In the ESL model, the structural topology changes are introduced by changing the orthotropic non-linear ESL stiffness properties, without any modifications in the structural FE model. This circumvents constly re-meshing and modeling, but bears an additional cost of running unit cell analysis with each of the configuration subject to investigation. This allows the optimization of a wide range of material and geometric configurations.

The stiffness of the ESL depends on the response of the mechanical behavior of the repeating periodic part of the stiffened panel called the unit cell (UC). The UC is composed of the plate and the stiffener, which can be applied later to homogenize the entire stiffened panel, see Fig. 7. In Section 2.2, the application of the boundary conditions used in the UC is explained. The results of the UC analysis are used to determine the stiffness matrix of the ESL. Furthermore, to better understand the effect of geometric and material non-linearities on the UC responses, a parametric study is performed and explained in Section 2.3.

2.2 Definition of the unit cell

An important part of successful ESL modeling is dependent on determining the correct stiffness. The stiffness of the ESL is obtained from the response of the UC. The shape of the UC is a rectangular cuboid where the width and length are fixed to the stiffener spacing. This size selection is based on the analysis in Section 2.3. The application of
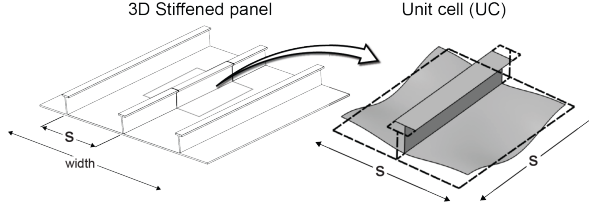
Figure 7: Determination of the unit cell (UC).

boundary conditions to the UC and the response needed to determine the stiffness of the ESL are discussed in the following.

The UC is simulated under six loading conditions as shown in Fig. 8. Periodicity is invoked by prescribed displacement boundary conditions applied on the UC edges according to the kinematics of the first-order shear deformation theory (FSDT). Displacements are enforced in a single direction, resulting in three uni-axial displacements ($\varepsilon_{11}^{(0)}, \varepsilon_{22}^{(0)}, \gamma_{12}^{(0)}$) and three curvatures ($\varepsilon_{11}^{(1)}, \varepsilon_{22}^{(1)}, \gamma_{12}^{(1)}$). There are two types of boundary conditions: periodic equation constraints (P) and displacement boundary conditions (BC). In Fig. 8, the first sub-figure illustrates the color-coding of the boundary condition and equation constraints which apply to the rest of the loading scenarios. There are always five prescribed kinematic constraints applied to each boundary node, with rotation around the z-axis left free because, according to FSDT, this degree of freedom is not taken into account. The periodic equation constraint (P) always involves two nodes at opposing edges of the UC. The displacement boundary condition (BC) is applied to the entire edge of the UC. These P and BC are generated with python script that automatically organizes and orders the node sets to facilitate the process.
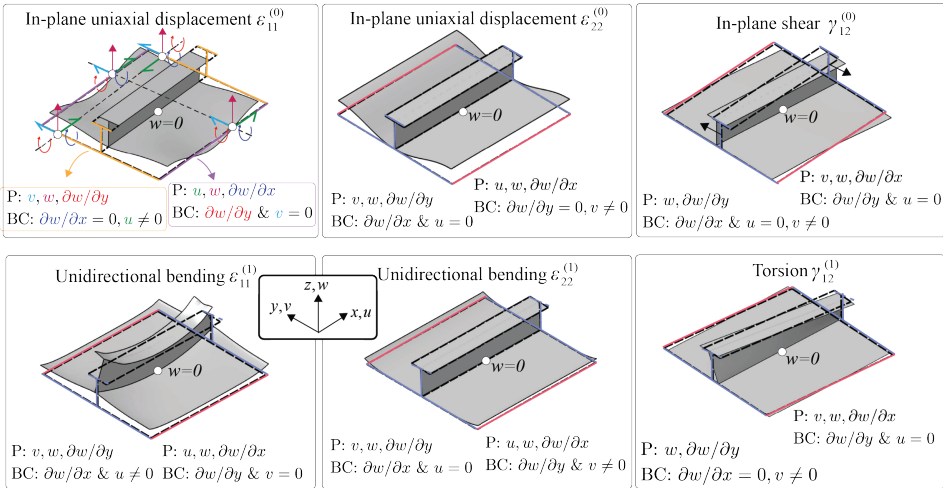

Figure 8: Boundary conditions used in the UC analysis.

The results of the UC analysis are presented in the membrane force and bending moment as shown in Fig. 9, for details see Publication I Section 3.2 and Goncalves et al. [46] Section 3.3. The first derivatives or slopes of these curves are used to determine the stiffness of the ESL. As these slopes vary in increasing strain, the stiffness of the ESL is non-linear. To consider non-linear stiffness in the ESL simulation, the UGENS or VUGENS

subroutine is invoked for implicit or explicit analysis, respectively. This subroutine allows the stiffness to change during the ESL simulation.
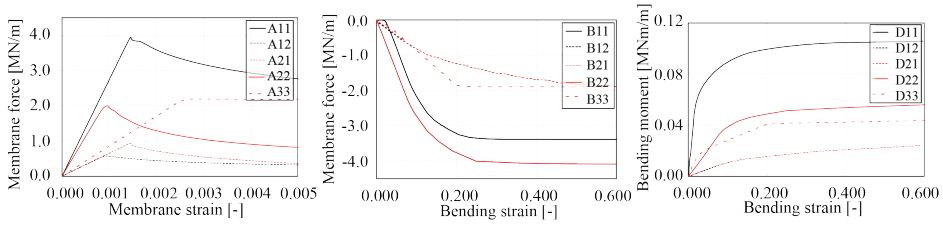

Figure 9: Membrane force and bending moment from the UC analysis (Publication I).

Further UC analysis is conducted to investigate the capability of the ESL to predict an axial force under shear loading. In Fig. 10, the axial force (N_{11}) exists during shear loading in the UC analysis. This force updates the stiffness component of A_{13} in the ESL model where in Publication I this component is assumed to be zero since the stiffened panel is subjected to pure compression. Therefore, for combined compression and shear loading on the stiffened panel, the stiffness of the ESL is extended by including the A_{13} as non-zero (Publication II).
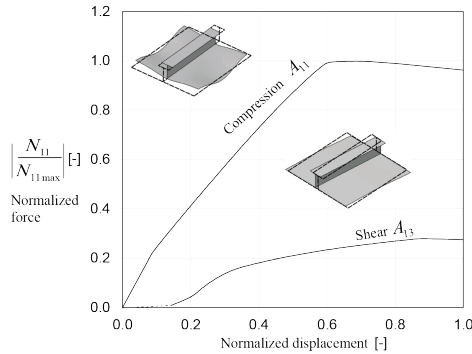
Figure 10: Development of axial forces under compression and shear loads (Publication II).

2.3 Parametric study with the unit cell

During compression, stiffened panels may experience buckling and yielding behavior, resulting in non-linear response. To capture this non-linear response also with the ESL model, the respective stiffness components need to be characterized with UC analysis. Since the UC can be considered as the basic building block of the stiffened panel, the UC analysis has to be repeated for each structural configuration that is analyzed (Publication I).

The size of the UC affects its stiffness, since it defines the allowable number of buckling half-waves during non-linear response and the evolution of the deformation shape. The width of the UC (s) is equal to the stiffener spacing, while the length (a) is varied to investigate the response, see Fig. 11. Based on the results, the UC of a/s=1.0 is selected because it has the lowest strain energy (area under the curve).

The buckling occurs in the unit cell with initial imperfection, thus lowering stiffness, see Fig. 12. As shown in Fig. 12, initial imperfections are needed to trigger buckling in the
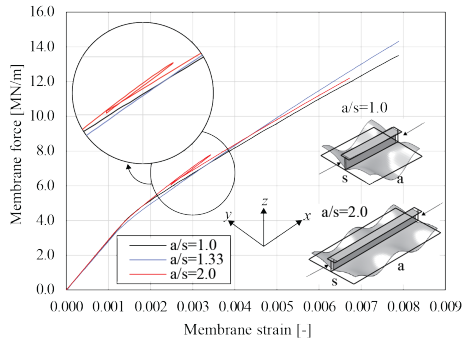
Figure 11: Effect of UC size on UC response (Publication I).

UC, and the amount of stiffness reduction depends on the severity of the imperfection. In Fig. 12, the severity of the buckling is defined by the amplitude x. For the UC without initial imperfection, buckling never occurs. This is because buckling is a bifurcation phenomenon and buckling does not occur without disturbance or trigger [49].
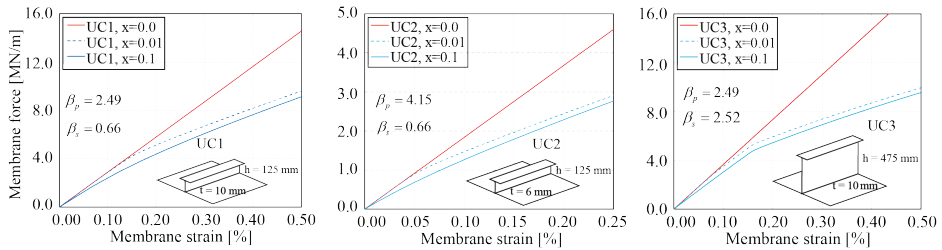

Figure 12: Effect of initial imperfections on membrane forces with different slenderness of plate (β_p) and stiffener (β_s) (Publication I).

In unit cell analysis, the effect of geometric and material non-linearity on the membrane responses was investigated with different panel configurations (Publication I), see Fig. 13. In Fig. 13 the effect of material non-linearity is quantified by membrane force difference between elastic and elastic-plastic analysis with both analyses having the same geometric non-linearity. The geometric non-linearity is quantified by the force difference between two elastic-plastic analyses, one having initial imperfections. Both of these non-linearities, geometric and material, have a marked effect on the UC response. Since both of these non-linearities are present in real panels, the UC response must account for this behavior to yield representative stiffness behavior.
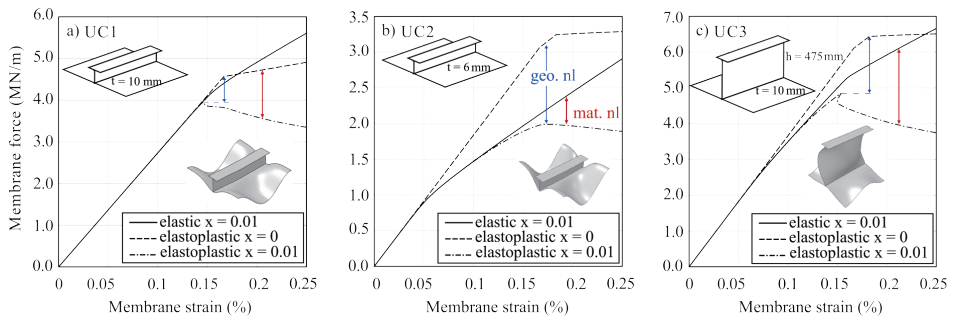
Figure 13: Effect of material and geometrical non-linearity on the unit cell response. The effect of geometric non-linearity is shown with a blue arrow approximately at the ultimate point. The effect of material non-linearity is indicated with a red arrow in qualitative terms (Publication I).

3 Ultimate strength of stiffened panel

3.1 Stiffened panel under uni-axial compression

Under uni-axial compressive loading, ESL can accurately capture the response of collapse behavior up to the ultimate stage, see Fig. 14. In the ESL homogenization concept, the relationship of stress resultants and strains is assumed to be evenly distributed throughout the panel. Based on this assumption, the ultimate strength analysis yields satisfactory results. However, the accuracy of the ESL decreases in the post-ultimate stage. At this stage, the inhomogeneity of progressive collapse is characterized by dominating buckling at a certain location. The strength of the stiffened panel drops significantly, making it difficult for the ESL to predict accurately.
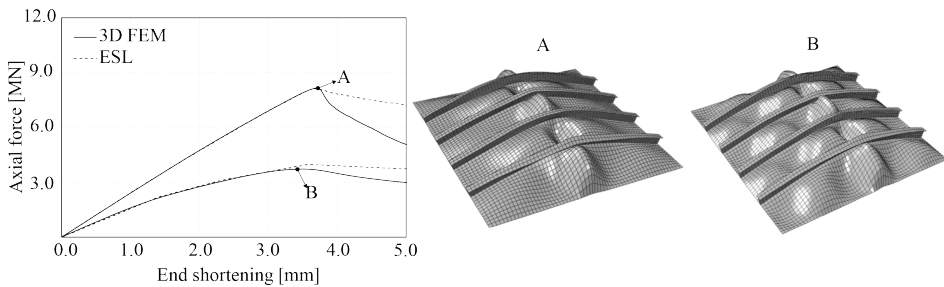

Figure 14: Load-end shortening curves and deformation shapes of stiffened panels in different configurations under uni-axial compression (Publication I).

The local buckling shape of the stiffened plate (e.g. the number of wavelengths between and along the plate field between stiffeners) depends on the panel configuration. The ESL topology that is a bare plate with secondary stiffeners removed cannot visualize this local behavior. Consequently, the local deflections are not directly comparable between 3D FE model and ESL model as demonstrated in Fig. 15. However, the response of local buckling is accounted in terms of the non-linear stiffness of the ESL. Therefore, the global response in terms of load end-shortening of grillage panel is predicted largely accurately.
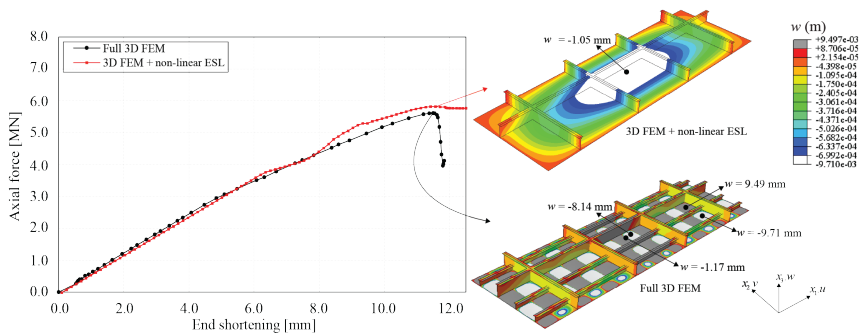

Figure 15: Load-end shortening curves and deformation shapes of a large grillage under uni-axial compression (Publication I).

27

3.2 Stiffened panel under combination of compression and shear

In the presence of shear (τ), the ultimate strength of the stiffened panel can be reduced compared to pure compression (σ), since shear can generate additional axial forces. A decrease in axial response occurs at the bifurcation point along with an increase in combination of compression and shear ratio (τ/σ), see Fig. 16. In addition to affecting the axial force, shear also contributes to the increase in panel deflection. The effect of the shear load on the reduction in the ultimate strength of the stiffened panel can be considered by including the ESL stiffness component of A_{13} as non-zero (Publication II). This improves the accuracy of the ESL in predicting the ultimate strength under a combination of compression and shear. Since shear is not present under compressive load, the ESL stiffness component of A_{13} has no effect on the reduction of axial force.
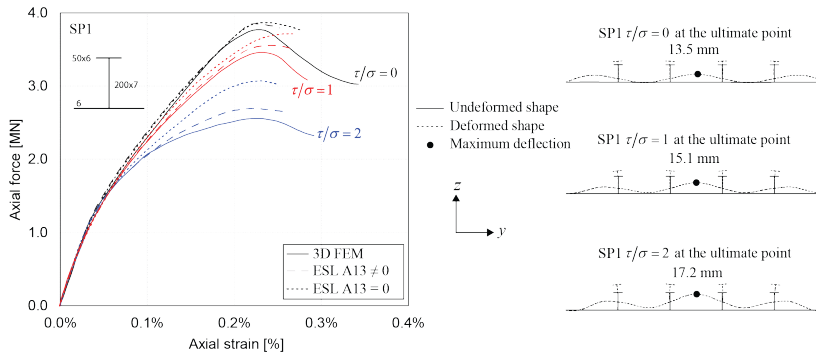

Figure 16: Axial force-strain curves and collapse modes of the stiffened panel under combination of compression and shear (Publication II).

To reveal a wide range of applicability, the accuracy of the ESL approach is analyzed based on the stiffened panel configurations and loading scenarios, see Fig. 17. Due to the increase in the stiffener web height and the removal of the flange, the stiffener can become unstable and experience local buckling. This collapse mode can cause large out-of-plane deformations in the stiffener web. In addition to panel configuration, the loading scenario affects the collapse mode. For example, the panel with the 450 mm web experiences tripping type of collapse under pure compression, but under compression and shear the collapse mode changes leading to interaction between local plate and stiffener web buckling modes (Publication II).

Recent investigations have demonstrated that lateral loads can reduce hogging ultimate strength up to 25% [50, p.377]. Therefore, lateral load influence on the accuracy of the ESL is assessed in Publication II, see Fig. 17. In general, lateral pressure increases the out-of-plane deformation. However, by comparing the error in analyses between the same stiffened panels with and without lateral pressure in Fig. 17, it is concluded that the accuracy of the ESL is not compromised by lateral loads.

To summarize the results in Fig. 17 and analyses in Publication II, a collapse mode formed by a combination of local buckling on the plate and stiffener reduces the accuracy of the ESL.
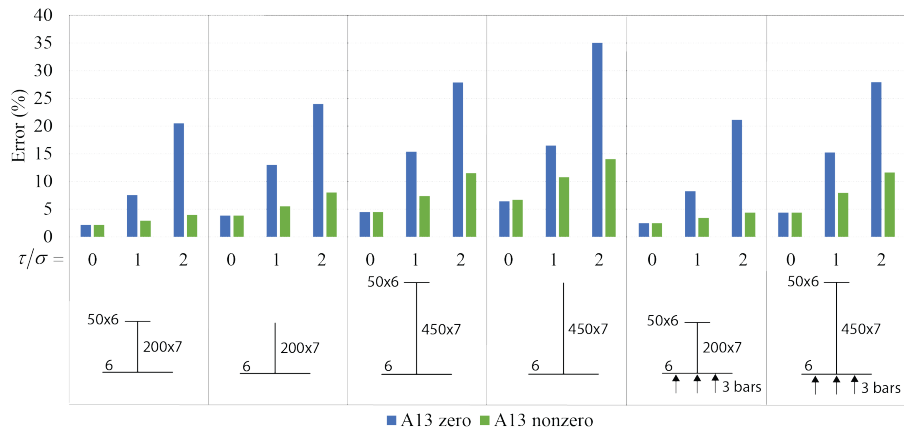
Figure 17: The error percentages of the ultimate strength resulted from ESL for several configurations of stiffened panels under a combination of compression, shear and lateral pressure (Publication II).

4 Ultimate strength of hull girder

4.1 One-compartment box girder

The ESL approach is used to predict the ultimate strength of the one-compartment box girder model. The model is subjected to bending load that causes compression in the deck and tension in the bottom. Analyses are performed with 3D FE and ESL models. The qualitative comparison of the deformations in Fig. 18 shows that the compartment level buckling obtained with the ESL method is similar to the 3D FE results.

Furthermore, in more quantitative terms, there is a close agreement between the 3D FEM and the ESL in terms of maximum bending moments; see Fig. 19(a). ESL simulations were performed with 50 mm, 300 mm and 600 mm mesh. All ESL element size configurations studied can accurately capture compartment-level buckling behavior, and for efficiency 600×600 mm mesh or two ESL elements between webframes is recommended. However, the accuracy of the ESL decreases if the stiffened panel experiences local buckling on the plate or the stiffener web (Publication II). Therefore, an investigation of the appropriate ESL element size for such simulations needs to be conducted in the future. In addition to providing the good accuracy, the ESL approach also gives shorter computation times than 3D FEM, see Fig. 19(b).
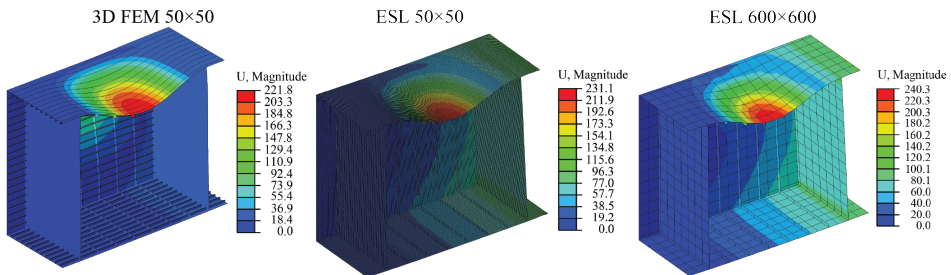

Figure 18: Deformation shape of the one-compartment box girder using 3D FE and ESL models (Publication III).
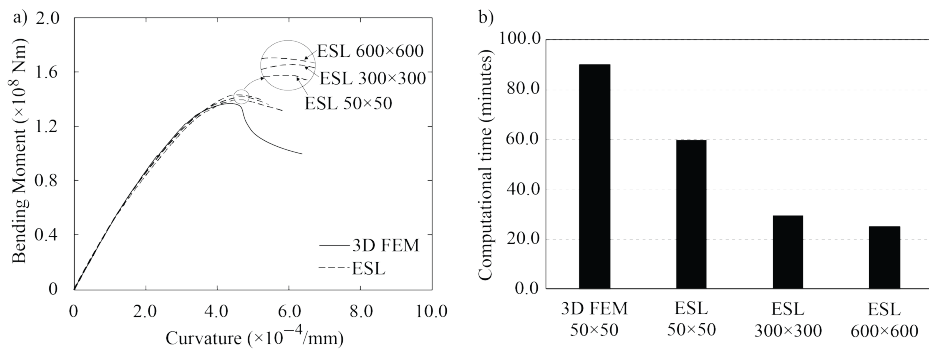

Figure 19: a) Bending moment – curvature curves obtained from 3D FEM and ESL with several element sizes. b) Computational time for 3D FEM and ESL with several element sizes. (Publication III).

4.2 Full-scale hull girder

Modeling the hull girder with ESL is especially advantageous, as the number of elements used can be reduced by up to 25% compared to the 3D FE model (Publication III). However, the accuracy of the ESL is still good in comparison with the results of the 3D FEM. The bending moment can be accurately predicted using the ESL approach until the ultimate stage, as shown in Fig. 20(a). In the post-ultimate stage, the accuracy of the ESL under sagging condition is better than under hogging condition. The difference in accuracy is due to the progressive collapse mode experienced in compressed structures. As explained in Section 3.2, the combined local buckling of the plate and the stiffener web reduces the accuracy of the ESL and the same local buckling interaction takes place in the double bottom structure under hogging condition, see Fig. 20(b). In contrast, there is no local buckling in the main deck structure under sagging conditions, resulting in a better accuracy for the ESL in the post-ultimate stage.
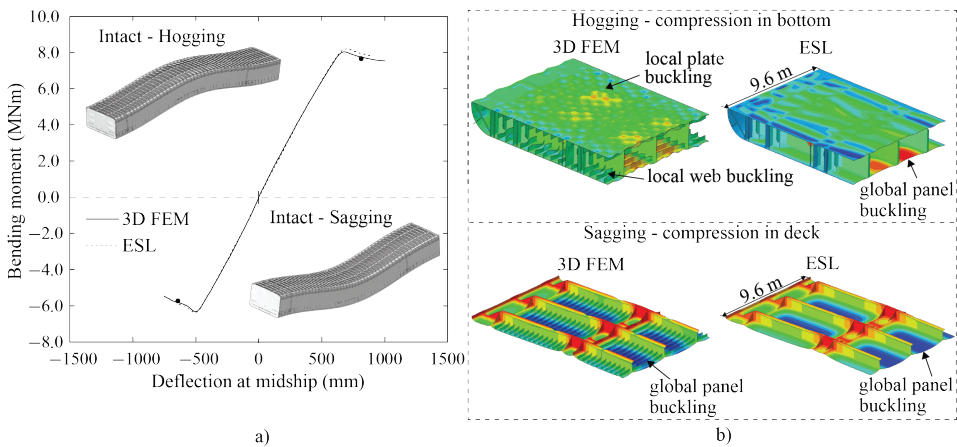

Figure 20: Response of an intact ship under vertical bending moment. (a) Bending moment-deflection curves. (b) Collapse mode in the double bottom and main deck structures under hogging and sagging conditions in the post-ultimate stage, respectively (Publication III).

Fig. 21 compares the longitudinal stress distribution in the outer shell of the main frame section obtained with 3D FEM and ESL. The longitudinal stresses obtained with the ESL approach are in good agreement with 3D FE results. The ship studied is made of high-strength steel (AH36) with a yield stress of 355 MPa. Figure shows that at the ultimate stage outer side shell has reached plastic stage in upper part. In compressed part of the structure there is some deviation between longitudinal stresses as already noted in Fig. 19. The longitudinal stress obtained from the ESL is calculated by dividing the axial force to cross-sectional area. In post-processing, the ESL element cannot provide the stress results due to the limitation of Abaqus.

As an application of the developed ESL approach, it is used in Publication III to assess the ultimate strength of damaged ships due to collision and grounding. The ultimate strength analysis is performed under vertical and horizontal bending moments. The reduction in bending moment due to collision and grounding obtained with 3D FEM and ESL are presented in Fig. 22. The overall accuracy of ESL simulations compared with 3D FEM is excellent, remaining within 3% in all cases. The accuracy of ESL is better than the results obtained from the incremental-iterative method or the CSR method as presented in Publication III.
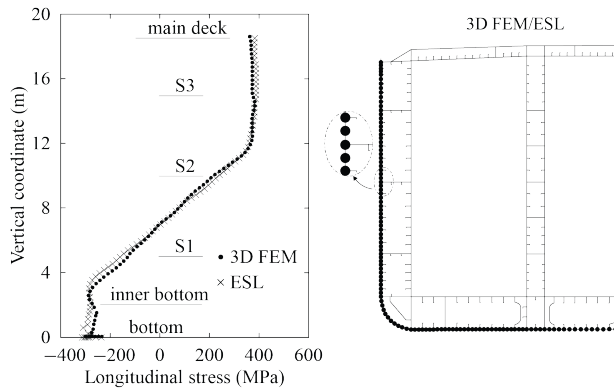
Figure 21: Distribution of longitudinal stress in the midship section using 3D FEM and ESL under hogging condition (Publication III).
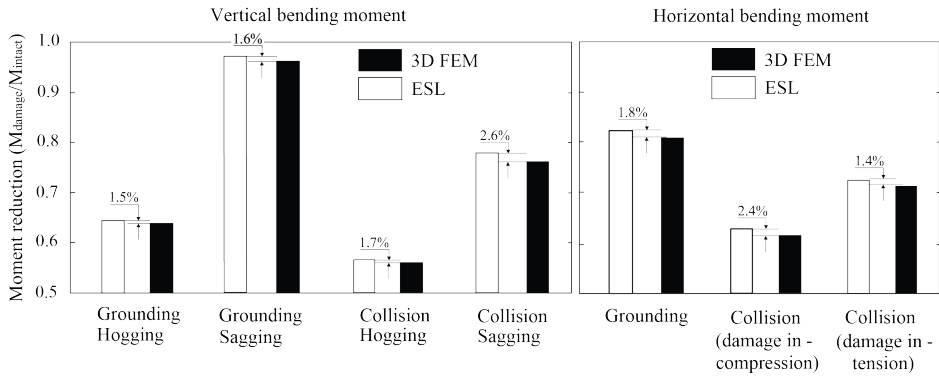

Figure 22: The moment reduction ratio due to grounding and collision damage under vertical and horizontal bending moments using the 3D FEM and ESL (Publication III).

5 Conclusions and future work

This thesis proposes an equivalent single layer (ESL) approach to predict the ultimate strength of the stiffened panel and hull girder. In the ESL approach, a single layer is used to replace the stiffened panel, providing a stiffness equivalent to that of the original panel. A novel aspect of this study is the implementation of the ESL model on stiffened panels, which are asymmetric in the thickness direction. Additionally, geometric and material non-linearities are considered in the unit cell analysis to capture the non-linear responses due to the buckling and yielding behavior. These non-linearities are included in the stiffness matrix of the ESL by way of Abaqus UGENS or VUGENS subroutines for implicit or explicit analysis, respectively. On the basis of the results, the ESL with non-linear stiffness is able to accurately predict the ultimate strength of stiffened panels. The error in ESL simulations compared to 3D FEM ranges between 3%–14% depending on the panel slenderness. In most cases, the ESL gives a more stiffer response. The lowest accuracy of the ESL is obtained when the stiffened panel experiences local buckling on both the plate and the stiffener web. The application of lateral loads on the stiffened panel does not deteriorate the accuracy of ESL in predicting the ultimate strength.

The use of the ESL approach is found to have substantial benefits in the ultimate strength analysis of a full-scale modeling of the hull girder. In comparison to 3D FEM, two ESL elements between webframes are about three times faster in terms of analysis time. Using these ESL elements, the compartment level buckling can be captured. The ESL approach is capable of well capturing the bending moment until the ultimate stage, but at the post-ultimate stage the accuracy depends on the type of collapse mode. Compared to panels that experience local buckling on both plate and stiffener web, panels that undergo global buckling yield better accuracy at the post-ultimate stage. In general, the ESL approach provides good ultimate strength predictions for intact and damaged ships under vertical and horizontal bending moments.

Several aspects need to be addressed in future research. The ESL mesh with two elements between webframes provides good accuracy in predicting overall compartment level collapse. Future investigations should try to improve the accuracy of the prediction under local buckling. In this study, the entire unit cell analysis process was automated using Python scripts, which read the structural data from a text file, prepare numerical models, and generate the ABCD stiffness matrices. In order to facilitate design optimization, it is necessary to prepare a database containing results from unit cell analysis with different configurations. Furthermore, in the post-processing stage, the ESL element cannot visualize the stress, so this aspect should be discussed in the future.

References

[1] DNVGL. *Direct strength analysis of hull structures in passenger ships*. DNV GL AS, 2016.

[2] A.F. Molland. *The maritime engineering reference book*. Butterworth-Heinemann, 2008.

[3] A. Hrennikoff. Solution of problems of elasticity by the framework method. *Journal of Applied Mechanics*, 4:169–175, 1941.

[4] R. Courant. Variational methods for the solution of problems of equilibrium and vibrations. *Bulletin of the American Mathematical Society*, 49(1):1–23, 1943.

[5] J.K. Paik, J.K. Seo, and D.M. Kim. Idealized structural unit method and its application to progressive hull girder collapse analysis of ships. *Ships and Offshore Structures*, 1(3):235–247, 2006.

[6] J. Jelovica. *Global buckling response of web-core steel sandwich plates influenced by general corrosion*. Doctoral thesis, School of Engineering, 2014.

[7] D. Quinn, A. Murphy, and C. Glazebrook. Aerospace stiffened panel initial sizing with novel skin sub-stiffening features. *International Journal of Structural Stability and Dynamics*, 12(5):1250060, 2012.

[8] J.K. Paik and B.J. Kim. Ultimate strength formulations for stiffened panels under combined axial load, in-plane bending and lateral pressure: a benchmark study. *Thin-Walled Structures*, 40(1):45–83, 2002.

[9] D.G. Stamatelos, G.N. Labeas, and K.I. Tserpes. Analytical calculation of local buckling and post-buckling behavior of isotropic and orthotropic stiffened panels. *Thin-Walled Structures*, 49(3):422–430, 2011.

[10] M. Shama. *Torsion and shear stresses in ships*. Springer Berlin Heidelberg, 2010.

[11] J.K. Paik. *Large-deflection and ultimate strength behavior of stiffened panels and grillages*. John Wiley Sons, Ltd, 2018.

[12] J. Caldwell. Ultimate longitudinal strength. *Trans RINA*, 10:411–430, 1965.

[13] J.K. Paik and A.E. Mansour. A simple formulation for predicting the ultimate strength of ships. *Journal of Marine Science and Technology*, 1:52–62, 1995.

[14] C.S. Smith. Influence of local compressive failure on ultimate longitudinal strength of a ship's hull. In *Proceedings of the International Symposium on Practical Design in Shipbuilding (PRADS), Tokyo, Japan*, 1977.

[15] A. Bayatfar, B.J. Kim, C.P. Chen, D. Wang, J. Boulares, J.M. Gordo, L. Josefson, M. Smith, P. Kaeding, P. Jensen, R. Ojeda, S. Benson, S. Vhanmane, S. Zhang, X. Jiang, and X. Qian. Report of ISSC 2015 Committee III. 1 Ultimate Strength. In *The 19th International Ship and Offshore Structures Congress*, 2015.

[16] Z. Pei, K. Iijima, M. Fujikubo, S. Tanaka, S. Okazawa, and T. Yao. Simulation on progressive collapse behaviour of whole ship model under extreme waves using idealized structural unit method. *Marine Structures*, 40:104–133, 2015.

[17] K. Masaoka. A rectangular plate element for ultimate strength analysis. In *Proceedings of the 2nd International Conference Thin-Walled Structures*, 1977.

[18] T. Lindemann and P. Kaeding. Application of the idealized structural unit method for ultimate strength analyses of stiffened plate structures. *Ship Technology Research*, 64(1):15–29, 2017.

[19] M. Fujikubo, P. Kaeding, D. Olaru, and Z. Pei. Development of ISUM plate element considering lateral pressure effects and its application to stiffened plate. In *Transactions of The West-Japan Society of Naval Architects The 109th West-Japan Society of Naval Architects Meeting (Joint Autumn Meeting of Three Societies of Naval Architects*, 2005.

[20] D.K. Kim, H.B. Kim, M.H. Mohd, and J.K. Paik. Comparison of residual strength-grounding damage index diagrams for tankers produced by the ALPS/HULL ISFEM and design formula method. *International Journal of Naval Architecture and Ocean Engineering*, 5(1):47–61, 2013.

[21] S. Benson, J. Downes, and R.S. Dow. Compartment level progressive collapse analysis of lightweight ship structures. *Marine Structures*, 31:44–62, 2013.

[22] M. Tekgoz, Y. Garbatov, and C.G. Soares. Strength assessment of an intact and damaged container ship subjected to asymmetrical bending loadings. *Marine Structures*, 58:172–198, 2018.

[23] T. Yoshikawa, A. Bayatfar, B.J. Kim, C.P. Chen, D. Wang, J. Boulares, J.M. Gordo, L. Josefson, M. Smith, and P. Kaeding. Report of ISSC 2015 Committee III. 1 Ultimate Strength. In *The 19th International Ship and Offshore Structures Congress*, 2015.

[24] M.E. Alfred, S.D. Benson, S.E. Hirdaris, and R.S. Dow. Design safety margin of a 10,000 TEU container ship through ultimate hull girder load combination analysis. *Marine Structures*, 46:78–101, 2016.

[25] F. Romano, F. Di Caprio, B. Auriemma, and U. Mercurio. Numerical investigation on the failure phenomena of stiffened composite panels in post-buckling regime with discrete damages. *Engineering Failure Analysis*, 56:116–130, 2015.

[26] X. Kong, Y. Yang, J. Gan, T. Yuan, L. Ao, and W. Wu. Experimental and numerical investigation on the detailed buckling process of similar stiffened panels subjected to in-plane compressive load. *Thin-Walled Structures*, 148, 2020.

[27] J. Slota, A. Kubit, T. Trzepieciński, B. Krasowski, and J. Varga. Ultimate load-carrying ability of rib-stiffened 2024-T3 and 7075-T6 aluminium alloy panels under axial compression. *Materials 2021, Vol. 14, Page 1176*, 14(5):1176, 2021.

[28] J.S. Gui and W.G. Da. Ultimate strength of u-type stiffened panels for hatch covers used in ship cargo holds. *Ships and Offshore Structures*, 16(3):280–291, 2020.

[29] D.K. Kim, H.L. Lim, and S.Y. Yu. Ultimate strength prediction of T-bar stiffened panel under longitudinal compression by data processing: A refined empirical formulation. *Ocean Engineering*, 192, 2019.

[30] J. Loughlan and N. Hussain. The in-plane shear failure of transversely stiffened thin plates. *Thin-Walled Structures*, 81:225–235, 2014.

[31] L. Pavlovčič, A. Detzel, U. Kuhlmann, and D. Beg. Shear resistance of longitudinally stiffened panels-part 1: Tests and numerical analysis of imperfections. *Journal of Constructional Steel Research*, 63(3):337–350, 2007.

[32] L. Pavlovčič, D. Beg, and U. Kuhlmann. Shear resistance of longitudinally stiffened panels-part 2: Numerical parametric study. *Journal of Constructional Steel Research*, 63(3):351–364, 2007.

[33] Y. Su, Z. Guan, X. Wang, Z. Li, J. Guo, and Y. Huang. Buckling and post-buckling behavior of titanium alloy stiffened panels under shear load. *Chinese Journal of Aeronautics*, 32(3):619–626, 2019.

[34] F. Wang, J.K. Paik, B.J. Kim, W. Cui, T. Hayat, and B. Ahmad. Ultimate shear strength of intact and cracked stiffened panels. *Thin-Walled Structures*, 88:48–57, 2015.

[35] J.N. Reddy. *Mechanics of laminated composite plates and shells*. CRC Press, 2003.

[36] J. Romanoff and P. Varsta. Bending response of web-core sandwich plates. *Composite Structures*, 81(2):292–302, 2007.

[37] J. Romanoff and A. Klanac. Design optimization of steel sandwich hoistable car decks applying homogenized plate theory. *Journal of Ship Production*, 24(02):108–115, 2008.

[38] J. Romanoff. Optimization of web-core steel sandwich decks at concept design stage using envelope surface for stress assessment. *Engineering Structures*, 66:1–9, 2014.

[39] E. Avi, I. Lillemäe, J. Romanoff, and A. Niemelä. Equivalent shell element for ship structural design. *Ships and Offshore Structures*, 10(3):239–255, 2015.

[40] M. Metsälä, B.R. Gonçalves, J. Romanoff, and J. Jelovica. Geometrically nonlinear bending response of a ship-like box girder using an enhanced single-layer theory. In C.G. Soares and Y. Garbatov, editors, *Progress in the Analysis and Design of Marine Structures-Proceedings of the 6th International Conference on Marine Structures, MARSTRUCT 2017*, 2017.

[41] T. Nordstrand. On buckling loads for edge-loaded orthotropic plates including transverse shear. *Composite Structures*, 65(1):1–6, 2004.

[42] T.S. Lok and Q.H. Cheng. Free vibration of clamped orthotropic sandwich panel. *Journal of Sound and Vibration*, 229(2):311–327, 2000.

[43] J. Jelovica, J. Romanoff, S. Ehlers, and P. Varsta. Influence of weld stiffness on buckling strength of laser-welded web-core sandwich plates. *Journal of Constructional Steel Research*, 77:12–18, 2012.

[44] J. Jelovica, J. Romanoff, and R. Klein. Eigenfrequency analyses of laser-welded web-core sandwich panels. *Thin-Walled Structures*, 101:120–128, 2016.

[45] J. Jelovica and J. Romanoff. Load-carrying behaviour of web-core sandwich plates in compression. *Thin-Walled Structures*, 73:264–272, 2013.

[46] B.R. Goncalves, J. Jelovica, and J. Romanoff. A homogenization method for geometric nonlinear analysis of sandwich structures with initial imperfections. *International Journal of Solids and Structures*, 87:194–205, 2016.

[47] M. Kõrgesaar, B.R. Goncalves, J. Romanoff, and H. Remes. Non-linear effective properties for web-core steel sandwich panels in tension. *International Journal of Mechanical Sciences*, 115:428–437, 2016.

[48] J. Romanoff, J. Jelovica, J.N. Reddy, and H. Remes. Post-buckling of web-core sandwich plates based on classical continuum mechanics: success and needs for non-classical formulations. *Meccanica*, 2020.

[49] T. Yao and M. Fujikubo. *Initial imperfections due to welding*. Butterworth-Heinemann, 2016.

[50] M. Kaminski, P. Rigo, S. Estefen, N. Pegg, Y. Chen, J. Pradillon, P. Kaeding, M. Samuelides, S. Ferraris, M. Fujikubo, R. Torhaug, C.G. Soares, Y.S. Choo, J.K. Paik, A. Shenoi, and X. Wang. Report of ISSC 2018 Committee III. 1 Ultimate Strength. In *The 20th International Ship and Offshore Structures Congress*, 2018.
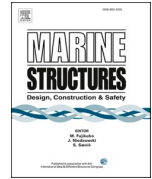
Appendix 1

I

T. Putranto, M. Kõrgesaar, J. Jelovica, K. Tabri, and H. Naar. Ultimate strength assessment of stiffened panel under uni-axial compression with non-linear equivalent single layer approach, *Marine Structures*, 78:103004, 2021

Ultimate strength assessment of stiffened panel under uni-axial compression with non-linear equivalent single layer approach

Teguh Putranto [a,b,*], Mihkel Kõrgesaar [a], Jasmin Jelovica [c], Kristjan Tabri [b], Hendrik Naar [b]

[a] *Estonian Maritime Academy, Tallinn University of Technology, Tallinna 19, 93819, Kuressaare, Estonia*
[b] *Department of Civil Engineering and Architecture, School of Engineering, Tallinn University of Technology, Ehitajate tee 5, 19086, Tallinn, Estonia*
[c] *Departments of Mechanical Engineering and Civil Engineering, The University of British Columbia, 6250 Applied Science Lane, V6T 1Z4, Vancouver, Canada*

ABSTRACT

Steel stiffened panels are widely used in engineering design and construction. However, numerical modeling and analysis effort for a three-dimensional (3D) stiffened panel may be notable, especially for the ultimate limit state of ship structures. Therefore, a homogenization method is outlined that transforms 3D stiffened panel into an Equivalent Single Layer (ESL) concerning the same mechanical behavior. ESL stiffnesses are obtained with a unit cell analyses based on stiffened panel where periodicity is imposed with boundary conditions based on a first-order shear deformation theory (FSDT). Stiffnesses were determined from the first derivative of a membrane force and bending moment obtained with numerical simulations. The effect of initial imperfection shape was included in the analysis to account for local and global buckling behavior. ESL with non-linear stiffness was implemented in Abaqus UGENS subroutine, allowing incremental evaluation of stiffness. Ultimate strength prediction of a steel grillage model with ESL finite element analysis was in excellent agreement with detailed 3D FEM analysis. The key in this analysis was consideration of non-linear ESL stiffness as linear analysis was unable to detect the point where ultimate strength capacity of the grillage was reached.

1. Introduction

Stiffened panels are composed of the plate and attached "stiffeners" that give the plate sufficient strength and rigidity to carry in-plane and out-of-plane loads. Although all-steel structural core sandwich panels are gaining popularity because of their better weight to stiffness ratio, the widespread use as load-carrying elements in ship structures is still somewhat limited because of different issues, such as integration with the rest of the structure and fatigue sensitivity of the joints [1]. Therefore, there is still an interest in marine, civil, and aerospace industries to utilize the advantages of the stiffened panels in optimizing the weight of structures [2]. Stiffened panels are the main constructional element in ship hull girders providing resistance to sagging and hogging for longitudinal strength. However, traditional finite element (FE) modeling of stiffened structures is time-consuming because all the structural elements are modeled explicitly. This is prohibitively expensive (time & cost) in the conceptual/preliminary design framework aiming to deliver stakeholders a *holistic* design that entails computer-aided generation, exploration, and selection of optimal designs [3].

---

* Corresponding author. Estonian Maritime Academy, Tallinn University of Technology, Tallinna 19, 93819, Kuressaare, Estonia.
E-mail address: teguh.putranto@taltech.ee (T. Putranto).

In ship structural ultimate limit state (ULS) analysis, different methods exist for fast calculation of global hull girder and/or local panel strength. The development of these approaches has been dictated by the rule compliance requirements and certain load cases [4]. Notably, classification societies generally consider only the 2D cross-sectional arrangement in ULS definition. The latter notion is probably the reason why purpose-built ALPS/HULL tool [5,6] for ULS assessment of global hull strength is applicable for a single cross-section rather than the entire hull girder. Moreover, this and other computational tools for ULS assessment are often purpose-built software for an in-house user base, which restricts their widespread application and community based on future developments. One example is the progressive collapse program (PROCOLL) of Benson et al. [7], which estimates the ultimate strength based on cross-sectional element's load-shortening curves. The method extends well established idealized structural unit method (ISUM) [8,9] by accounting for overall buckling modes between bulkheads or other discontinuous transverse structures instead of only interframe buckling, see Ref. [10]. Another example is the coupled beam method developed by Naar et al. [11] for ULS assessment of large passenger ships, where ship structure is represented with longitudinal and vertical beams coupled together using non-linear springs. The latter method has been recently updated to account ultimate strength of hull girder with grounding damage [12]. Therefore, there is a definite potential for a computer-aided design tool that is implemented in the commercial software enabling computationally efficient ULS assessment of ship hull girder.

The purpose of the present study is to provide the first building block for such a tool. Thereby, a method is presented for stiffened panel ultimate strength assessment using equivalent single layer (ESL) theory. In this approach stiffeners with attached plating are represented by an appropriate stiffness matrices in ESL framework and modeled with traditional shell elements, while primary structural members (e.g., webframes) are modeled explicitly. Such a method is implemented in a commercial code and is efficient without sacrificing much the accuracy while being accessible to a wide range of users through the open-source distribution of the developed method.

1.1. ESL models for ship and other structures

Equivalent single layer theory is a generalization of mathematical models that started with Kirchoff-Love plate theory and Euler-Bernoulli beam theory. Many books are dedicated to these topics; Reddy [13] presents the foundation of the theories, generalizes them concerning transverse shear deformation, and shows applications to several engineering problems. The idea is to replace a complex, discrete material distribution within a plate or a panel with a homogenized continuum by modeling the stiffness correctly. Several studies over the last few decades involved ESL for bending, buckling, and vibration response of, primarily, composite structures. A review of the applications to sandwich panels in the early days can be found in Noor et al. [14]. More recently, the method has been used to model sandwich panels with discrete plates in the core [15]. The approach reduces the computational and analysis pre-processing time and thus, can be effectively coupled with optimization frameworks [16,17] to provide holistic designs already in the conceptual design stage.

Moreover, the application of ESL theory is not limited to sandwich panels. Avi et al. [18] used the equivalent single layer method to obtain homogenized stiffness properties of stiffened panels in the linear range. An obtained equivalent plate element was subsequently used to assess ship global and local static and vibration response. However, the review by Romanoff et al. [19] calls for more advanced analysis related to ESL to strengthen and extend the theory for its widespread application.

The homogenization scheme transforms the 3D stiffened panel model to the ESL model with the same stiffness. This is achieved by involving the linear and non-linear stiffness matrix in the definition of ESL. The linear stiffness matrix has been used in the orthotropic material modeling of ship-like box girder and ship side shell to study structural response under global and local bending loads [18,20]. ESL was used to predict linear buckling of corrugated cardboard panels [21] and vibration of truss-core sandwich panels [22]. Furthermore, it was used as an alternative to 3D shell modeling to analyze the effect of production quality on linear buckling and vibration of sandwich panels, see Jelovica et al. [23] and Jelovica et al. [24], respectively. These studies did not consider the non-linear stiffness matrix during simulation since the emphasis was on the linear response. The linear part of the ESL stiffness matrix can be defined directly in the Abaqus software. To account for non-linearity, UGENS subroutine in the Abaqus must be used. This UGENS based approach has been shown to be effective in non-linear mechanical behavior analyses of sandwich panels under compression [25] or tension [26] loads. Apparently, with the non-linear ESL stiffness matrix, the change in stiffness throughout deformation can be considered, resulting in a better overall response prediction.

While the above studies have amply demonstrated the advantages of ESL homogenization for the analysis of sandwich panels that are symmetric in the thickness direction, the extensions of this method for asymmetric (in the thickness direction) stiffened panels are missing. The asymmetry amplifies the coupling between axial and bending response, which needs appropriate consideration. Therefore, this study focuses on the load-carrying behavior analysis of stiffened panels with the ESL under the uni-axial compression load. The challenge and novelty in this development are in the determination of progressively changing stiffness matrices for stiffened panels that, as opposed to sandwich panels, are asymmetric in thickness direction. Furthermore, compared to earlier studies, we account for the material non-linearity in the ESL framework, which is shown to have a strong influence on the panel response. This way, the paper extends the works of Goncalves et al. [25] and Jelovica and Romanoff [27] to the analysis of stiffened panels.

The outline of the paper is the following. First, we define periodic boundary conditions for a unit cell composed of a plate and a single stiffener that acts as a basic building block of the stiffened panel. Thereby, this unit cell is used to transform the detailed 3D FEM of stiffened panel into the single layer. The buckling response of the unit cell is analyzed with respect to unit cell size ratio and elastoplastic material properties. These analyses provide the stiffness matrix for the definition of ESL and guide the definition of unit cell size and initial imperfections. In Section 4, a 3 × 3 m stiffened panel was analyzed with the detailed 3D FEM approach. The response was compared with the ESL estimate that provided general validation for the homogenization approach. In Section 5, the

ultimate strength of a stiffened grillage representative of an actual ship structure was modeled with 3D FEM and ESL approach. In this part, ESL was only used to replace plates with longitudinal stiffeners while larger structural stiffening members (girders and web-frames) were modeled explicitly. Results show that ESL based approach can capture the ultimate strength with high accuracy.

2. The equivalent single layer (ESL) approach for stiffened panels

2.1. Shell kinematics and constitutive equations

Stiffened panels with the plate, web, and flange are here considered as a subclass of a laminate plate following shell kinematics, for which the ESL theory was initially developed. The shell kinematics and constitutive equations for such an element are explained in the following.

With the same assumption and restriction introduced by the classical laminate theory, the displacement field of first-order shear deformation theory (FSDT) is defined with Equations (1)–(3). From these equations, it is known that the displacement component is composed of two parts, i.e., extensional (u^0, v^0, w^0) and bending (φ_1, φ_2, φ_3) responses.

$$u = u^0 + x_3 \varphi_1 \tag{1}$$

$$v = v^0 + x_3 \varphi_2 \tag{2}$$

$$w = w^0 + x_3 \varphi_3 \tag{3}$$

FSDT assumes that the plate thickness does not change during deformation, thus

$$\varphi_3 = \frac{\partial w}{\partial x_3} = 0 \tag{4}$$

As shown in Fig. 1, the point p moves in x_1 direction because of the extensional and bending responses. Under bending, transverse normals of the deformed shell do not remain perpendicular to the midplane. The strains (ε_{11}, ε_{22}, γ_{12}) are linear through the laminated thickness, and the transverse shear strains (γ_{13}, γ_{23}) are constant in the first-order laminated theory. Therefore, the non-linear strain field can be expressed by Equation (5).

$$
\begin{bmatrix} \varepsilon_{11} \\ \varepsilon_{22} \\ \gamma_{12} \\ \gamma_{13} \\ \gamma_{23} \end{bmatrix} =
\begin{bmatrix} \varepsilon_{11}^{(0)} \\ \varepsilon_{22}^{(0)} \\ \gamma_{12}^{(0)} \\ \gamma_{13}^{(0)} \\ \gamma_{23}^{(0)} \end{bmatrix} + x_3
\begin{bmatrix} \varepsilon_{11}^{(1)} \\ \varepsilon_{22}^{(1)} \\ \gamma_{12}^{(1)} \\ \gamma_{13}^{(1)} \\ \gamma_{23}^{(1)} \end{bmatrix} =
\begin{bmatrix} \dfrac{\partial u^0}{\partial x_1} + \dfrac{1}{2}\left(\dfrac{\partial w^0}{\partial x_1}\right)^2 \\[2mm] \dfrac{\partial v^0}{\partial x_2} + \dfrac{1}{2}\left(\dfrac{\partial w^0}{\partial x_2}\right)^2 \\[2mm] \dfrac{\partial u^0}{\partial x_2} + \dfrac{\partial v^0}{\partial x_1} + \dfrac{\partial w^0}{\partial x_1}\dfrac{\partial w^0}{\partial x_2} \\[2mm] \dfrac{\partial w^0}{\partial x_1} + \varphi_1 \\[2mm] \dfrac{\partial w^0}{\partial x_2} + \varphi_2 \end{bmatrix} + x_3
\begin{bmatrix} \dfrac{\partial \varphi_1}{\partial x_1} \\[2mm] \dfrac{\partial \varphi_2}{\partial x_2} \\[2mm] \dfrac{\partial \varphi_1}{\partial x_2} + \dfrac{\partial \varphi_2}{\partial x_1} \\[2mm] 0 \\[2mm] 0 \end{bmatrix} \tag{5}
$$

where

$$\varphi_1 = \frac{\partial u}{\partial x_3}, \varphi_2 = \frac{\partial v}{\partial x_3} \tag{6}$$

In Equation (7) the superscript $^{(0)}$ and $^{(1)}$ indicate membrane and bending strains, respectively. Strains include von Karman non-linearity, which allows moderate rotations of the shell, important for the post-buckling response. In the shell constitutive behavior, the stiffness of the plate is due to the extension (A_{ij}), bending (D_{ij}), coupling of extension caused by bending (B_{ij}), and coupling of bending caused by extension (C_{ij}). The plate stiffness is expressed by the relation of membrane force (N_{ij}), bending moment (M_{ij}), and strain (ε_{ij},
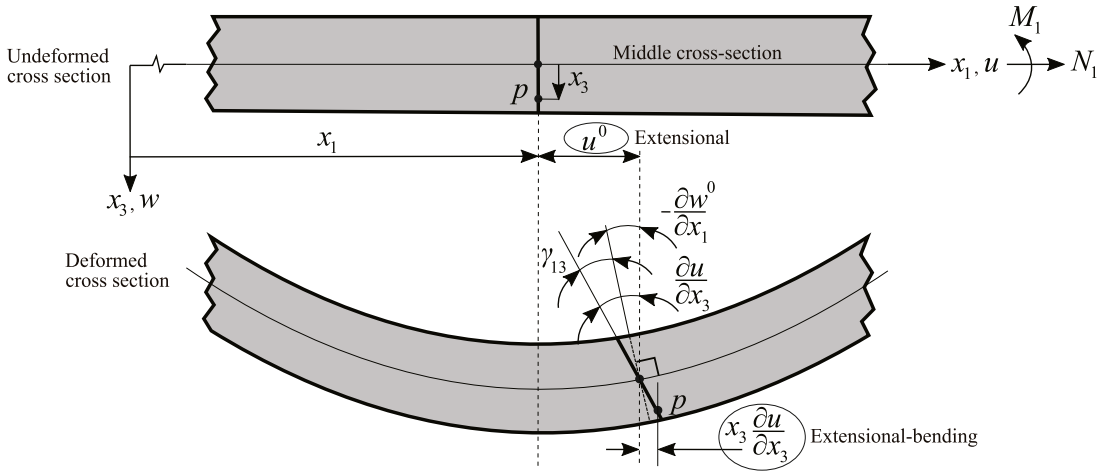
Fig. 1. Shell kinematic of deformation behavior in the first-order shear deformation theory.

$$
\begin{bmatrix} N_{11} \\ N_{22} \\ N_{12} \\ M_{11} \\ M_{22} \\ M_{12} \end{bmatrix} = \begin{bmatrix} A_{11} & A_{12} & 0 & B_{11} & B_{12} & 0 \\ A_{21} & A_{22} & 0 & B_{21} & B_{22} & 0 \\ 0 & 0 & A_{33} & 0 & 0 & B_{33} \\ C_{11} & C_{12} & 0 & D_{11} & D_{12} & 0 \\ C_{21} & C_{22} & 0 & D_{21} & D_{22} & 0 \\ 0 & 0 & C_{33} & 0 & 0 & D_{33} \end{bmatrix} \begin{bmatrix} \varepsilon_{11}^{(0)} \\ \varepsilon_{22}^{(0)} \\ \gamma_{12}^{(0)} \\ \varepsilon_{11}^{(1)} \\ \varepsilon_{22}^{(1)} \\ \gamma_{12}^{(1)} \end{bmatrix} \tag{7}
$$

γ_{ij}), as shown in Equation (7).

The transverse shear force is given by Equation (8).

$$
\begin{bmatrix} Q_1 \\ Q_2 \end{bmatrix} = \begin{bmatrix} D_{Q1} & 0 \\ 0 & D_{Q2} \end{bmatrix} \begin{bmatrix} \gamma_{13} \\ \gamma_{23} \end{bmatrix} \tag{8}
$$

where D_{Q1} and D_{Q2} are the transverse shear stiffnesses of the ESL in the stiffener direction and transverse to the stiffener, as shown in Fig. 2, respectively. These variables are calculated by using Equations 9 and 10 as in Avi et al. [18].

$$
D_{Q1} = k_{13} \left(G_p t_p + G_w h_w + G_f h_f \right) \tag{9}
$$

$$
D_{Q2} = k_{23} G_p t_p \tag{10}
$$

where t_p is the plate thickness, h_w is the web height and t_f is the flange thickness. It is clear from Equation (9) that stiffener height gives majority of the transverse shear stiffness in direction 1. The shear moduli of the web G_w and flange G_f are a function of the plate G_p and calculated as follows.
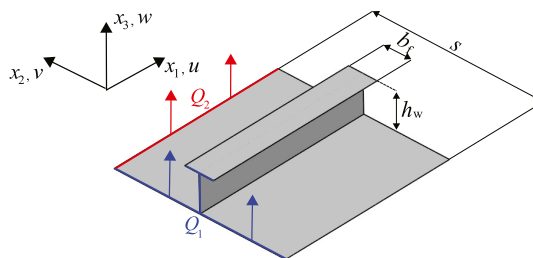

Fig. 2. Definition of transverse shear forces in the stiffened panel.

$$G_w = G_p \frac{t_w}{s} \tag{11}$$

$$G_f = G_p \frac{b_f}{s} \tag{12}$$

where t_w is the thickness of the web stiffener, b_f is the flange length and s is the stiffener spacing. For stiffened panel, longitudinal k_{13} and transverse k_{23} shear correction factors are calculated as follows:

$$k_{23} = \frac{5}{6} \tag{13}$$

$$k_{13} = \frac{\tau_{13(avg)}}{\tau_{13(max)}} \tag{14}$$

The average shear stress is calculated by dividing the shear force to the effective shear area:

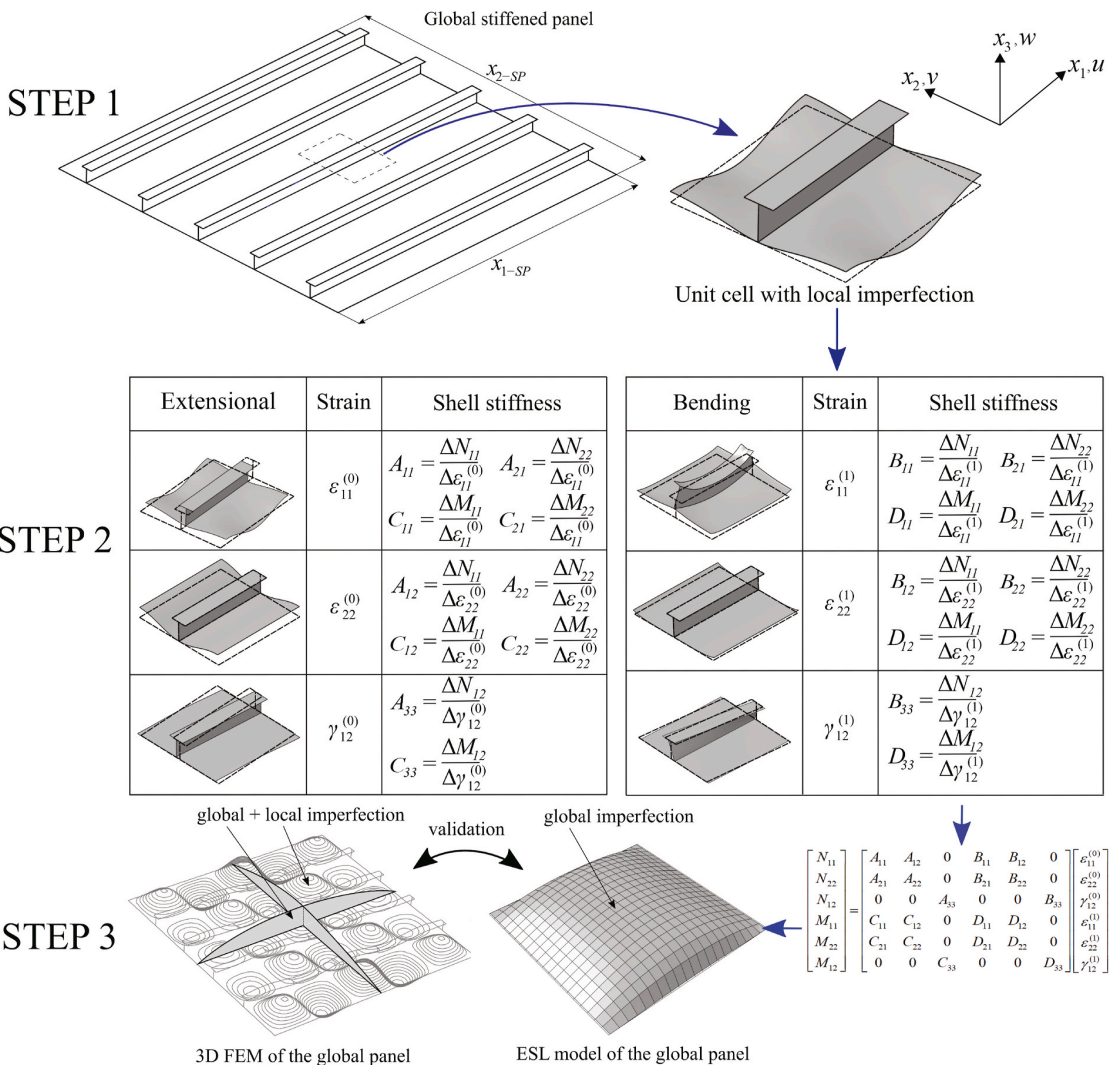$$\tau_{13(avg)} \approx \frac{Q_{x_3}}{A_w + t_w t_p + t_w h_f} \tag{15}$$

Fig. 3. Flowchart of the ESL approach.

where A_w is the cross-sectional area of the stiffener web. Finally, we can calculate the maximum shear stress:

$$\tau_{13(max)} \approx \frac{Q_{x_3}\left(A_p\left(2x_{3,NA} - t_p\right) + t_w\left(x_{3,NA} - t_p\right)^2\right)}{2I_{x_3}t_w} \tag{16}$$

where $x_{3,NA}$ is the neutral axis and I_{x_3} is the second moment of area of the plate-stiffener combination, respectively. Because of the large deformations and buckling, the location of the neutral axis changes. For this reason, in the following we refer to a neutral axis as the reference axis. However, according to the FSDT the position of neutral axis is not updated during the calculations and thus, the updated neutral axis location is also not considered in UGENS subroutine. Furthermore, it is worth mentioning that transverse shear stiffnesses remain constant during the analysis. The reason is that UGENS subroutine accepts only constant transverse shear stiffness values. This limitation could be bypassed by a complete new element definition using user-defined element (UEL) subroutine, which would provide freedom in defining the characteristics of an element, but would also be more challenging to implement. Nonetheless, UGENS capabilities to predict the post-buckling response were showcased in Goncalves et al. [28] on a sandwich panel which is very sensitive to any variation of the transverse shear stiffness. As D_{Q2} was approximated as constant there during progressive failure, it justifies using the same approach for the current analysis of stiffened panels.

2.2. Transition between scales

Micromechanics is the study of composite material considering the mechanical behavior in the microstructure level. In micromechanics, the concept of a unit cell, also known as a representative volume element, is used as a basic building block of the whole structure. We employ mainly the same concept, however in our case the "microstructure" is the plate with a stiffener, which can later be used to homogenize the entire grillage where larger structural components (girders and webframes) are still modeled explicitly. A unit cell analysis in Section 3.1 provides the average extensional, bending and shear stiffness coefficients used to define the non-linear stiffness of the ESL model. Thereby, the ESL approach adopted in this paper follows these steps represented in the flowchart in Fig. 3:

1. Definition of the unit cell model and its characteristics (material definitions, geometrical imperfections, size).
2. Definition of periodic boundary conditions.
3. Response analysis of unit cell models generated at Step 1. Definition of stress resultant vs. strain relations.
4. Composition of non-linear stiffness matrix for macroscale ESL analysis.

2.3. Initial imperfections

It is well known that initial imperfections affect the buckling response of the stiffened panels [29]. To account this, local imperfections are considered in the unit cell analysis, while global imperfections are superimposed later in the actual global panel analysis. These local imperfections of the unit cells correspond to the first eigenmode obtained with each of the boundary conditions given in Section 3.2. Thereby, stiffness matrix of the ESL accounts for the local imperfections. The global imperfection is the deformation shape
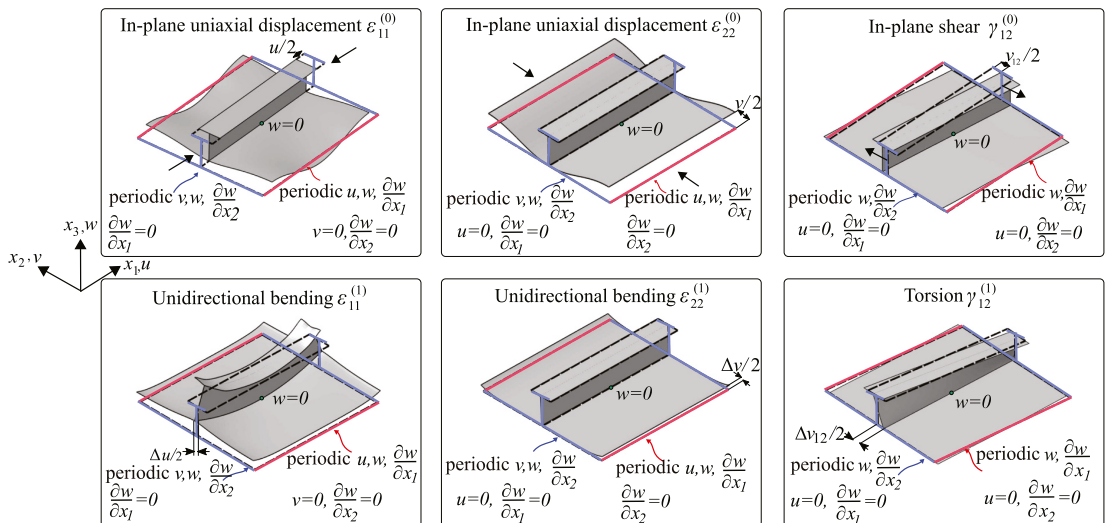

Fig. 4. Unit cell displacement boundary condition on the strain definitions of the FSDT.

of the entire panel corresponding to the first eigenmode. This first eigenmode is obtained for both, detailed 3D FEM and reduced ESL model. The eigenmodes are scaled by imperfection scale factor as explained in Section 3.3.1 to obtain different level of imperfection.

We note in passing, that while the scope of unit cell analysis in present paper is limited to initial imperfections, it is not by any means exhaustive of ESL capabilities. The analyst could choose the specifics of unit cell according to desired needs, obtain the stiffness properties and transfer those to UGENS subroutine that is a basis for ESL framework. For instance, the unit cell analysis could account for the effect of initial stiffener deflections or initial pre-stress in the structural members.

3. Unit cell analysis

3.1. Definition of the unit cell

Following the steps defined in the flowchart in Fig. 3, unit cell of a stiffened panel is composed of a plate and a longitudinal stiffener. The shape of a unit cell is a rectangular cuboid where width is fixed to the stiffener spacing, but length is varied to study the effect of unit cell size. Such definition of the size expedites the adoption of unit cell later in macroscale analysis. In other words, the unit cell becomes a discretization element combining plate and stiffener in grillage or hull girder analysis. Similarly to Goncalves et al. [25], the unit cell is modeled with shell elements (S4R) in Abaqus element library to reduce the computational effort. For compatibility with shell element macroscale analysis, plane stress is assumed to prevail in the unit cells.

3.2. Relations between the displacements and internal forces

The second step of the methodology, as shown in Fig. 3, involves the definition of the boundary conditions. Fig. 4 explains the boundary conditions used in the unit cell of the stiffened panel. Boundary conditions are defined to ensure compatibility with the kinematics of the FSDT. According to FSDT, the deformation is decomposed to the membrane and bending types as indicated in Fig. 4, which leads to 6 different boundary conditions: two uniaxial deformations in the different direction ($\varepsilon_{11}^{(0)}, \varepsilon_{22}^{(0)}$), shear ($\gamma_{12}^{(0)}$), two uni-directional rotations in the different directions ($\varepsilon_{11}^{(1)}, \varepsilon_{22}^{(1)}$), and torsion ($\gamma_{12}^{(1)}$). Therefore, displacements and constraints are enforced so that they are always symmetric along the parallel faces. In Fig. 4 this symmetry is highlighted either with red or blue color. As a result, the boundary condition is either simple translational (u, v, w) or rotational (u', v', w') fixture or it is periodic. Zero translation of the unloaded edge perpendicular to loading direction leads to a plane strain state. The periodic boundary condition is achieved in the numerical model with an equation constraint (Abaqus) to ensure displacement compatibility along the parallel edges. The out-of-plane translation w in a single node middle of the plate below the stiffener is constrained to restrain the vertical movement of the unit cell (Fig. 4). This also ensured that no rigid-body modes appeared during a simulation. For bending and torsion cases, imposed displacement varies linearly from the flange to the plate with the zero value at the neutral axis.

The third step of the methodology, as shown in Fig. 3, involves the calculation of internal force and moment resultants. The resultant force (F_1, F_2, F_{12}) and moment ($F_1 x_{3,NA}, F_2 x_{3,NA}, F_{12} x_{3,NA}$) are calculated from the respective force components measured on the unit cell edges. Therefore, free body cut in Abaqus is defined that is composed of plate, web, and flange edges for x_2-x_3 plane, and plate edge for x_1-x_3 plane (Fig. 5). The resultant moments are obtained by defining the reference axis location in the free-body cut definition over which forces are summed. These procedures are performed only on one opposing cross-section edge, assuming that the response is symmetric. These resultant force and moment are then divided by the unit cell length to obtain shell equivalent membrane force (N_{ij}) and bending moment (M_{ij}), respectively, as shown in Equation 17–22. The strains are calculated from the division of displacement or curvature (as shown in Fig. 4) by initial length (L_1, L_2, as shown in Fig. 5).

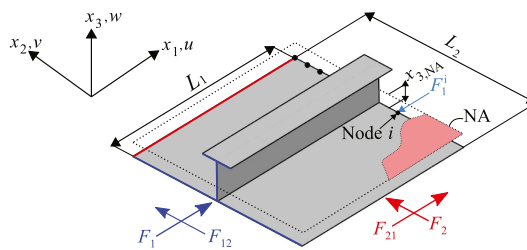$$N_{11} = \frac{\sum_{i=1}^{n} F_1^i}{L_2} \quad \varepsilon_{11}^{(0)} = \frac{u}{L_1} \tag{17}$$

Fig. 5. Schematic of force and moment extractions from the unit cell. The location of free-body cuts defined in the post-processing stage are highlighted in color. For simplicity F_1 is shown only for loading in x_1 direction. (For interpretation of the references to color in this figure legend, the reader is referred to the Web version of this article.)

$$N_{22} = \frac{\sum_{i=1}^{n} F_2^i}{L_1} \quad \varepsilon_{22}^{(0)} = \frac{v}{L_2} \tag{18}$$

$$N_{12} = \frac{\sum_{i=1}^{n} F_{12}^i}{L_2} \quad \gamma_{12}^{(0)} = \frac{v_{12}}{L_2} \tag{19}$$

$$M_{11} = \frac{\sum_{i=1}^{n} F_1^i x_{3,NA}^i}{L_2} \quad \varepsilon_{11}^{(1)} = \frac{\Delta u}{L_1 x_{3,NA}} \tag{20}$$

$$M_{22} = \frac{\sum_{i=1}^{n} F_2^i x_{3,NA}^i}{L_1} \quad \varepsilon_{22}^{(1)} = \frac{\Delta v}{L_2 x_{3,NA}} \tag{21}$$

$$M_{12} = \frac{\sum_{i=1}^{n} F_{12}^i x_{3,NA}^i}{L_2} \quad \gamma_{12}^{(1)} = \frac{\Delta v_{12}}{L_2 x_{3,NA}} \tag{22}$$

3.3. Parametric study

A parametric study is performed to get a better understanding of the response of the unit cell considering variability in initial imperfections, unit cell sizes, and material non-linearity. Three unit cell configurations consisting of plate and attached T-profiled stiffener are considered in the following, see Table 1. The first two unit cells have different plate thickness to determine the effect of local plate buckling on the response. In the third unit cell (UC3) stiffener slenderness is significantly reduced compared to UC2 by increasing the web height, while still satisfying the DNV GL buckling requirement $t_w \geq h_w/C_w \sqrt{R_{eH}/235}$ [30]. The objective is to promote interaction between buckling modes in the unit cell level (stiffener buckling vs local plate buckling) and determine whether the ESL framework can capture the 3D response across the variability considered. The ESL analyses with stiffened panels are presented in Section 4.

In all unit cells structural steel elastoplastic material properties were used with yield stress of $\sigma_y = 355$ MPa, elastic modulus of $E = 210$ GPa, and poisson ratio of $\upsilon = 0.3$. Numerical simulations were performed with Abaqus/Standard. The analysis type for all simulations was the modified Riks static method, which determines the static equilibrium state for force and moment during the unstable stage of the response. The square-shaped elements in the simulation had 15 mm edge length, which was deemed sufficient based on the convergence analysis performed with 7.5 mm elements.

3.3.1. Effect of initial imperfections

The inclusion of initial imperfections prevents sudden bifurcation-type buckling and guarantees the stability of the numerical solution and monotonic increase in strain energy with load increase [25,29]. As explained in Section 2.3, eigenmode analyses are performed with each of the boundary conditions to obtain the initial imperfection shape. Analysis procedure type is the linear buckling analysis. We emphasize that the eigenmode shapes are used here for the sake of simplicity as a numerical trick to trigger local buckling. If analyst wants to account the effect of actual measured imperfections on local buckling, such imperfections should be represented in the unit cell level. In contrast, if the aim is to account actual measured global imperfections as in Ref. [31] on the panel global response, such imperfections should be represented in the FE model discretized with ESL elements instead of considering them on the unit cell level. Thereby, the length scale over which the imperfections are averaged corresponds to the length of the finite element, independent whether the standard 3D FEM model or 2D homogenized ESL model is considered.

The obtained imperfection shape in the unit cell comprises of sinusoidally formed waves, which in the global panel level would lead to multiple waves in the panel domain. The maximum imperfection amplitude w_{max} depends on the panel slenderness β that is a function of panel geometry and the material properties [31],

$$\beta = \frac{s}{t} \sqrt{\frac{\sigma_y}{E}} \tag{23}$$

Table 1
Unit cell configurations. All units in mm.

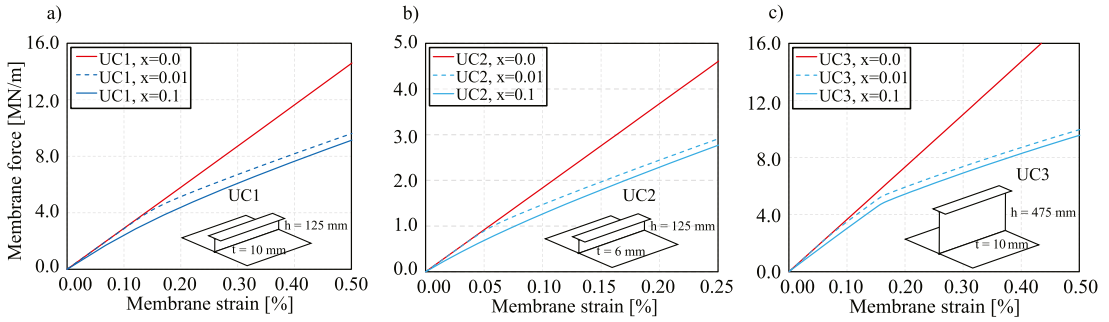|	Length × Breadth	Plate Thickness	Stiffener web Height × thickness	Stiffener flange Height × thickness	DNV GL web thickness requirement
Unit cell 1 (UC1)	600 × 600	10	125 × 7.8	100 × 4	2.03
Unit cell 2 (UC2)	600 × 600	6	125 × 7.8	100 × 4	2.03
Unit cell 3 (UC3)	600 × 600	10	475 × 7.8	100 × 4	7.73

Fig. 6. Effect of initial imperfection on the axial load for UC1 (a), UC2 (b), and UC3 (c).

$$\frac{w_{max}}{t} = x\beta^2 \qquad\qquad (24)$$

where $s = 600$ mm is the stiffener spacing, $t = 10$ mm is the plate thickness and x is the Faulkner's imperfection scale factor. Simulations were performed with three scale factors to obtain zero imperfection $x = 0$ ($w_{max} = 0$ mm), slight imperfection $x = 0.01$ ($w_{max} = 0.61$ mm) or average imperfection $x = 0.1$ ($w_{max} \approx 6$ mm). The level of imperfections and terminology used is consistent with DNV GL guidelines [30]. Analyses are performed with unit cells UC1, UC2, and UC3.

The results with three imperfection scale factors in Fig. 6 show that imperfections in the plate lead to an instability in the panel compared with analysis without imperfection. Furthermore, response shows some dependence on the imperfection level and slenderness of stiffeners. In UC3 with slender stiffener the buckling point is more pronounced compared with analyses with stocky stiffener UC1 and UC2. In UC1 buckling instability occurs approximately at the membrane strain of 0.0015. At this point the maximum equivalent stress in the simulation is 550 MPa, that agrees with the analytical estimate $N_c = k_c(\pi/s)^2 \cdot E \cdot t^2/(12(1 - v^2)) = 553$ MPa, where $k_c = 10.5$ comes from the clamped boundary condition on all edges, see Ref. [32].

3.3.2. Effect of unit cell size

The size of the unit cell affects its stiffness, since it defines the allowable number of buckling half-waves during non-linear response and the evolution of the deformation shape. At any point in the analysis, the structure is assumed to be in static equilibrium, meaning that the principle of minimum potential energy applies. Therefore strain energy of the system needs to be at minimum [13]. The strain energy corresponds to the area under the force-deflection curve. The unit cell UC1 from Table 1 was taken as a "seed" geometry that was subject to different size configurations. Analyzed unit cells had the slight initial imperfection ($x = 0.01$) and three different size configurations, namely $a/s = 1.0$, 1.33, and 2.0, where s is the stiffener spacing and a is the length of the unit cell. Therefore, stiffness is modulated by changing the length a while fixing the stiffener spacing s. The analyses are performed under uniaxial compression ($\varepsilon_{11}^{(0)}$).

During the simulation, the unit cell length reduction and forces are traced as explained in Section 3.2 and plotted in Fig. 7. While the initial stiffness is size independent, the strain energy is minimized for the $a/s = 1.0$. Curves in Fig. 7 shows how the unit cell with an aspect ratio of $a/s = 2.0$ exhibits a snap-back behavior, during which the deformation mode abruptly switches from two to four half-
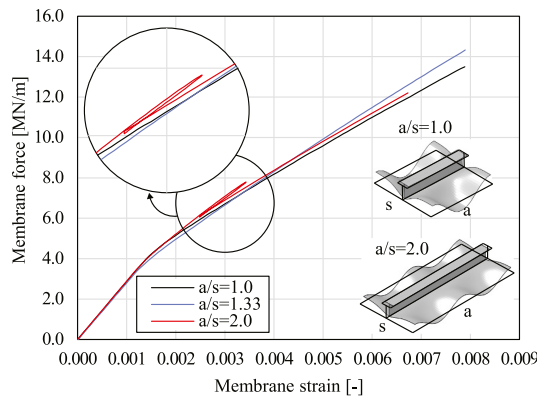

Fig. 7. Effect of unit cell aspect ratio a/s on the axial response of UC1.

waves in x_1 direction. Simulation can handle this as Riks arc length method is used in the analysis. Therefore, $a/s = 1.0$ was used in the following analysis. Analyses with other unit cells UC2 and UC3 showed qualitatively the same results, but are not shown here for sake of brevity.

3.3.3. Material properties

This section studies the effect of material non-linearity on the unit cell response. Therefore, an equivalent stress-plastic strain curve is introduced characterizing a structural steel with an initial yield strength of 355 MPa. The current flow stress σ_f depends on the equivalent plastic strain $\bar{\varepsilon}$ following the modified Swift hardening rule [33,34], see Equation 25 and 26.

$$\sigma_f(\bar{\varepsilon}) = \begin{cases} \sigma_0 \ if \ \bar{\varepsilon} \leq \varepsilon_L \\ K\left(\bar{\varepsilon}_0 + \bar{\varepsilon}\right)^n \quad if \ \bar{\varepsilon} > \varepsilon_L \end{cases} \tag{25}$$

$$\bar{\varepsilon}_0 = \left(\frac{\sigma_0}{K}\right)^{1/n} - \varepsilon_L \tag{26}$$

where K and n are the parameters defining the work hardening, σ_0 is the initial yield strength. To account for the existence of the Lüders plateau, which is characteristic to marine grade structural steels [35,36], the hardening is delayed until the plastic strain reaches the plateau strain $\bar{\varepsilon} = \varepsilon_L$, while the parameter $\bar{\varepsilon}_0$ enforces continuity of the stress-strain curve at that point. Analyses are performed with UC1, UC2, and UC3 with (x = 0.01) and without (x = 0) initial imperfection. By switching the initial imperfection off, we can distinguish the non-linearities in response due to geometry and material.

Membrane force obtained from simulations is plotted in Fig. 8 as a function of membrane strain showing the effect of material and geometrical non-linearity on the response. Results show that the effect of geometric non-linearity on ultimate point (indicated with blue arrow) is less prevailing in the analyses with thick plates (UC1 & UC3, Fig. 8a,c) compared with thin plates (UC2, Fig. 8b). In the analysis with the thinner plate in Fig. 8b the effect of geometric non-linearity (x = 0.01) has more pronounced effect on the response compared with the thick plate. Nevertheless, importance of geometric non-linearity is demonstrated with slender frame (UC3) elasto-plastic analyses, where it causes the stiffener web buckling and sudden load drop in response as shown in Fig. 8c. Furthermore, differences between elastic and elastoplastic response convey the importance of considering metal plasticity in the unit cell level. With elastic analyses ultimate strength point cannot be determined.

4. Numerical example with stiffened panel

In this example the theory presented above is applied to model the response of stiffened panel (ESL approach) and the results are compared with detailed 3D FEM analysis results. The stiffened panel is chosen for its common use in the marine and civil applications. The stiffened panel is modeled with four longitudinal stiffeners with distance of 600 mm. The panels are essentially built from the discrete unit cell geometries of UC1, UC2, and UC3 from Table 1.

4.1. Detailed 3D stiffened panel

For the comparative 3D FEM analyses a FE model is set up as shown in Fig. 9. The element type used is S4R and the element size is 50×50 mm. The same elasto-plastic material properties are used as in the unit cell analysis. The simulation is performed by Abaqus in two steps. The first step is the bifurcation-type (linear) buckling analysis of the stiffened panel. The resulting first eigenmode is used as
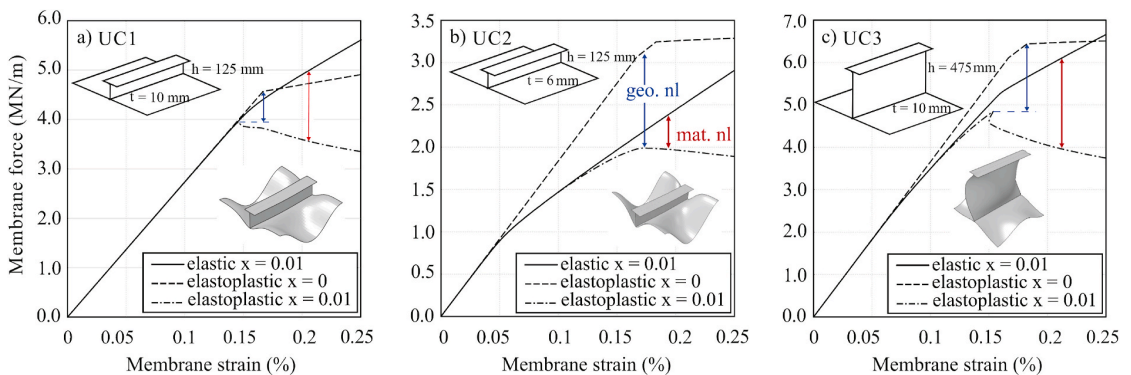

Fig. 8. Effect of material and geometrical non-linearity on the unit cell response. The effect of geometric non-linearity is shown with blue arrow approximately at the ultimate point. The effect of material non-linearity is indicated with red arrow in qualitative terms. (For interpretation of the references to color in this figure legend, the reader is referred to the Web version of this article.)
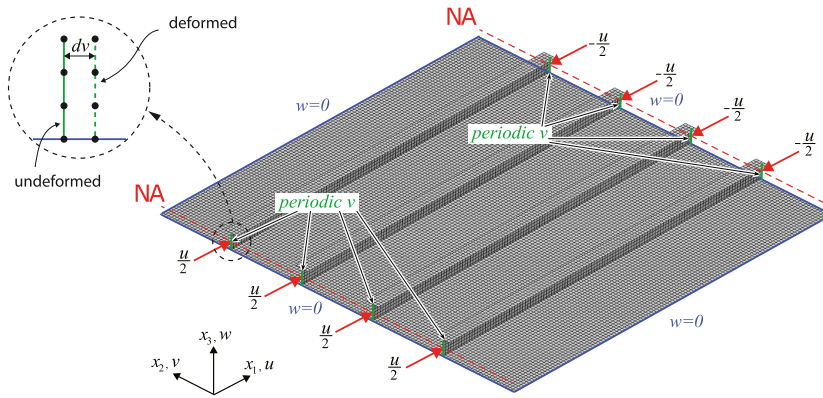
Fig. 9. The geometry of the stiffened panel simply supported on the edges.

an initial imperfection on the global level. The slight imperfection factor ($x = 0.01$) is used. In the second step the force and moment responses are obtained by progressive increase of end displacements using the modified Riks static method. The stiffened panel is compressed by the applied displacement at the nodes where neutral axis crosses the stiffener webs, see Fig. 9. To avoid the local buckling in the web edges due to the prescribed displacement, the local thickness of stiffener web elements is increased five times. All edges of the plate are constrained in the x_3 direction for translation, but still allowed to deform in the x_2 direction as shown in Fig. 9. The periodic boundary condition implies that in each stiffener separately, web nodes are tied together using Abaqus equation constraint option to have the same deformation displacement in the respective direction.

4.2. ESL stiffened panel

ESL model is prepared by using element type S4R and the mesh density of 150×150 mm. Non-linear material properties in ESL are included through non-linear stiffnesses, and the element is defined as shell general section (Abaqus). Additionally, linear analysis are performed with ESL linear stiffness matrices, which can be defined in Abaqus without calling the UGENS subroutine. Comparison between linear and non-linear analyses will show the importance of considering non-linearity in ABD matrices.

The simulation is carried out with the same procedure as the detailed 3D FEM. First, the global imperfection shape of the ESL model is obtained with the bifurcation-type (linear) buckling analysis. The imperfection scaling factor ($x=0.01$ where $w_{max} = 0.6$ mm) is used. Note that while the unit cell analysis already included the imperfections, they need to be accounted in the global model to promote also global buckling as opposed to only local buckling. Finally, ESL panel is loaded in uniaxial compression using displacement applied in x_1 direction. The boundary condition of ESL is simple support for each side, while translation in x_3 direction is constrained. Additionally, a single node in the middle of the panel was constrained in x_2 direction to prevent rigid body motions.

In shell general section (Abaqus), element stiffness of ESL is composed of 4 submatrices (ABCD matrix), explained in Eq. (7). The stiffness matrix is obtained by following the calculation procedure in Section 3.2. The nonlinear stiffness matrix of ESL is shown in Fig. 10a and Fig. 10b for the elastic and elastoplastic material properties, respectively. The (C) submatrix is zero because of moment equilibrium during extension. The B11 submatrix is initially zero as forces are balanced in the beginning. When the curvature increases, plate is compressed while the flange is stretched leading to a non-zero B11 submatrix. For small strains (<0.001), the A12 and A21 submatrices are the same, but local buckling of the plate causes the stiffnesses to become non-linear. The in-plane shear (A33) and torsional stiffnesses (D33) are not very influential for the current case study. For elastoplastic material properties, the (A) submatrix becomes negative after the yield point as seen by the negative slope of the force-strain graph. As shown in Fig. 10c (same behavior as in Fig. 8b), the plate thickness reduction corresponding to case UC2 leads to local plate buckling prior to reaching ultimate strength (A11 matrix).

4.3. Response comparison: ESL and 3D FEM

Fig. 11 presents the load-end shortening curves for 3D FEM and ESL with elastic material properties. Overall perfect agreement is achieved in initial stages of global buckling between the ESL and 3D FEM. The starting point of the global buckling marked in the figure occurs at the same displacement for ESL and 3D FEM. Subsequent response is non-linear while the plate field displays early signs of local buckling as shown in Fig. 11 insert. This local buckling is believed to cause the differences in response at later stages of analysis between 3D model and linear ESL. In contrast, non-linear ESL demonstrates softening in response at late stage of analysis that is comparable to 3D model.

Buckling and elastoplastic collapse dominate the ultimate strength of structures in compression [4,30]. Therefore, we proceed to analyze how non-linearity influences the response of the stiffened panel calculated with the ESL model. In case of the thick plate and stocky stiffeners the ultimate strength is reached when local plate buckling occurs, accompanied by material yielding, after which load
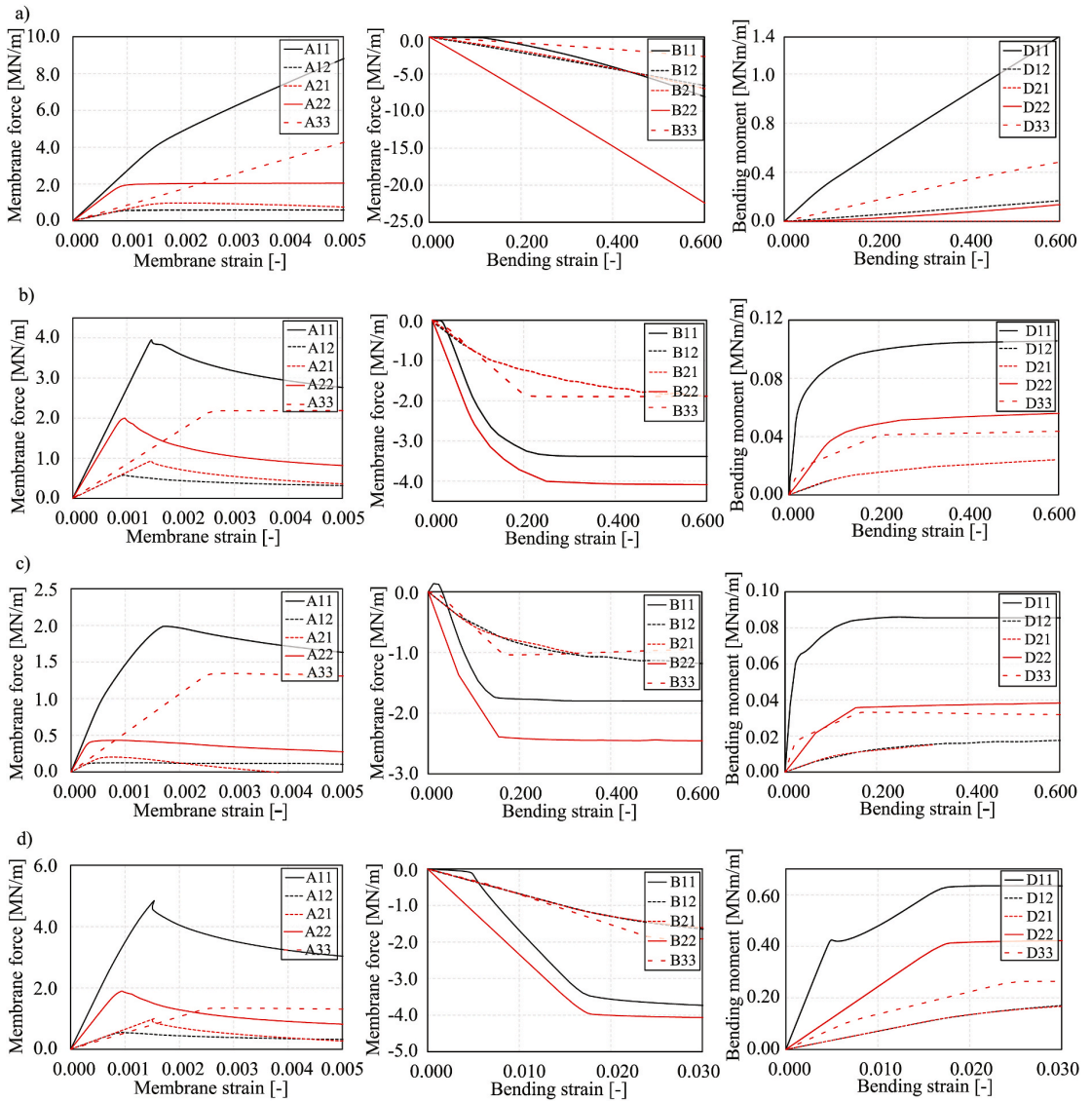
Fig. 10. Non-linear stiffnesses of the unit cell: elastic with UC1 (a); elastoplastic with UC1 (b); elastoplastic with UC2 (c); and elastoplastic with UC3 (d).

suddenly drops (see UC1 in Fig. 12a). This load drop signifies the stiffened panel's ultimate load-carrying capacity and demonstrates the importance of including non-linear stiffness in ESL analysis. The case with thinner plate (UC2) provokes earlier local plate buckling and more gradual stiffness loss before ultimate strength. For these two cases, non-linear ESL can capture the ultimate point with good accuracy. In case of the slender stiffener the results are promising as well, as shown in Fig. 12b. Reduction of stiffener's slenderness led to stiffener web buckling in the unit cell level as demonstrated with unit cell analysis in Fig. 8c and the same response is observed in 3D stiffened panel in Fig. 12b. Besides web buckling, stiffeners in 3D model also show tripping failure, but in the post-ultimate regime, as shown in Fig. 12b. Non-linear ESL analysis can capture the ultimate point with good accuracy, but loses fidelity in the post-ultimate strength range, similar to UC1 and UC2 shown in Fig. 12a. Whether and how this affects the ultimate strength prediction in ship hull girder level should be further investigated. In contrast, constant stiffness ESL does not give any indication that ultimate strength has been attained.

4.3.1. The effect of ESL element size on the response

The mesh sensitivity of ESL model is studied to see the effect on the stiffened panel response. Three element size configurations are
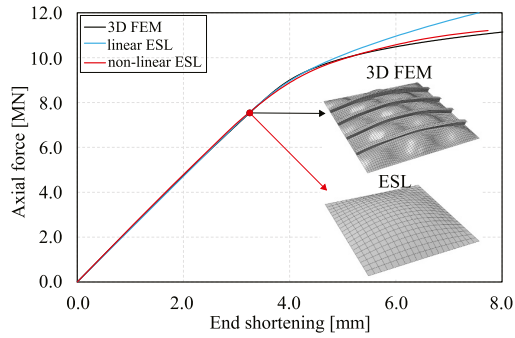
Fig. 11. Load-end shortening curves from three methods and deformed shape for elastic material with plate thickness, $t_p = 10$ mm (unit cell UC1).
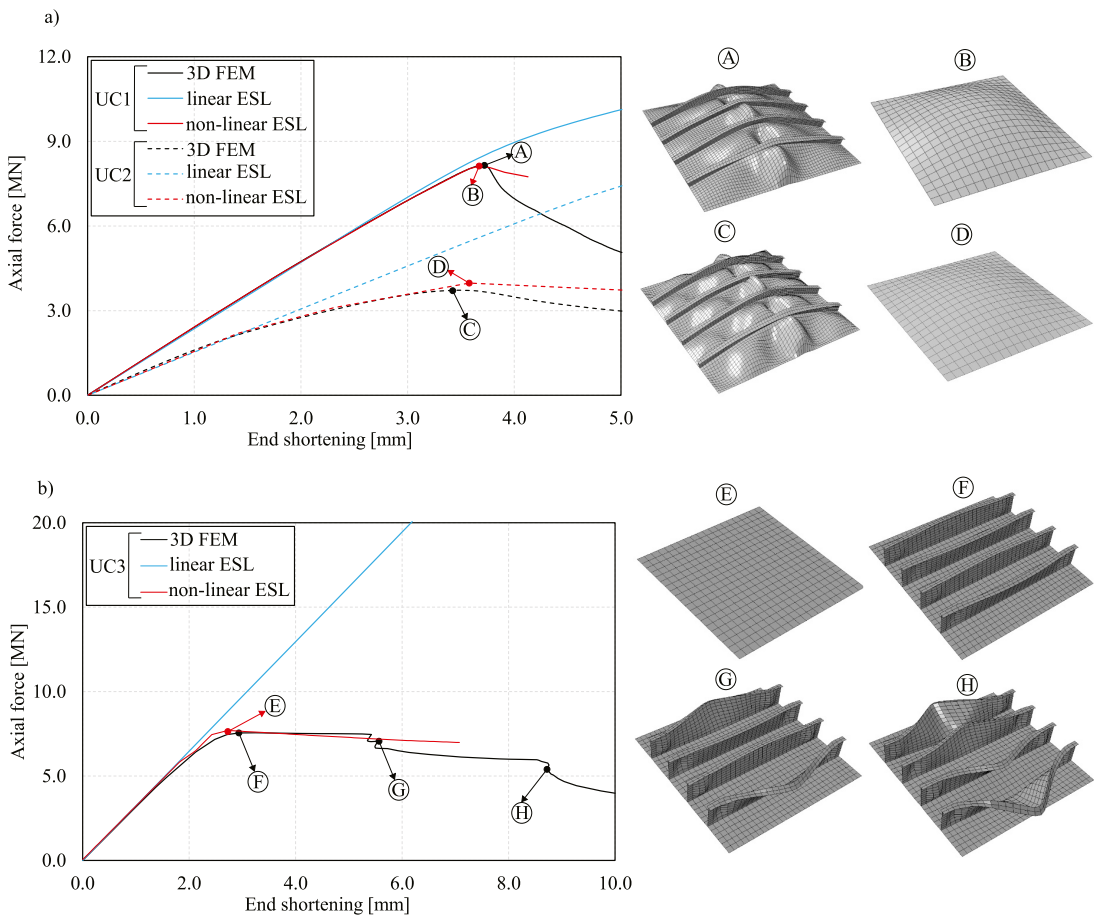

Fig. 12. Load-end shortening curves of stiffened panels. Unit cells UC1 and UC2 with stocky stiffeners (a). Unit cell UC3 with slender stiffener (b). Deformation scaling factor used in 3D FEM pictures is 10.

tested: 75×75 mm, 150×150 mm, and 500×500 mm. The same stiffness matrices corresponding to the UC2 case. As shown in Fig. 13, for all practical purposes results are independent of the ESL element length. In terms of computational efficiency, the analysis time of 500 mm meshed model was ~5 times faster than 75 mm model.
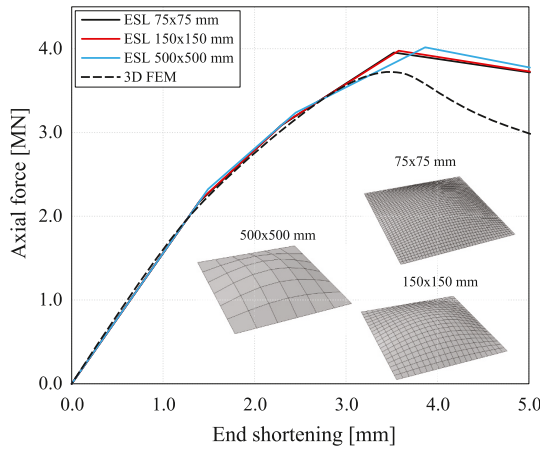
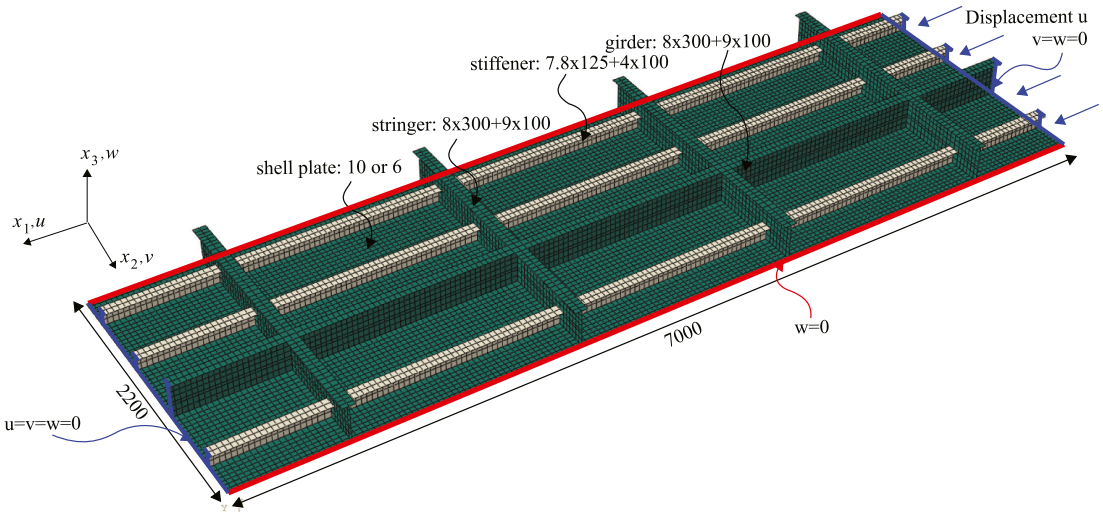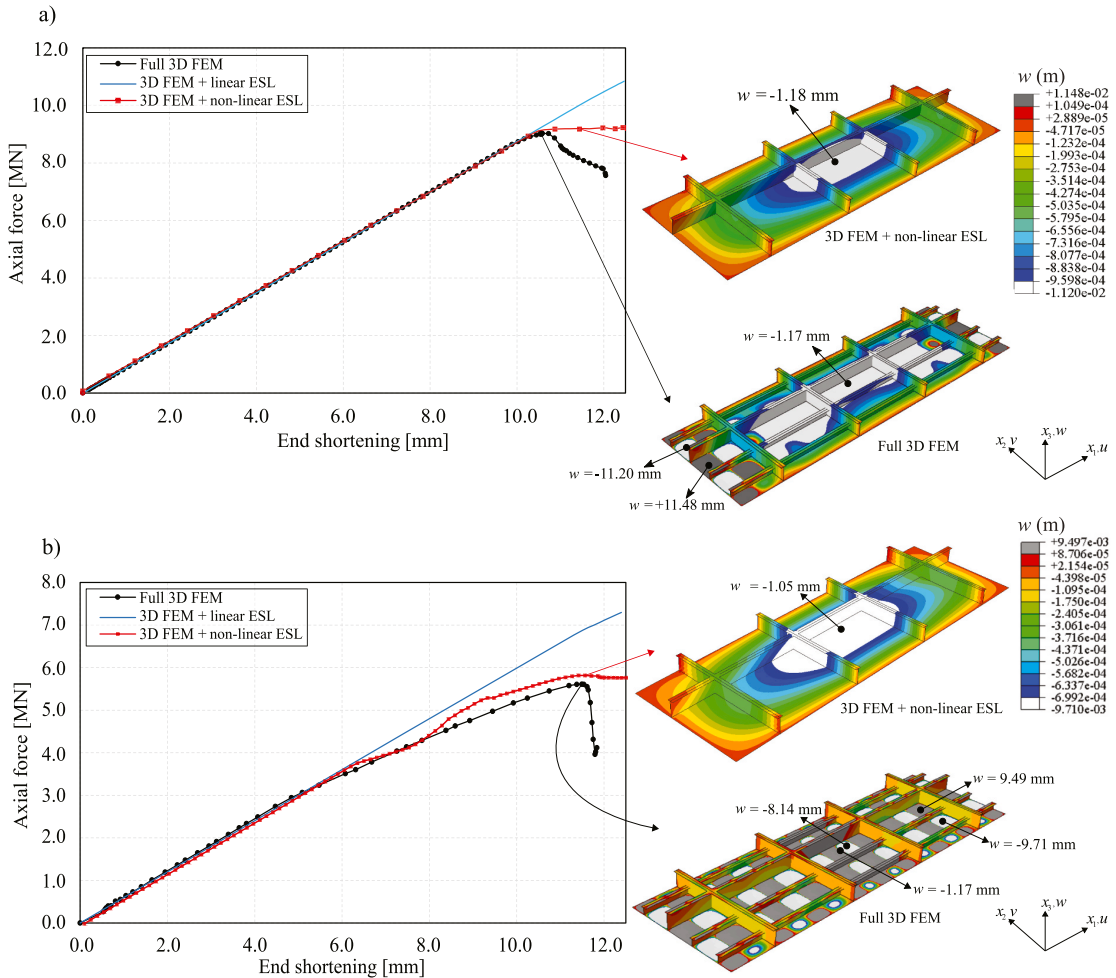**Fig. 13.** Load-end shortening curves of three different element sizes.

Fig. 14. Structural geometry and boundary conditions applied to the grillage model (dimensions in mm).

5. Numerical example with large grillage

This example shows how the ESL can be applied in structural analysis in conjunction with detailed 3D FEM modeling. In other words, ESL methodology is applied only in some parts of the structure while larger structural supporting components like girders and webframes are still modeled explicitly.

Grillage model is composed of longitudinal stiffeners, stringers, and one girder. The structural scantlings and imposed boundary conditions used in the model are shown in Fig. 14. Displacement compression is applied at $x_1 = 0$, and transverse edges are constrained as simple support. To avoid the x_2 and x_3 translation, the aft and fore edges are restrained in respective direction, while transverse edges are free to displace in the x_2 direction. In ship construction, this model can represent a part of a bottom, inner bottom, side, or a deck structure. The analyses are performed with two grillage configurations based on the unit cells UC1 and UC2. Three analysis methods are used: 1) Full 3D FEM, 2) 3D FEM + non-linear ESL and 3) 3D FEM + linear ESL. In all analyses a 12 mm displacement is applied at one end of the panel to exert compression. In ESL simplification, the plate sections with longitudinal stiffeners are replaced with ESL elements, while the rest of the structure is modeled explicitly. Non-linear ESL uses UGENS subroutine for simulation while linear ESL only considers the initial stiffness portion without invoking UGENS subroutine. The ABD stiffnesses are given in Fig. 10.

Fig. 15 shows that a good agreement is obtained between load-end shortening curves for the non-linear ESL and the full 3D FEM, for both plate-stiffener combinations (UC1 and UC2). The ultimate strength cannot be identified based on the linear ESL analysis. Side

Fig. 15. Load-end shortening curves for large grillage. Plate-stiffener combinations for UC1 (a) and UC2 (b). Coloured contours for ESL and full 3D model use the same legend limits.

figures of Figs. 15a and b show the contours of out-of-plane displacement in the deformed configuration approximately at the same applied displacement for the full 3D and ESL analysis. In case of UC1 (Fig. 15a) the maximum deformation in the mid-panel of ESL model is 1.18 mm downward, which agrees well with the full 3D model at the same location. At the fore and aft section in the full 3D model the plate buckles locally, which marks also the point of ultimate strength. Although the non-linear ESL cannot visualize this local plate buckling due to software limitations, the response curve precisely captures this point.

In case of UC2 (Fig. 15b) the thinner 6 mm plate buckles locally across the grillage in 3D model. These local buckles are not presented visually in ESL model so deformations are not comperable. Nevertheless, the global out-of-plane deformation measured in 3D model between two local buckles (1.17 mm) compares well with non-linear ESL analysis measured at the same location (1.05 mm).

In both analyzed cases the ESL cannot capture the post-buckling load drop demonstrated by the full 3D model, which is similar to when it was used for the stiffened panel analysis. Although the post-buckling response obtained with the non-linear ESL is slightly different from the full 3D model, we once more highlight its clear advantage over the constant stiffness ESL, which cannot ascertain the exact point of collapse. Linear ESL excludes the non-linearities caused by the material and geometry.

6. Conclusion

This study proposes a homogenization method for stiffened panels to assess their ultimate strength. Linear and non-linear stiffness matrices of an equivalent single layer (ESL) are used in the calculation. The stiffnesses are composed of extensional, coupling, bending and transverse shear components based on the first-order shear deformation theory. On the unit cell level, geometrical imperfections

and non-linear material properties are considered. Global geometric imperfections are incorporated on the panel level. Our analysis with large grillage structure exemplifies that non-linear ESL model can accurately predict the global ultimate strength of the panel stiffened with stiffeners (represented with equivalent single layer approach) and larger stiffening elements (modeled explicitly). In contrast, the linear ESL analysis captured the stiffness of the grillage accurately but did not provide the point of collapse. However, analysis with stiffened panels showed that even the non-linear ESL cannot capture the post-ultimate response of the panels.

The proposed method posts computational efficiency compared with full 3D analysis (not quantified in the paper) but can significantly reduce the model preparation time as different structural configurations are realized by modification of stiffness matrices. This circumvents the laborious 3D modelling effort. The approach offers a pathway for efficient ship hull girder design tool. However, further work is needed to validate the approach for more extensive range of boundary and loading conditions. Moreover, present analysis demonstrated that in the current implementation approach fails to capture the post-ultimate softening. How this affects the global hull girder analysis should be part of further research.

Declaration of competing interest

The authors declare that they have no known competing financial interests or personal relationships that could have appeared to influence the work reported in this paper.

Acknowledgments

References

[1] Kortenoeven J, Boon B, de Bruijn A. Application of sandwich panels in design and building of dredging ships. J Ship Prod 2008;24:125–34.
[2] Quinn D, Murphy A, Glazebrook C. Aerospace stiffened panel initial sizing with novel skin sub-stiffening features. Int J Struct Stabil Dynam 2012;12:1250060. https://doi.org/10.1142/S0219455412500605.
[3] Vassalos D. In: Papanikolaou A, editor. Risk-based ship design BT - risk-based ship design: methods, tools and applications. Berlin, Heidelberg: Springer Berlin Heidelberg; 2009. p. 17–96. https://doi.org/10.1007/978-3-540-89042-3_2.
[4] IMO.. IACS common structural rules for bulk carriers and oil tankers. 2012.
[5] Paik JK, Seo JK, Kim DM. Idealized structural unit method and its application to progressive hull girder collapse analysis of ships. Ships Offshore Struct 2006;1: 235–47. https://doi.org/10.1533/saos.2006.0129.
[6] Paik J, Thayamballi A. Ultimate limit state design of ship hulls. 2008.
[7] Benson S, Downes J, Dow RS. Compartment level progressive collapse analysis of lightweight ship structures. Mar Struct 2013;31:44–62. https://doi.org/10.1016/j.marstruc.2013.01.001.
[8] Ueda Y, Sherif R. An ultimate transverse strength analysis of ship structure. J Soc Nav Archit Jpn 1974;1974:309–24.
[9] Yukio U, Rashed SMH. The idealized structural unit method and its application to deep girder structures. Comput Struct 1984;18:277–93. https://doi.org/10.1016/0045-7949(84)90126-3.
[10] Benson S, Downes J, Dow RS. Overall buckling of lightweight stiffened panels using an adapted orthotropic plate method. Eng Struct 2015;85:107–17. https://doi.org/10.1016/j.engstruct.2014.12.017.
[11] Naar H, Varsta P, Kujala P. A theory of coupled beams for strength assessment of passenger ships. Mar Struct 2004;17:590–611. https://doi.org/10.1016/j.marstruc.2005.03.004.
[12] Tabri K, Naar H, Kõrgesaar M. Ultimate strength of ship hull girder with grounding damage. Ships Offshore Struct 2021;15:S161–75. https://doi.org/10.1080/17445302.2020.1827631.
[13] Reddy J. Mechanics of laminated composite plates and shells. CRC Press; 2003. https://doi.org/10.1201/b12409.
[14] Noor AK, Burton WS, Bert CW. Computational models for sandwich panels and shells. Appl Mech Rev 1996;49:155–99. https://doi.org/10.1115/1.3101923.
[15] Romanoff J, Varsta P. Bending response of web-core sandwich plates. Compos Struct 2007;81:292–302. https://doi.org/10.1016/j.compstruct.2006.08.021.
[16] Romanoff J, Klanac A. Design optimization of steel sandwich hoistable car decks applying homogenized plate theory. J Ship Prod 2008;24:108–15.
[17] Romanoff J. Optimization of web-core steel sandwich decks at concept design stage using envelope surface for stress assessment. Eng Struct 2014;66:1–9. https://doi.org/10.1016/j.engstruct.2014.01.042.
[18] Avi E, Lillemäe I, Romanoff J, Niemelä A. Equivalent shell element for ship structural design. Ships Offshore Struct 2015;10:239–55. https://doi.org/10.1080/17445302.2013.819689.
[19] Romanoff J, Jelovica J, Reddy JN, Remes H. Post-buckling of web-core sandwich plates based on classical continuum mechanics: success and needs for non-classical formulations. Meccanica 2020:1–16. https://doi.org/10.1007/s11012-020-01174-6. https://aaltodoc.aalto.fi/handle/123456789/45158.
[20] Metsälä M, Gonçalves BR, Romanoff J, Jelovica J. Geometrically nonlinear bending response of a ship-like box girder using an enhanced single-layer theory. Prog Anal Des Mar Struct - Proc 6th Int Conf Mar Struct MARSTRUCT 2017 2017:289–96. https://doi.org/10.1201/9781315157368-34.
[21] Nordstrand T. On buckling loads for edge-loaded orthotropic plates including transverse shear. Compos Struct 2004;65:1–6. https://doi.org/10.1016/S0263-8223(03)00154-5.
[22] Lok TS, Cheng QH. Free vibration of clamped orthotropic sandwich panel. J Sound Vib 2000;229:311–27. https://doi.org/10.1006/jsvi.1999.2485.
[23] Jelovica J, Romanoff J, Ehlers S, Varsta P. Influence of weld stiffness on buckling strength of laser-welded web-core sandwich plates. J Constr Steel Res 2012;77: 12–8. https://doi.org/10.1016/j.jcsr.2012.05.001.
[24] Jelovica J, Romanoff J, Klein R. Eigenfrequency analyses of laser-welded web-core sandwich panels. Thin-Walled Struct 2016;101:120–8. https://doi.org/10.1016/j.tws.2016.01.002.
[25] Reinaldo Goncalves B, Jelovica J, Romanoff J. A homogenization method for geometric nonlinear analysis of sandwich structures with initial imperfections. Int J Solid Struct 2016;87:194–205. https://doi.org/10.1016/j.ijsolstr.2016.02.009.
[26] Kõrgesaar M, Goncalves BR, Romanoff J, Remes H. Non-linear effective properties for web-core steel sandwich panels in tension. Int J Mech Sci 2016;115–116: 428–37. https://doi.org/10.1016/j.ijmecsci.2016.07.021.
[27] Jelovica J, Romanoff J. Load-carrying behaviour of web-core sandwich plates in compression. Thin-Walled Struct 2013;73:264–72. https://doi.org/10.1016/j.tws.2013.08.012.
[28] Goncalves BR, Jelovica J, Romanoff J. Abaqus UGENS subroutine for nonlinear analysis of periodic panels. 2016.
[29] Paik JK. Ultimate limit state analysis and design of plated structures. 2018. https://doi.org/10.1002/9781119367758.

[30] DNV GL AS. Rules for classification ships. 2015. p. 105. Oct. 2015 Part 3 Hull [Chapter 8] Buckling.

[31] Faulkner D. A review of effective plating for use in the analysis of stiffened plating in bending and compression. J Sh Res 1975;19:1–17.

[32] Singer J, Arbocz J, Weller T. Buckling experiments: experimental methods in buckling of thin-walled structures, vol. 1; 2002. https://doi.org/10.1002/9780470172995.

[33] Storheim M, Amdahl J, Martens I. On the accuracy of fracture estimation in collision analysis of ship and offshore structures. Mar Struct 2015;44:254–87. https://doi.org/10.1016/j.marstruc.2015.09.006.

[34] Swift HW. Plastic instability under plane stress. J Mech Phys Solid 1952;1:1–18. https://doi.org/10.1016/0022-5096(52)90002-1.

[35] Ehlers S, Varsta P. Strain and stress relation for non-linear finite element simulations. Thin-Walled Struct 2009;47:1203–17. https://doi.org/10.1016/j.tws.2009.04.005.

[36] Kõrgesaar M, Romanoff J, Remes H, Palokangas P. Experimental and numerical penetration response of laser-welded stiffened panels. Int J Impact Eng 2018;114:78–92. https://doi.org/10.1016/j.ijimpeng.2017.12.014.
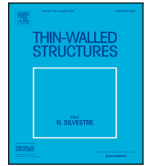
Appendix 2

II

T. Putranto, M. Kõrgesaar, and J. Jelovica. Ultimate strength assessment of stiffened panels using equivalent single layer approach under combined in-plane compression and shear, *Thin-Walled Structures*, 180:109943, 2022

Full length article

Ultimate strength assessment of stiffened panels using Equivalent Single Layer approach under combined in-plane compression and shear

Teguh Putranto [a,*], Mihkel Kõrgesaar [a], Jasmin Jelovica [b]

[a] *Department of Civil Engineering and Architecture, Kuressaare College, Tallinn University of Technology, Tallinna 19, 93819, Kuressaare, Estonia*
[b] *Departments of Mechanical Engineering and Civil Engineering, The University of British Columbia, 6250 Applied Science Lane, V6T 1Z4, Vancouver, Canada*

ARTICLE INFO

ABSTRACT

Equivalent Single Layer (ESL) approach is extended to model ultimate strength of stiffened panels under a combination of in-plane compression and shear. Ultimate strength under this combined loading depends on the loading path and could be lower than for only uni-axial compression since shear load can produce axial forces. Thus, to account for this effect, the recent ESL model is extended to include A_{13} stiffness component as non-zero value. Procedure to accurately obtain A_{13} is presented. In ESL approach, a stiffened panel is transformed into a two-dimensional (2D) single layer with the same stiffness obtained from unit cell simulations. To obtain non-linear stiffness matrix of ESL, elastic–plastic material properties and initial imperfection were applied to the unit cell. ESL responses were validated by comparing numerical and experimental results from the literature. Several stiffened panel configurations were analyzed to obtain different collapse modes. Combined loads were applied for shear to compression ratio of 0, 1, and 2. Lateral pressure loading was also considered in the simulations. Analyses were carried out based on the load sequences consisting of: 1) compression and shear loaded simultaneously and 2) shear applied first, followed by compression. The results show that the modified ESL can well capture the effect of shear load on ultimate strength in comparison to a detailed 3D FEM model of stiffened panels. The accuracy of the ESL varies depending on the collapse mode of stiffened panels.

1. Introduction

Stiffened panels are widely used in thin-walled structures that can be found in civil, aerospace, and marine engineering. Stiffened panels are the main load-bearing components, having many benefits such as excellent strength to weight ratio and ease of fabrication. During operation of a structure, stiffened panel will be subjected to complex, combined in-plane and lateral loading scenarios. These scenarios can lead to different types of buckling modes and subsequent collapse of the panel, and ultimately, the entire structure [1–4]. Therefore, it is important to analyze possible collapse scenarios and to provide efficient tools for estimating the collapse loads. This study focuses on combined in-plane compression and shear. Additionally, lateral pressure is considered.

In terms of buckling and ultimate strength analysis of stiffened panels, shear loads have seen less attention compared with pure compression loads [5,6]. However, if shear loads exceed a load-carrying capacity, bridge, aircraft, or hull structures may buckle and collapse [7, 8] and the failure will occur earlier for thin-walled structures [9]. In stiffened panels, the stiffeners are mainly employed to prevent elastic buckling as well as to increase the shear buckling strength [10]. Slender stiffeners are able to withstand shear loads, however, local

web buckling can occur under compression loads [11,12]. Additionally, shear buckling strength is influenced by boundary conditions and plate thicknesses of the stiffened panel. Critical shear buckling load of stiffened panels decreases when it is simply supported rather than clamped [13] and has thinner plate and stiffeners thicknesses [14]. Several researchers also then explained how the structural behavior and ultimate strength of stiffened panel under combined loads. Using FE simulations, Hussain and Loughlan [15] found that the ultimate strength of stiffened panel reduces with increasing shear to compression ratio. Furthermore, under combined loading, the out-of-plane deflection is larger in comparison with pure compression loading [16].

Combined loading occurs frequently, thus an efficient method is needed to account for different loads in ultimate strength analysis of stiffened structures. Equivalent Single Layer (ESL) approach has been shown to be computationally efficient and accurate for predicting the structural strength under compression. In ESL, 3D stiffened panel is represented as a 2D plate with uniform stiffness where each finite element has the same properties. The ESL with constant stiffness was effective in capturing the global buckling strength of sandwich panels [17–19] and vibration response of stiffened panels [20,21]. However, ESL with constant stiffness cannot account for local buckling in a stiffened

---

* Corresponding author.
 E-mail address: teguh.putranto@taltech.ee (T. Putranto).

panel and a non-linear material behavior. Nevertheless, local buckling is a relevant failure mode in the non-linear analysis of sandwich [22] and stiffened panels [23,24]. ESL with non-linear stiffness can account for local buckling and non-linear material responses. The ESL has been shown to be effective in the non-linear uni-axial compression–tension analysis [25–27]. The above studies considered membrane (**A**), membrane-bending (**B**) and bending (**D**) matrices, but approximated the axial force caused by the shear, the term A_{13}, to be zero, which effectively discards the effect of shear.

Therefore, the work of Putranto et al. [27] is extended by including the A_{13} term in the ESL stiffness matrix definition. The effect of this term on the ultimate strength of stiffened panels is shown under combined compression and shear accompanied by lateral pressure. Several stiffened panel configurations are analyzed to account for different failure modes. To consider local buckling, initial imperfection is applied in unit cell. Additionally, elastic–plastic properties are used so that unit cell experiences yielding. In this way, local buckling and yielding behavior can be accounted for in the global ESL simulation. Stiffened panels are subjected to a combination of compression and shear loads by varying the load ratio. Analysis is also carried out by two different loading sequences: (1) compression and shear applied simultaneously and (2) shear applied first, followed by compression. This study finds that ESL with $A_{13} \neq 0$ can accurately predict the ultimate strength of stiffened panel under combination of compression and shear loads.

2. Overview of the ESL approach

The ESL approach is derived from the 3D elasticity theory following appropriate assumptions regarding the shell kinematics of deformation or stress state through the laminate thickness. Effectively, the 3D continuum problem of stiffened panel composed of plate, web, and flange can be reduced to a 2D shell continuum problem as an ESL. Here, the ESL theory is based on the first-order shear deformation theory (FSDT) explained in the following.

2.1. First-order shear deformation theory (FSDT)

The FSDT is the extension of classical laminated plate theory (CLPT) or Kirchhoff plate theory by including a transverse shear strain through the kinematic assumptions. The transverse shear strain is assumed to be constant throughout the laminate thickness. The displacement field of FSDT associated with the shell continuum in Eqs. (1), (2), (3) is composed of two parts, i.e., membrane u^0, v^0, w^0 and bending $\partial u/\partial x_3$, $\partial v/\partial x_3, \partial w/\partial x_3$ components [28]:

$$u = u^0 + x_3 \frac{\partial u}{\partial x_3}; \tag{1}$$

$$v = v^0 + x_3 \frac{\partial v}{\partial x_3}; \tag{2}$$

$$w = w^0 + x_3 \frac{\partial w}{\partial x_3}. \tag{3}$$

The $\partial w/\partial x_3$ is zero since there is no rotation around the x_3 direction. A deformed shell element in the ESL approach is based on the FSDT or Reissner–Mindlin plate theory. Accordingly, the transverse normals do not remain perpendicular to the midplane since transverse shear strains (γ_{13}) are considered, as illustrated in Fig. 1. Due to membrane and bending responses, point C is displaced in the x_1 direction.

2.2. Compliance and stiffness

In the ESL approach, the non-linear von Karman strains are accounted for which means that the ESL element has the capability to represent geometrical non-linearity (moderate rotation). Thus, for cases
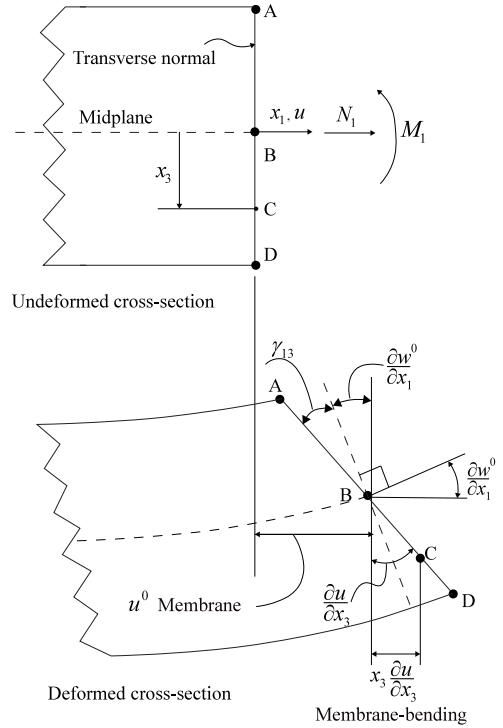

Fig. 1. Geometry of deformation based on the FSDT.

of small strain and moderate rotation, the strain–displacement relations are given by Eq. (4) [29].

$$
\begin{Bmatrix} \varepsilon_{11} \\ \varepsilon_{22} \\ \gamma_{12} \\ \gamma_{13} \\ \gamma_{23} \end{Bmatrix} = \begin{Bmatrix} \varepsilon_{11}^0 \\ \varepsilon_{22}^0 \\ \gamma_{12}^0 \\ \gamma_{13}^0 \\ \gamma_{23}^0 \end{Bmatrix} + x_3 \begin{Bmatrix} \varepsilon_{11}^1 \\ \varepsilon_{22}^1 \\ \gamma_{12}^1 \\ \gamma_{13}^1 \\ \gamma_{23}^1 \end{Bmatrix} = \begin{Bmatrix} \frac{\partial u^0}{\partial x_1} + \frac{1}{2}\left(\frac{\partial w^0}{\partial x_1}\right)^2 \\ \frac{\partial v^0}{\partial x_2} + \frac{1}{2}\left(\frac{\partial w^0}{\partial x_2}\right)^2 \\ \frac{\partial u^0}{\partial x_2} + \frac{\partial v^0}{\partial x_1} + \frac{\partial w^0}{\partial x_1}\frac{\partial w^0}{\partial x_2} \\ \frac{\partial w^0}{\partial x_1} + \frac{\partial u}{\partial x_3} \\ \frac{\partial w^0}{\partial x_2} + \frac{\partial v}{\partial x_3} \end{Bmatrix} +
$$
$$
x_3 \begin{Bmatrix} \frac{\partial^2 u}{\partial x_1 \partial x_3} \\ \frac{\partial^2 v}{\partial x_2 \partial x_3} \\ \frac{\partial^2 u}{\partial x_2 \partial x_3} + \frac{\partial^2 v}{\partial x_1 \partial x_3} \\ 0 \\ 0 \end{Bmatrix} \tag{4}
$$

where $(\varepsilon_{11}^0, \varepsilon_{22}^0)$ are the in-plane membrane strains, (γ_{12}^0) is the in-plane shear strain, $(\varepsilon_{11}^1, \varepsilon_{22}^1)$ are the bending strains, (γ_{12}^1) is the torsional strain, and $(\gamma_{13}^0, \gamma_{23}^0)$ are the transverse shear strains. Based on the FSDT, $(\gamma_{13}^1, \gamma_{23}^1)$ are zero as there are no rotations around the x_3 axis. Accordingly, all strain components follow from the kinematics and are linearly related to the plate thickness. Therefore, the stress resultants can be written in a compact form as in Eq. (5):

$$
\begin{Bmatrix} \{N\} \\ \{M\} \\ \{Q\} \end{Bmatrix} = \begin{bmatrix} [A] & [B] & 0 \\ [C] & [D] & 0 \\ 0 & 0 & [D_Q] \end{bmatrix} \begin{Bmatrix} \{\varepsilon^0\} \\ \{\varepsilon^1\} \\ \{\gamma^0\} \end{Bmatrix} \tag{5}
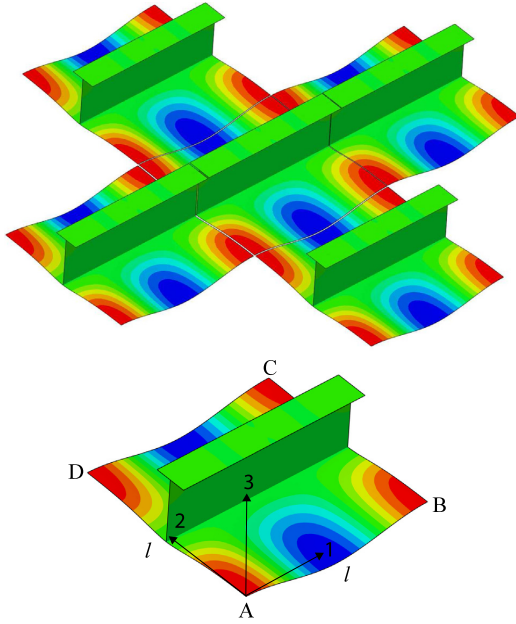$$

Fig. 2. Deflection of UC under uni-axial compression representing $j = 3$. Displacements in all directions are periodic but not shown for brevity.

where $\{\varepsilon^0\}$, $\{\varepsilon^1\}$, and $\{\gamma^0\}$ are the in-plane membrane, bending, and transverse shear strains, respectively. **A**, **B**, **C** and **D** are the 3×3 matrices of the membrane, membrane-bending, bending-membrane, and bending stiffnesses, respectively. Additionally, $\mathbf{D_Q}$ is the 2×2 matrix of the transverse shear stiffness. The response of the plate is expressed by using membrane force $\{N\}$, bending moment $\{M\}$, and transverse shear force $\{Q\}$ matrices. To consider the change of **ABCD** stiffness matrix during simulation, UGENS subroutine is used. Inner workings of UGENS subroutine is explained in Appendix A.

2.3. Unit cell analysis

The stiffness matrices are obtained with unit cell (UC) analyses. In contrast to the stiffened panel analysis presented in the next section, the boundary conditions imposed on the UC must comply with ESL homogenization theory and presumption that UC is a periodic unit of a larger structure. Therefore, the edges of the UC must remain periodic throughout loading. For periodic boundary condition, displacement u constrained at nodes in the UC are written by Eqs. (6),(7) [30], ε is the strain in the UC, l is the UC length, and j is the direction of 1,2,3 as illustrated in Fig. 2.

$$u_j^{BC} - u_j^{AD} = \varepsilon_{11}^0 l \qquad (j = 1, 2, 3) \tag{6}$$

$$u_j^{CD} - u_j^{AB} = \varepsilon_{11}^0 l \qquad (j = 1, 2, 3) \tag{7}$$

The basic dimension of UC selected is a square shape where the size is the stiffener spacing. This size is obtained from analyzing the response of UC in the different size configurations, see in Ref. [27]. The width of UC is constant since it refers to the stiffener spacing, while the length of one is varied. UC is subjected to uni-axial compression. A strain energy criterion is used here to determine the dimension of UC [25]. The square shape of UC has the minimum strain energy which has the smallest area under the membrane force–membrane strain curve.

The procedure for calculating the ESL stiffness matrix is explained briefly; for further details see [27]. Firstly, the unit cell representing a periodic part of the stiffened panel needs to be determined. This unit cell is then subjected to six loading conditions based on the FSDT as shown in Fig. 3. As a result, non-linear membrane forces and bending moments are obtained due to local buckling and yielding. Finally, the non-linear stiffness is obtained from the calculation of the first derivative of those results as shown in Appendix B.

The boundary condition definitions and terminology used throughout the paper related to shear simulation are further explained in Fig. 4. Notably, the figure highlights the differences in boundary conditions between UC analysis denoted as *periodic simple shear* (Fig. 4(a)) and stiffened panel analysis (Fig. 4(b) and (c)). The details related to latter two conditions in Fig. 4(b) and (c), relaxed *pure shear* and *simple shear*, respectively, will be explained in the following Sections.

The shear displacement U is applied at the nodes on the UC edges as shown in Fig. 4(a). Furthermore, UC is simply supported with one additional constraint. Namely, to prevent the vertical rigid body motion, the translations are fixed in the node at the middle of the plate below the stiffener. The shear and axial forces are obtained by summing the respective components on the cross-sectional area cutting through the plate and stiffener. The membrane force per unit length is $N_{12} = \sum F_{12}/L$ where $\sum F_{12}$ is the total shear forces and L is the length of the unit cell. The shear angle is $\gamma = \tan^{-1}(2v)/L$ where v is the applied shear displacement. Therefore, the in-plane membrane (shear and axial) force vs. shear angle relations are obtained and used to determine the A_{33} and A_{13}, respectively.

2.4. Effect of shear stiffness on axial force

According to the ESL stiffness matrix in Eq. (5), the axial force (N_{11}) can be obtained as follows:

$$N_{11} = A_{11}\varepsilon_{11}^0 + A_{12}\varepsilon_{22}^0 + A_{13}\gamma_{12}^0 + B_{11}\varepsilon_{11}^1 + B_{12}\varepsilon_{22}^1 + B_{13}\gamma_{12}^1 \tag{8}$$

In our previous work where the focus was on in-plane compression loading [27], the axial forces due to shear A_{13} and torsion B_{13} were taken as zero. Under complex loading scenarios where compression and shear are both active, the axial force increases due to shear. Thus, the A_{13} is expressed by:

$$A_{13} = \frac{\partial N_{11}}{\partial \gamma_{12}^0} \tag{9}$$

where N_{11} is the axial force and γ_{12}^0 is the shear strain. The latter is calculated from the shear displacement (δv) divided by the length of the unit cell (L).

Comparative UC analysis were performed under compression (Fig. 3(a)) and shear (Fig. 3(c)) according to the description given in Section 2.3. The resulting axial force for UC under compression and shear are presented in Fig. 5, where curves are normalized against peak normal force attained in compression analysis. Under compression all three UCs depict the same mechanistic behavior with linear increase in force prior to elastic buckling, which is followed by the non-linear stage until maximum load. The onset of elastic shear buckling is more obvious under shear load with axial force component (N_{11}) increasing suddenly at about 20% of maximum applied displacement. For these three investigated cases, this axial force due to shear reaches a maximum of 25% of the N_{11} in compression analysis. This increase implies that the axial stiffness under shear (A_{13}) is relevant in the post-buckling stage when loading deviates from uni-axial compression. Finally, the torsion component is still kept zero ($B_{13} = 0$) as the torsion plays a minor role in buckling analysis of most structural applications, see e.g. [31].
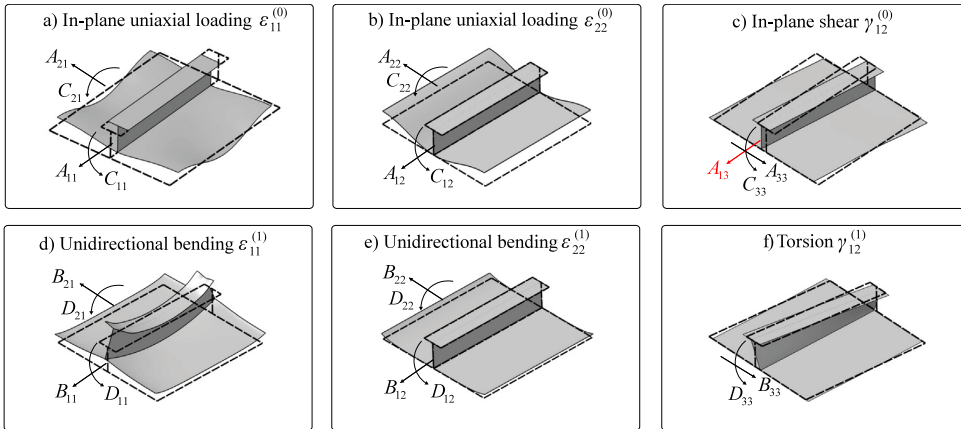
Fig. 3. Determination of stiffness coefficients from unit cell analysis according to [27]. The A_{13} component previously ignored in the earlier study is highlighted in red. (For interpretation of the references to color in this figure legend, the reader is referred to the web version of this article.)
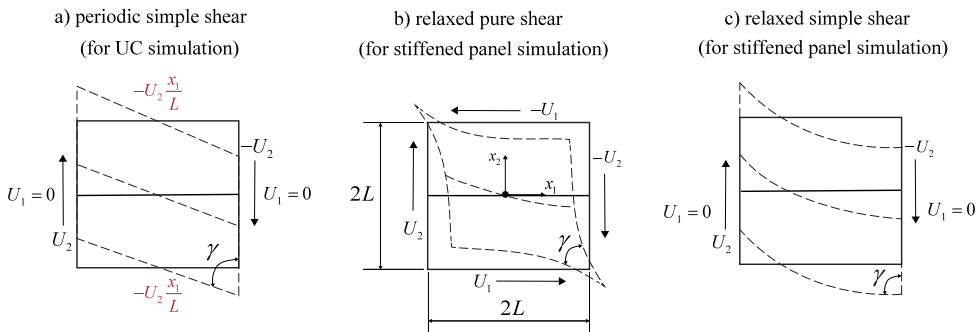

Fig. 4. Schematic of relaxed and periodic boundary conditions for simple and pure shears. Imposed displacement loads are marked with black arrows while imposed equation constraints are marked in red. Equation constraint formulation assumes an origin of the coordinate system in the middle of the panel. (For interpretation of the references to color in this figure legend, the reader is referred to the web version of this article.)

3. Validation of the ESL approach with numerical and experimental results

3.1. Numerical simulations

The numerical simulations are performed using Abaqus FEA software. Shell element S4R is selected for its capability to model high distortions and numerically efficient reduced integration and formulation. S4R element is suitable for both thin and thick plates and has six degrees of freedom per node allowing accurate displacements (axial, shear, bending, and torsion). The simulations are performed with an implicit solver using the modified Riks method.

In the 3D FE model of the stiffened panel, both plate and stiffeners are modeled explicitly in their position, while an ESL model is represented with a 2D meshed flat plate. This is where the ESL obtains its computational efficiency, in addition to having stiffness defined beforehand. To include the non-linear stiffness of ESL, the UGENS subroutine is invoked. In 3D FE and UC analyses the material behavior is described with elastic-perfectly plastic isotropic von Mises model. In ESL simulations no material definition is given as the behavior is governed by stiffness matrices.

3.1.1. Boundary and loading conditions

Stiffened panels are simply supported with displacements constrained at the panel edges in the x_3 direction ($U_3 = 0$). The shear displacements (δu and δv) are applied at the nodes on the panel edges for plate and stiffeners as shown in Fig. 6. Without additional constraints applied on panel edges, these boundary conditions are referred to as *relaxed pure shear* in Fig. 4(b) and distinguished from the ones used in UC analysis (Fig. 4(a)). The boundary conditions correspond to the ones used in both reference studies [5,32].

Shear forces are obtained from the cross-sectional cut transverse to the stiffener direction, as can be seen in Fig. 6. The obtained shear forces are multiplied by two to account for the symmetry of the panel. To obtain the average shear stress (τ), the total shear forces ($\sum F_{12}$) are divided by the cross-sectional area. The shear angle is $\gamma = \tan^{-1}(2v)/L$ where v is the applied shear displacement and L is the length of the panel. The obtained $\tau - \gamma$ relation is compared with the results from the literature.

3.1.2. Initial imperfections

Plate can experience local buckling under compression and shear. To consider the buckling behavior, initial imperfections need to be applied on the stiffened panel. The geometric configuration of the initial local and global imperfections is obtained from the first eigenmode of buckling analysis under compression. The maximum imperfection amplitude ($w_{\max}$) is calculated based on Eq. (10)

$$\frac{w_{\max}}{t} = x\left(\frac{b}{t}\right)^2 \frac{\sigma_0}{E}, \tag{10}$$
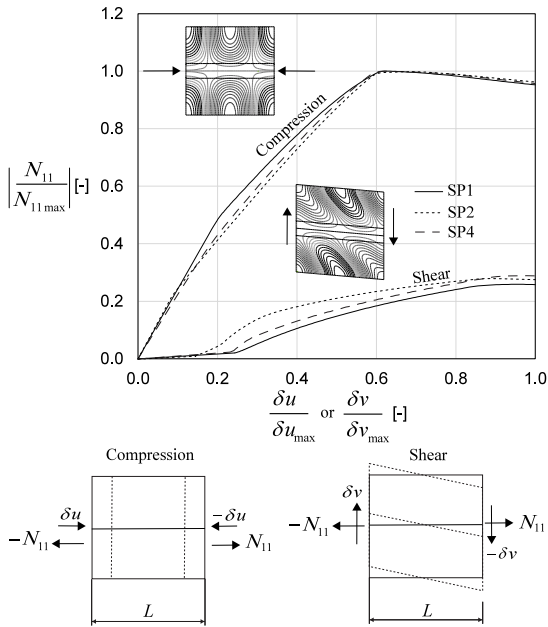
Fig. 5. Axial force development under compression and shear loads for several unit cell configurations (see Table 2).

where t is the plate thickness, b is the stiffener spacing, σ_0 is the yield stress, and E is the elastic modulus [33,34]. According to Li et al. [35], the x-factor values for local plate distortion amplitude spread in the range from 0 (without imperfection) to 0.1 (average imperfection). Unit cell analysis with three x-factors ($x = 0$, 0.025, and 0.1) were performed showing that some imperfection is needed to cause elastic buckling in unit cell. Therefore, in this study DNV's [34] suggested value corresponding to slight imperfection of $x = 0.025$ was used. The residual stresses were not considered.

Global imperfections are typically characterized by a half-wave in both length and width directions, while local imperfections have multiple waves in the model as can be seen in Fig. 7 for 3D FEM. Both models have the same global and local imperfections, but the local one is handled differently in ESL than 3D FEM. For 3D FEM model, local and global imperfections are directly superimposed. For ESL model, global imperfections are explicitly modeled, while local ones are considered in UC analyses. ESL model cannot visualize local imperfection, however local imperfections have been considered in the non-linear stiffness of ESL.

The mesh convergence study of 3D FE and ESL models is carried out to determine the element size that gives a reasonably accurate result. The convergence is achieved when further mesh refinement does not yield significant changes in the ultimate strength. In 3D simulations, the same result is obtained with mesh size of 25×25 mm and 50×50 mm. In ESL models, 50×50 mm mesh gives nearly the same result as 100×100 mm mesh. Therefore, for saving computational time, the element sizes used in continuation for 3D FE and ESL models are 50×50 mm and 100×100 mm, respectively.

3.2. Numerical validation of ESL under shear

The presented ESL method is validated with two stiffened panel simulations from literature. The details of the panel configurations and material properties are given in Table 1. Loughlan and Hussain [32] considered a stiffened panel with a single stiffener, while model of

Wang et al. [5] had three stiffeners. In both models, elastic-perfectly plastic material properties without strain hardening were used.

First, the 3D FEM simulation results under pure shear agree well with reference analysis where also pure shear boundary conditions were used (Fig. 8). This in general validates the adopted simulation methodology and boundary conditions. At the beginning, the slope of the curves (stiffness) is linear until the structure undergoes local plate buckling which is marked by "×". Once buckling occurs, the stiffness gradually decreases until the maximum shear stress is achieved. The corresponding ESL simulation can capture both the shear buckling response and ultimate shear strength quite accurately.

Besides pure shear, the response of the panels is also analyzed under simple shear. First, it is instructive to explain why these analyses under simple shear are conducted. In simple shear (Fig. 4(c)), as opposed to pure shear (Fig. 4(b)), two panel edges are kept straight during simulation. This allows imposing both shear and compression loads in a single simulation either in sequence or in parallel, and more importantly, provides a way to post-process and compare the simulation results in a consistent manner. Such combined analyses are presented in Section 4. The analyses presented here demonstrate the difference in response between the two types of shear loads.

The boundary conditions for simple shear are given in Fig. 6. Namely, the edges where shear displacement is applied do not move axially (transverse to shear direction). Comparing the 3D FEM numerical simulation results in Fig. 8(a), it is clear that variations between the curves are small and that for all practical purposes it is reasonable to assume that both boundary conditions lead to same response. Note that under much larger deformations (more than 10% strain) the differences between pure and simple shear can be quite significant, e.g. see [36]. The ESL simulation results with panels under simple shear practically overlapped to ones obtained under pure shear. While the A_{13} stiffness does not affect the magnitude of shear stress, it captures the axial stress very well as can be seen in Fig. 8(b).

Additionally, axial stress–shear strain curves presented in Fig. 8(b) show that the axial stress under pure shear is much smaller than one under simple shear. Before shear buckling occurs (indicated with the "×" mark), the axial stress is relatively small under simple shear. Notable increase in axial stress occurs after shear buckling. This increase in axial stress is captured accurately when A_{13} stiffness is included in the ESL definition. In contrast, ESL with $A_{13} = 0$ gives very small axial stress. This component of axial stress is caused by the axial stretching of the element when panel is under shear. Thus, ESL needs to consider contribution from the shear load when modeling the axial force.

3.3. Experimental validation of the ESL under shear

In-plane shear experiments with composite stiffened panels described in Bai et al. [37] are used to validate ESL simulations. Panels are subjected to pure shear condition by application of tensile loads at the diagonal ends. Testing configuration and material are described in [37]. Namely, unit cell analyses were performed with orthotropic material properties to capture the composite behavior. For these properties, elastic modulus along the X and Y, in-plane shear modulus and Poisson's ratio are 177 GPa, 8.05 GPa, 4.37 GPa and 0.32, respectively. The stiffened panel consists of four stiffeners and two transverse frames. In ESL model, stiffeners are removed, but transverse frames are still modeled in detail.

Fig. 9(a) compares the shear load–displacement curves and deflection contours between experimental, 3D FEM, and ESL results. The response generated by ESL captures the trend of 3D FEM and experiment well. The maximum load is 11.51% higher compared with experiments. Furthermore, at the ultimate strength, deflection contours in simulations (ESL and 3D FEM) show good correlation with experimentally observed two wavelength patterns as shown in Fig. 9(b). This is consistent with the result presented in Fig. 8, which shows that A_{13} stiffness has little effect on the change of the shear stress, but has a great impact on changes in axial stress.
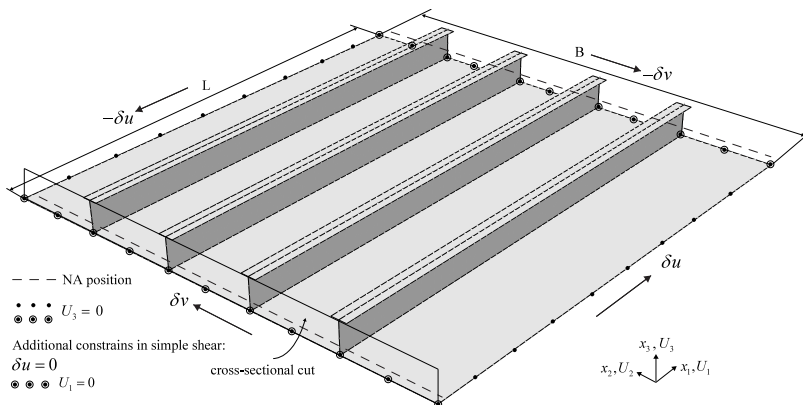
Fig. 6. Loading and boundary conditions on idealized stiffened panel under pure shear. Legend explains modification of these boundary conditions for the case study analysis in Section 4.1.

Table 1

Dimension and material properties of two stiffened panel configurations. t_p, t_w, and t_f are the plate, web, and flange thicknesses, respectively, h_w is the web height, b_f is the breadth of flange, and $l_p \times b_p$ are the length and breadth of stiffened panel, respectively. E, v, and σ_Y are the elastic modulus, Poisson's ratio, and yield stress of material.

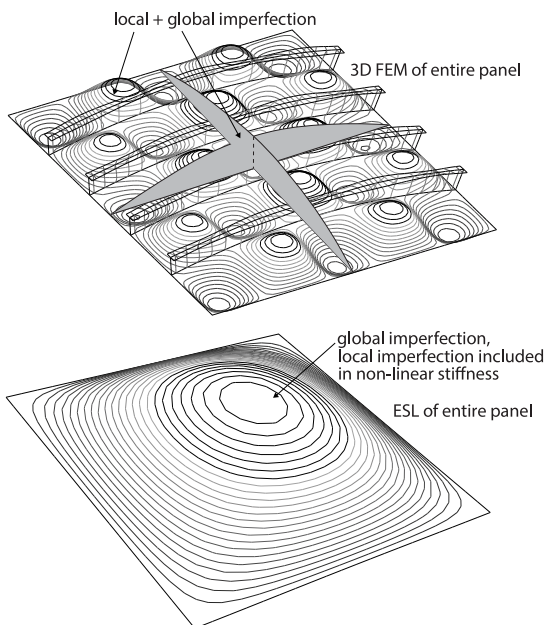| Stiffened panel	$l_p \times b_p \times t_p$ (mm)	$h_w \times t_w$ (mm)	$b_f \times t_f$ (mm)	E (GPa)	v	σ_Y (MPa)
Loughlan and Hussain [32]	$1000 \times 500 \times 5$	12.5×5	–	71.7	0.33	300
Wang et al. [5]	$2850 \times 3400 \times 5$	350×9	125×13	205.8	0.3	350

Fig. 7. Global and local imperfections applied in the 3D FEM and ESL models.

3.4. Experimental validation of the ESL under compression

Under compression load, stiffened panels may experience different collapse modes depending on the geometric configuration. It is well established that these collapse modes, and interaction between different modes, can be predicted using detailed 3D non-linear FE simulations.

However, to make sure the results are valid, the experimental results can be used for comparison. In this section, two experiments from Xu and Soares [38] and Paik et al. [39] are used. They consist of four longitudinal stiffeners and two transverse frames. However, the resulting collapse modes of the two specimens are different. In ESL model, stiffeners in the x direction are removed and considered only in UC model, as can be seen in Figs. 10 and 11.

In the experiment of Xu and Soares [38], stiffened panel called FB3B2F6 experiences an overall collapse of plating and stiffener at the ultimate point, as can be seen in Fig. 10. Relationship between actual measured stress to yield stress ratio (S_a/S_y) and actual measured strain to yield strain ratio ($\varepsilon_a/\varepsilon_y$) is presented. The stiffened panel is deflected upward so that the stiffeners experience tension and the plates suffer global buckling because of compression. This deformation behavior is the same as predicted by the updated ESL model. In this case, A_{13} stiffness has no effect on changes in axial stress since no shear load is applied. Additionally, a good agreement is obtained regarding prediction of the ultimate strength where the updated ESL result is 10.7% greater than the experiment, which could be due to different geometric imperfections in experiments and potential residual stresses not considered in simulations. Initial stiffness of stiffened panel in the test is slightly smaller than one in the updated ESL and 3D FEM models, since panels were not fully in contact with support during initial displacement in the test.

In the experiment of Paik et al. [39], collapse mode is stiffener tripping and plate local buckling; this behavior can be captured by 3D FEM simulation, as can be seen in Fig. 11. In updated ESL model, stiffener tripping cannot be visualized since they are not modeled; however, the response is captured in the unit cell analysis. Because the ESL approach adheres to the homogenization theory, the location of stiffener tripping at the ultimate point cannot be predicted accurately. Therefore, there is a decrease of ESL accuracy in comparison to the experiment; ESL overestimates ultimate strength by 13.1%.

4. Case studies

In this section, the loading scenarios of combined in-plane shear and compression with several stiffened panel configurations studied
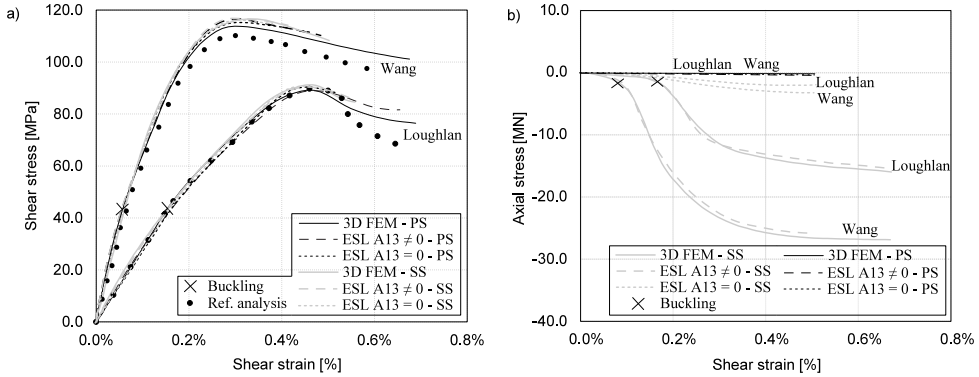
Fig. 8. Responses of (a) shear stress–shear strain curves of panel and (b) axial stress–shear strain curves of panel under simple (SS) and pure shear (PS).
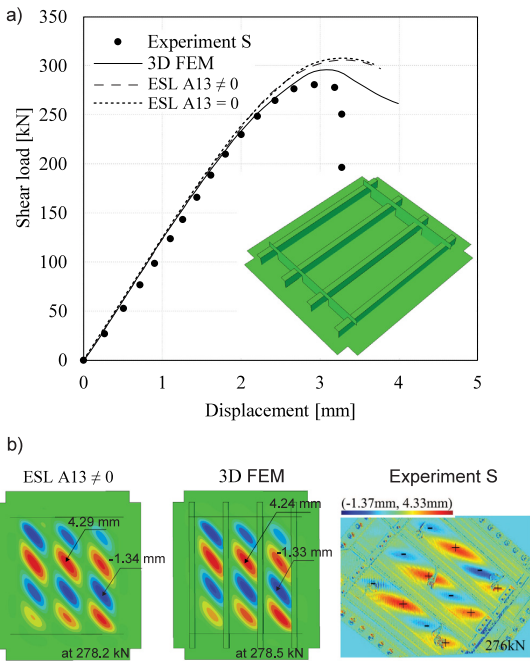

Fig. 9. (a) Shear load–displacement curves and (b) deflection contours for ESL, 3D FEM, and shear test from Bai et al. [37].

are explained. These loading scenarios are presented in Fig. 12. The considered panels are representative of ones used in ship structures. The baseline configuration denoted as SP1 in Table 2 corresponds to a flat plate with four T-shaped longitudinal stiffeners with the spacing of 600 mm. To obtain different failure modes, the baseline configuration is modified. To decrease buckling strength of the stiffener, the flange of SP1 is removed forming SP2. In SP3, the web height is increased compared with SP1 so that the stiffener may be expected to experience torsional buckling (tripping). In SP4, the configuration is the same as SP3 but without the flange in order to analyze the stiffener web buckling for slender flat bars. The web slenderness ratio is calculated based on Eq. (11) [40]:

$$\beta = \frac{h_w}{t_w} \sqrt{\frac{\sigma_0}{E}} \qquad (11)$$

To prevent local web buckling, classification society rules stipulate maximum allowed slenderness of $\beta_c \leq \left(C_w / \sqrt{\sigma_0} \right) \sqrt{\sigma_0 / E}$ where σ_0 is the yield stress, E is the Young's modulus, C_w is the coefficient of stiffener type of 282 and 400 for flat bar and T-profile, respectively. Accordingly, maximum slenderness for flat bar webs is $\beta_c = 1.96$ and for stiffeners with flange $\beta_c = 2.78$. As seen in Table 2 the case study profiles were designed more slender than allowed by class rules with purpose to trigger easier buckling and thereby, challenge the ESL to capture the response. The assumption here was that when ESL methodology can capture the response in these more challenging cases, it will also work for more conventional cases compliant with class rules.

4.1. Loading scenarios

The panels were subjected to combined in-plane shear and compressive loading. Shear to compression ratio (denoted as τ/σ) was varied as $\tau/\sigma = 0$, 1 and 2. According to DNV [34], the maximum shear to compression ratio in ships is 1, however, this ratio is increased to 2 for more thorough analysis. Furthermore, the loads are imposed either simultaneously or sequentially. To account for various conditions encountered in practice, the panels are subjected to uniform lateral pressure of 3 bar. The loading scenarios are shown in Fig. 12.

In-plane shear application is slightly different compared with validation case studies performed in Section 3. Instead of relaxed pure shear, boundary conditions on the panels correspond to relaxed simple shear as shown in Fig. 4(c). Under simple shear there is no imposed shear displacement in the same direction where compression is imposed (δu), thus shear will not interfere with compression loading. Thereby, it is easier to compare the axial force–strain curves between the pure compression ($\tau/\sigma = 0$) and combined loading ($\tau/\sigma = 1$ and $\tau/\sigma = 2$).

Compression displacement is applied in the stiffener direction at the neutral axis, as shown in Fig. 6. Shear displacement is applied in the nodes of the plate and stiffeners. During compression, the nodes in the plate of loaded edges have to move simultaneously in the axial direction. However, the plate may deform non-linearly as the plate and stiffeners have different stiffness. In order to keep loaded edges of the plate straight, equation constraints were used in the corresponding nodes to enforce the same axial displacement (periodic U_1) along the loaded edge. Moreover, to avoid a local web buckling due to applied displacement in the neutral axis, the thickness of local elements (1 row of elements) of the web is increased five times. Vertical translations at plate edges are restrained by setting $U_3 = 0$. These boundary conditions result in simply supported stiffened panel.

To consider the material non-linearity, elastic–plastic steel properties are employed with an initial yield stress of $\sigma_0 = 355$ MPa and flow
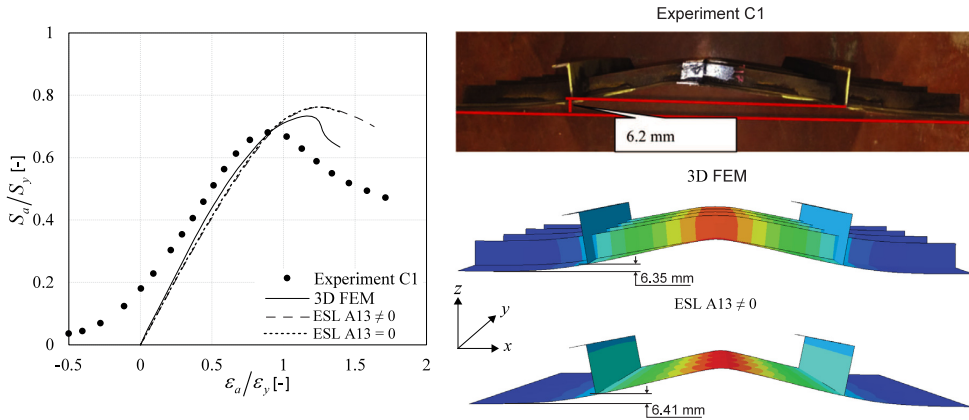
Fig. 10. Load-end shortening curves and deformation behavior for updated ESL, 3D FEM and compression test from Xu and Soares [38].
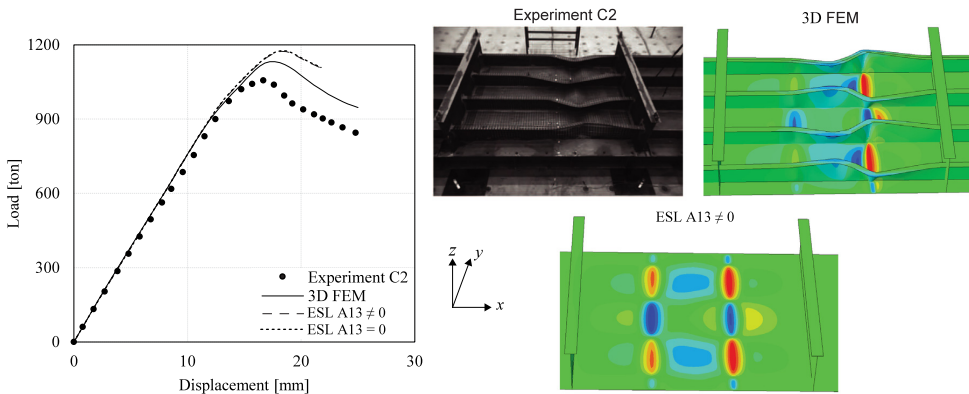

Fig. 11. Load-end shortening curves and deformation behavior for updated ESL, 3D FEM and compression test from Paik et al. [39].
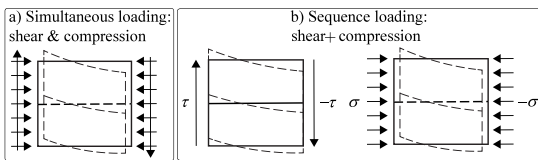

Fig. 12. (a) Simultaneous and (b) sequence loading scenarios in stiffened panel case study analyses. Only single stiffener shown for illustrative purposes.

stress given as

$$\sigma_f(\bar{\varepsilon}) = \begin{cases} \sigma_0 & \text{if } \bar{\varepsilon} \leq \varepsilon_L \\ K(\bar{\varepsilon}_0 + \bar{\varepsilon})^n & \text{if } \bar{\varepsilon} > \varepsilon_L \end{cases} \qquad (12)$$

where $\bar{\varepsilon}_0 = (\sigma_0/K)^{1/n} - \varepsilon_L$, $\bar{\varepsilon}$ is the effective plastic strain, $\varepsilon_L = 0.006$ is the plateau strain, and $K = 530$ MPa and $n = 0.26$ are the parameters of work hardening.

5. Results and discussions

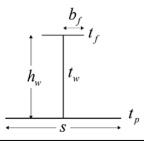### 5.1. Effect of shear to compression ratio

In this section, the ultimate strength of stiffened panel is analyzed based on the effect of load ratio. Shear and compression loads are

applied simultaneously. In general, higher shear to compression load ratio reduces panel's stiffness in post-buckling stage. In Fig. 13(a), SP1 configuration shows that maximum load carried by the panel reduces about 35% when pure compression ($\tau/\sigma = 0$) is accompanied by the shear ($\tau/\sigma = 2$). Moreover, similar reduction in ultimate strength is observed for all other stiffened panel configurations, see Fig. 13(b,c,d). Clearly, reduction of ultimate strength is caused by the increase of shear load. As already suggested by the analysis of Fig. 5, the shear load generates an additional axial force component. Furthermore, the deflection at the ultimate point is presented in Fig. 13(a) on the right hand side. It is clear that by increasing the load ratio, the out-of-plane deformation is getting larger. Comparative simulations are performed with the ESL method. In Fig. 13(a), ESL with $A_{13} \neq 0$ predicts the response with very good accuracy despite the increasing shear component. In contrast, the accuracy of the ESL without A_{13} component (ESL $A_{13} = 0$) deteriorates considerably more with increasing shear.

5.2. Effect of collapse mode

Stiffened panel collapse mode is highly dependent on structural configuration. Collapse mode in SP1 configuration indicates a failure pattern in which the ultimate strength occurs due to combination of local and global plate buckling. In this mode, a failure of plate–stiffener combination is typically evident at mid-span, which is often referred to as a plate-induced failure [41]. Under this collapse mode, local and

Table 2
Panel configurations used in the analysis.

Name	L × B × t_p (mm)	h_w × t_w (mm)	b_f × t_f (mm)	β	Configuration
SP1	3000 × 3000 × 6	200 × 7	50 × 6	1.18	Baseline
SP2	3000 × 3000 × 6	200 × 7	–	1.18	Flat bar
SP3	3000 × 3000 × 6	450 × 7	50 x 6	2.66	Slender stiffener
SP4	3000 × 3000 × 6	450 × 7	–	2.66	Slender stiffener made of flat bar

global deflections occur simultaneously either for $\tau/\sigma = 0$ or $\tau/\sigma = 2$, as can be seen in Fig. 13(a). The stiffener web does not buckle under pure compression. However, stiffener web buckling occurs on increasing shear load and causes the ESL accuracy to decrease slightly, as can be seen in Fig. 16. The updated ESL predicts load-end shortening curves accurately including local and global buckling for this collapse mode.

Compared to SP1 configuration, in SP2 the stiffener flange is removed. This reduces the shear resistance of the stiffened panel [42] and allows higher local deformations in the stiffener web. Consequently, bending stiffness of the stiffener is reduced thus it buckles easier, see Fig. 13(b). Stiffener web buckling under compression is well captured by the updated ESL formulation which includes A_{13} stiffness component considering an increased shear, as can be seen in Fig. 13(b).

SP3 has significantly more slender stiffeners than SP1. Stiffener tripping occurs in SP3 under pure compression, however the collapse mode is different when shear is applied. Under combined shear and compression load, this type of stiffener reduces the buckling load of stiffeners and promotes interaction between local plate and stiffener web buckling modes. Consequently, compared to local and global plate buckling and smooth response displayed by SP1 panel for combined load in Fig. 13(a), the response curve of SP3 in Fig. 13(c) displays more pronounced bifurcation to post-buckling stage especially for the case $\tau/\sigma = 2$. Overall, increasing shear load has similar degrading effect on ultimate strength as in previous configurations. For this complicated scenario the updated ESL overestimates the initial elastic buckling load, but overall trend is still well captured.

SP4 configuration has the same overall dimensions as SP3, except that stiffener flange is removed. This type of profile is prone to a more excessive local buckling of stiffener web. Comparing the collapse modes of SP3 and SP4 in Figs. 13(c) and (d), the stabilizing effect of flange is obvious. Nevertheless, the removal of flange only marginally reduces the ultimate strength as seen in Fig. 13(d). Ultimate strength obtained from 3D FEM results is still well predicted by the updated ESL, however the accuracy decreases with increasing shear.

5.3. Effect of lateral pressure

Lateral pressure effect is studied with two panel configurations: SP1 and SP3, see Fig. 14. Lateral pressure is applied simultaneously with shear and compression loads. Recall that without lateral pressure SP1 led to a local and global plate buckling mode while SP3 exhibited complex interactive mode with local plate buckling and stiffener tripping. Lateral pressure contributes to an increase in bending moment, which in turn will cause a higher global deflection before the axial and shear load applications. Since the collapse mode does not change, but the load required to attain the global collapse mode is reduced, overall ultimate strength of SP1 is significantly reduced under lateral pressure. Under the same pressure, higher section modulus of SP3 panel leads to a lower global deflections compared with SP1. Furthermore, since collapse of SP3 was dictated by local modes, the ultimate strength of SP3 is not significantly affected by lateral pressure. The ESL accuracy decreases with the application of pressure. One would assume that this is because pressure is not included in the unit cell analysis. Subsequent

consideration of pressure in UC simulations did not rectify the situation. These results are not shown for brevity.

The differences in pressure effect on these two panels deserve a further insight. It is clear that under pressure the ESL response of SP1 panel is too stiff (Figs. 13(a) vs. 14(a)). Further comparison of panel response showed that lateral pressure shortens the elastic buckling wavelength. Since this cannot be accounted for with square-shaped unit cell (UC) the new set of stiffness properties were determined with rectangular UC which is doubled in length. As the rectangular UC can accommodate the global deflection more easily the buckling wavelength effect will be now included in stiffness matrices. In the SP1 panel, ESL results with stiffness obtained from rectangular UC analysis show clear improvement in Fig. 14(a) (curve with gray overlay). In Fig. 14(b), similar approach adopted to SP3 panel, whereby stiffness is obtained by rectangular UC, did not yield any improvements since panel did not experience global deflection under pressure and thus, no change in buckling wavelength. These analyses show that UC size is an important parameter that should be further investigated.

5.4. Effect of loading sequence

In contrast to previous analysis where shear and compression acted simultaneously, the loads here are applied in sequence with shear applied first, followed by compression. Shear loads induce an axial force as can be seen in Fig. 15(a). After the shear buckling, the axial force increases significantly. At point A, the axial force magnitude of -1.12 MN is captured at the end of the shear simulation for $\tau = 2\sigma$. This force will be the starting value for the compression load in the next step, as shown in Fig. 15(b). Due to this starting position, the initial axial force for $\sigma = \tau/2$ is negative, however, the maximum axial force is not significantly affected by the amount of shear load applied at the beginning. As the shear load increases at the beginning, the panel begins to buckle in shear, causing a different initial stiffness under compression. This sequence loading is less critical than simultaneous loading, thereby providing higher buckling load. ESL with $A_{13} = 0$ cannot capture accurately the initial axial force due to shear loading. Updated ESL, on the other hand, closely matches the 3D model result.

5.5. Summary of the results

All the case study analyses are summarized in Fig. 16 in terms of normalized maximum load. Normalization of ultimate load is done with respect to 3D FEM results. Under pure compression ($\tau/\sigma = 0$), load-end shortening curves of ESL with $A_{13} = 0$ and $A_{13} \neq 0$ show relatively similar results. The axial force represented by A_{13} stiffness does not have a role when panels are subjected to pure compression. However, the contribution from A_{13} stiffness introduced to the ESL framework in this paper becomes significant when shear force is increased ($\tau/\sigma = 1$ and 2). Namely, ESL with $A_{13} \neq 0$ yields more accurate results than one with $A_{13} = 0$. In the worst-case scenario (SP4, $\tau/\sigma = 2$), ESL with $A_{13} \neq 0$ overestimates the ultimate load by 14% while this one for $A_{13} = 0$ overestimates the load by 35%.
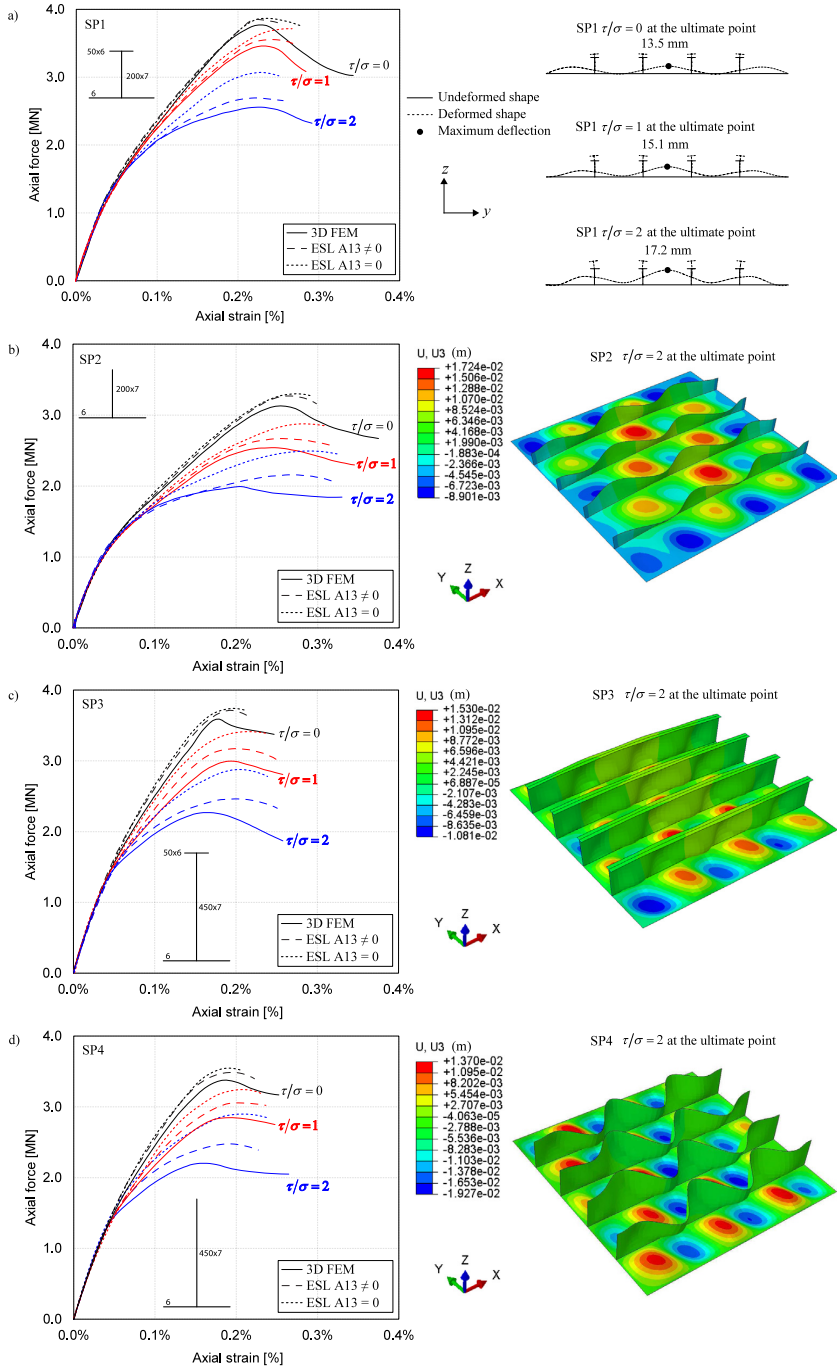
Fig. 13. Axial force-strain curves and collapse modes of (a) SP1, (b) SP2, (c) SP3, and (d) SP4 in variation of shear to compression ratios.

Comparison of results in Fig. 16 further shows that the accuracy of ESL is affected by the collapse mode of stiffened panel. ESL gives more accurate results for collapse mode consisting of local and global

plate buckling mode (SP1) compared with modes where stiffener web buckling is active (SP2, SP3 and SP4). Clearly, the extreme local buckling of stiffener web mode observed in SP4 case is not well handled
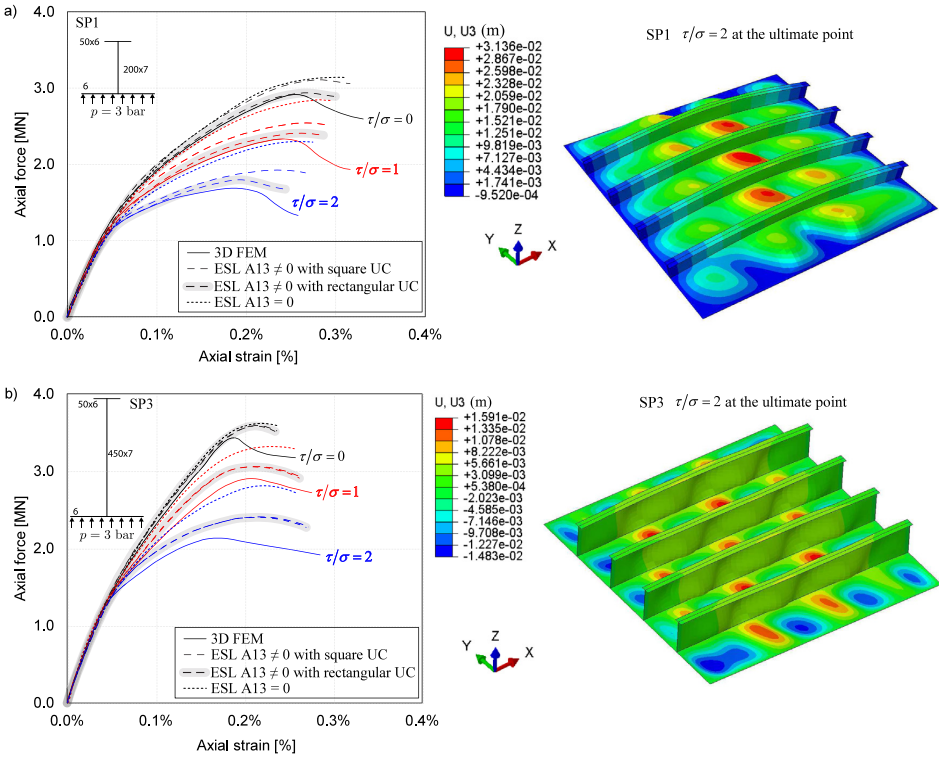
Fig. 14. Axial force–strain curves and structural behavior of (a) SP1 and (b) SP3 with lateral pressure of 3 bar in variation of shear to compression ratios.
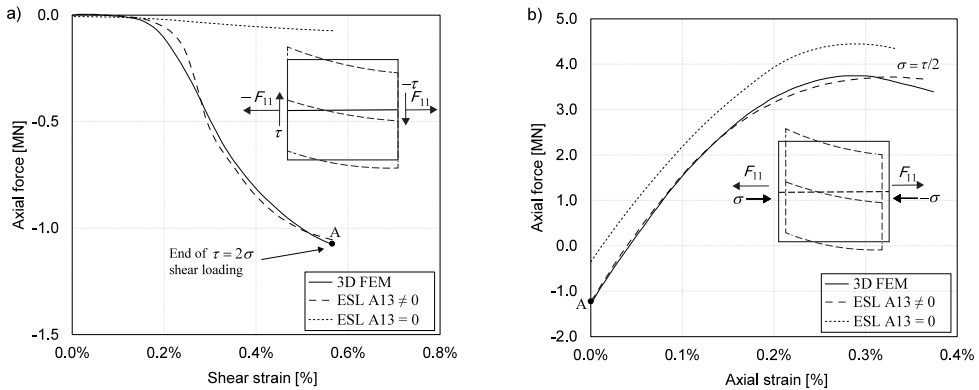

Fig. 15. Numerical results of SP1 for (a) axial force–shear strain curves under shear (first load) followed by; (b) axial force–axial strain for under compression (second load).

by ESL method. Additionally, when lateral pressure is added, there is an increasing global buckling. To obtain good ESL accuracy under lateral pressure, UC length should account for buckling wavelength.

Possible reason for the reduced accuracy of the ESL in case of significant local buckling of stiffener web is that the unit cell is not adjusted for this kind of failure mode. Suitable unit cell model for tripping should be developed in future.

6. Conclusion

In this paper, ESL stiffness is modified by including the effect of in-plane shear (A_{13}). The A_{13} stiffness models the axial force due to shear load. The modified ESL can model the ultimate strength of stiffened panel under combination of compression and shear. The shear component in ESL stiffness matrix is calculated by simulating the response of the unit cell with periodic boundary condition. Validation of ESL is carried out using 3D FEM and experimental results from
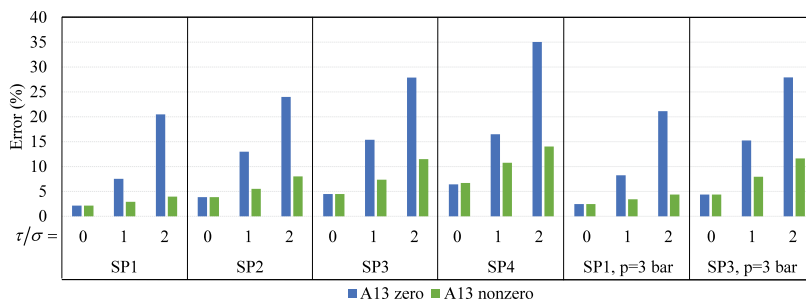
Fig. 16. Error percentages of ultimate strength resulted from ESL for all loading conditions and stiffened panel configurations.
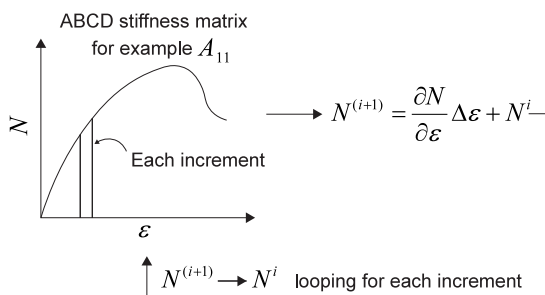

Fig. A.1. Inner workings for UGENS subroutine.

literature. Several stiffened panel configurations are chosen in order to obtain different collapse modes. Shear to compression ratio is varied to examine the change of axial force due to shear load. Furthermore, stiffened panel is subjected to lateral pressure, in addition to other loads. Moreover, two loading sequences are considered.

The purpose of using the ESL approach is to reduce a three-dimensional continuum problem to an equivalent two-dimensional problem, for which numerical modeling effort is significantly reduced. Furthermore, beside modeling effort, the computational effort is also reduced, first because ESL model does not include stiffeners, and second, because coarser mesh is sufficient for ESL in comparison to 3D model. Therefore, number of elements in calculations is reduced. Overall reduction in modeling and computational time is advantageous in optimization of structures since different stiffened panel configurations can be considered by appropriate stiffness matrices circumventing the need for 3D modeling. Current investigation shows that despite the homogenization the response in terms of critical buckling load and deflection for several geometric configurations of stiffened panels is captured with good accuracy.

The ESL accuracy depends on the configurations of the stiffened panel, which is related to the resulting collapse mode. In general, for the combinations of compression and shear, the differences in ultimate strength results between ESL and 3D FEM are 3%–14% with ESL showing consistently more stiffer response. In this study, the lowest accuracy was observed for SP4 where the stiffener is more slender than in other configurations. Additionally, application of lateral pressure decreases the ESL accuracy. This was due to the shortened buckling wavelength under pressure when panel experienced global bending due to pressure. Square-shaped unit cell was not able to capture this, while rectangular unit cell did and thus, provided more accurate response. When panel did not bend globally, the application of pressure did not affect the ESL response. These results suggest that it is advisable to include pressure in unit cell analysis, while unit cell size should be further investigated. Change of the loading sequence from simultaneous to sequence loading

did not negatively affect the ultimate strength predictions with the modified ESL. Future research may consider unit cell analysis aimed at improving ESL accuracy in case of predominant local buckling of stiffener web and under more complex loading condition.

CRediT authorship contribution statement

Teguh Putranto: Conceptualization, Investigation, Methodology, Validation, Writing – original draft, Writing – review & editing. **Mihkel Kõrgesaar:** Conceptualization, Project administration, Supervision, Writing – review & editing. **Jasmin Jelovica:** Conceptualization, Project administration, Writing – review & editing.

Declaration of competing interest

The authors declare that they have no known competing financial interests or personal relationships that could have appeared to influence the work reported in this paper.

Acknowledgments

Appendix A

UGENS subroutine is a user-defined subroutine available in the Abaqus software that is used to represent the non-linear mechanical behavior of shell element. Fig. A.1 shows the inner workings of UGENS subroutine. Membrane force and bending moment are obtained from the six loading conditions of a unit cell. The first derivative of these curves is the ESL stiffness coefficient ($\partial N/\partial\varepsilon$). The resulting force and moment are calculated from the multiplication of strain increment ($\Delta\varepsilon$) and stiffness coefficient. For the first increment, N^i is zero. For the next increment, $N^{(i+1)}$ becomes N^i. This process is repeated from the first increment to the last increment. At each increment, the total strain changes and affects the calculation of the stiffness coefficient.

Appendix B

The relation between stress resultants (N_{ij}, M_{ij}) and strains (ε_{ij}^0, γ_{ij}^0, ε_{ij}^1, γ_{ij}^1) is given by [25]:

$$
\begin{bmatrix}
N_{11} \\
N_{22} \\
N_{12} \\
M_{11} \\
M_{22} \\
M_{12}
\end{bmatrix}
=
\begin{bmatrix}
A_{11} & A_{12} & A_{13} & B_{11} & B_{12} & 0 \\
A_{21} & A_{22} & 0 & B_{21} & B_{22} & 0 \\
A_{31} & 0 & A_{33} & 0 & 0 & B_{33} \\
C_{11} & C_{12} & 0 & D_{11} & D_{12} & 0 \\
C_{21} & C_{22} & 0 & D_{21} & D_{22} & 0 \\
0 & 0 & C_{33} & 0 & 0 & D_{33}
\end{bmatrix}
\begin{bmatrix}
\varepsilon_{11}^0 \\
\varepsilon_{22}^0 \\
\gamma_{12}^0 \\
\varepsilon_{11}^1 \\
\varepsilon_{22}^1 \\
\gamma_{12}^1
\end{bmatrix}
\tag{B.1}
$$

where the calculation of $ABCD$ stiffnesses are expressed by:

$$
\begin{bmatrix}
A_{11} & A_{12} & A_{13} & B_{11} & B_{12} & 0 \\
A_{21} & A_{22} & 0 & B_{21} & B_{22} & 0 \\
A_{31} & 0 & A_{33} & 0 & 0 & B_{33} \\
C_{11} & C_{12} & 0 & D_{11} & D_{12} & 0 \\
C_{21} & C_{22} & 0 & D_{21} & D_{22} & 0 \\
0 & 0 & C_{33} & 0 & 0 & D_{33}
\end{bmatrix}
=
$$

$$
\begin{bmatrix}
\frac{\partial N_{11}}{\partial \varepsilon_{11}^0} & \frac{\partial N_{11}}{\partial \varepsilon_{22}^0} & \frac{\partial N_{11}}{\partial \gamma_{12}^0} & \frac{\partial M_{11}}{\partial \varepsilon_{11}^0} & \frac{\partial M_{11}}{\partial \varepsilon_{22}^0} & 0 \\
\frac{\partial N_{22}}{\partial \varepsilon_{11}^0} & \frac{\partial N_{22}}{\partial \varepsilon_{22}^0} & 0 & \frac{\partial M_{22}}{\partial \varepsilon_{11}^0} & \frac{\partial M_{22}}{\partial \varepsilon_{22}^0} & 0 \\
\frac{\partial N_{11}}{\partial \varepsilon_{11}^0} & 0 & \frac{\partial N_{11}}{\partial \gamma_{12}^0} & 0 & 0 & \frac{\partial M_{12}}{\partial \gamma_{12}^0} \\
\frac{\partial N_{11}}{\partial \varepsilon_{11}^1} & \frac{\partial N_{11}}{\partial \varepsilon_{22}^1} & 0 & \frac{\partial M_{11}}{\partial \varepsilon_{11}^1} & \frac{\partial M_{11}}{\partial \varepsilon_{22}^1} & 0 \\
\frac{\partial N_{22}}{\partial \varepsilon_{11}^1} & \frac{\partial N_{22}}{\partial \varepsilon_{22}^1} & 0 & \frac{\partial M_{22}}{\partial \varepsilon_{11}^1} & \frac{\partial M_{22}}{\partial \varepsilon_{22}^1} & 0 \\
0 & 0 & \frac{\partial N_{12}}{\partial \gamma_{12}^1} & 0 & 0 & \frac{\partial M_{12}}{\partial \gamma_{12}^1}
\end{bmatrix}
\tag{B.2}
$$

The transverse shear forces are expressed as follows:

$$
\begin{bmatrix}
Q_1 \\
Q_2
\end{bmatrix}
=
\begin{bmatrix}
D_{Q1} & 0 \\
0 & D_{Q2}
\end{bmatrix}
\begin{bmatrix}
\gamma_{13} \\
\gamma_{23}
\end{bmatrix}
\tag{B.3}
$$

where D_{Q1} and D_{Q2} are the shear stiffnesses of the ESL in the stiffener direction and transverse to the stiffener, respectively. These stiffnesses are calculated by [43]:

$$
D_{Q1} = k_{13} \left(G_p t_p + G_w h_w + G_f t_f \right) \tag{B.4}
$$

$$
D_{Q2} = k_{23} G_p t_p \tag{B.5}
$$

where t_p is the plate thickness, h_w is the web height, and t_f is the flange thickness. k_{12} is the shear correction factor in the stiffener direction which is calculated from the average shear stress $\left(\tau_{xz} \right)_{avg}$ divided by the maximum shear stress $\left(\tau_{xz} \right)_{max}$ and the value varies around 0.7–0.8 [43]. k_{23} is the shear correction factors in the perpendicular to stiffener direction and is 5/6. The shear moduli of the web (G_w) and flange (G_f) are a function of the plate (G_p) and calculated from the following equation:

$$
G_w = G_p \frac{t_w}{s} \tag{B.6}
$$

$$
G_f = G_p \frac{b_f}{s} \tag{B.7}
$$

where t_w is the web thickness, b_f is the breadth of flange, and s is the stiffener spacing.

References

[1] J.K. Paik, B.J. Kim, Ultimate strength formulations for stiffened panels under combined axial load, in-plane bending and lateral pressure: a benchmark study, Thin-Walled Struct. 40 (1) (2002) 45–83, http://dx.doi.org/10.1016/S0263-8231(01)00043-X.

[2] D.G. Stamatelos, G.N. Labeas, K.I. Tserpes, Analytical calculation of local buckling and post-buckling behavior of isotropic and orthotropic stiffened panels, Thin-Walled Struct. 49 (3) (2011) 422–430, http://dx.doi.org/10.1016/j.tws.2010.11.008.

[3] M. Shama, Torsion and shear stresses in ships, in: Torsion and Shear Stresses in Ships, Springer, Berlin Heidelberg, 2010, pp. 1–277, http://dx.doi.org/10.1007/978-3-642-14633-6.

[4] T. Yao, M. Fujikubo, Buckling/plastic collapse behavior and strength of rectangular plate subjected to uni-axial thrust, in: Buckling and Ultimate Strength of Ship and Ship-Like Floating Structures, Elsevier, 2016, pp. 75–155, http://dx.doi.org/10.1016/B978-0-12-803849-9.00004-6.

[5] F. Wang, J.K. Paik, B.J. Kim, W. Cui, T. Hayat, B. Ahmad, Ultimate shear strength of intact and cracked stiffened panels, Thin-Walled Struct. 88 (2015) 48–57, http://dx.doi.org/10.1016/J.TWS.2014.12.001.

[6] M. Gaiotti, M. Fujikubo, N. Grasso, C.M. Rizzo, Effect of shear stresses on the ultimate strength of the hull girder of a containership, Int. J. Offshore Polar Eng. 26 (2016) 183–191, http://dx.doi.org/10.17736/IJOPE.2016.JC649.

[7] S. Zhang, P. Kumar, S.E. Rutherford, Ultimate shear strength of plates and stiffened panels, 3 (2008) 105–112. http://dx.doi.org/10.1080/17445300701739642.

[8] D.C. da Silva, M.V. Donadon, M.A. Arbelo, A semi-analytical model for shear buckling analysis of stiffened composite panel with debonding defect, Thin-Walled Struct. (2021) 108636, http://dx.doi.org/10.1016/J.TWS.2021.108636.

[9] E.B. Machaly, S.S. Safar, M.A. Amer, Numerical investigation on ultimate shear strength of steel plate shear walls, Thin-Walled Struct. 84 (2014) 78–90, http://dx.doi.org/10.1016/J.TWS.2014.05.013.

[10] Y. Peng, Y. Ma, W. Sun, W. Zhang, Z. Wang, Z. Yang, Buckling fatigue behavior of 2a97 al-li alloy stiffened panels under shear loading, Eng. Fail. Anal. 128 (2021) http://dx.doi.org/10.1016/J.ENGFAILANAL.2021.105575.

[11] Z.Y. Wang, F. Yuan, Y. Chen, Q. Wang, T. Chen, X. Zhou, Z. Liu, Fatigue resistance of post-buckled slender trapezoidal corrugated webs in girders with stiff flanges, Eng. Struct. 198 (2019) 109478, http://dx.doi.org/10.1016/J.ENGSTRUCT.2019.109478.

[12] M.F. Hassanein, O.F. Kharoob, Behavior of bridge girders with corrugated webs: (I) real boundary condition at the juncture of the web and flanges, Eng. Struct. 57 (2013) 554–564, http://dx.doi.org/10.1016/J.ENGSTRUCT.2013.03.004.

[13] N.A. Dos Santos Rizzo, D. Do Amaral Amante, S.F. Estefen, Ultimate shear strength of stiffened panels for offshore structures, in: Proceedings of the International Conference on Offshore Mechanics and Arctic Engineering-OMAE, Vol. 4A, American Society of Mechanical Engineers (ASME), 2014, http://dx.doi.org/10.1115/OMAE2014-23155.

[14] U.K. Mallela, A. Upadhyay, Buckling load prediction of laminated composite stiffened panels subjected to in-plane shear using artificial neural networks, Thin-Walled Struct. 102 (2016) 158–164, http://dx.doi.org/10.1016/J.TWS.2016.01.025.

[15] N. Hussain, J. Loughlan, Buckling and post-buckling performance of stiffened webs subjected to interactive shear and compression, in: Eighth International Conference on Thin-Walled Structures-ICTWS 2018, Lisbon, Portugal, July 24-27, 2018, 2018.

[16] Q. Chen, P. Qiao, Post-buckling analysis of composite plates under combined compression and shear loading using finite strip method, Finite Elem. Anal. Des. 83 (2014) 33–42, http://dx.doi.org/10.1016/J.FINEL.2014.01.002.

[17] J. Jelovica, J. Romanoff, S. Ehlers, P. Varsta, Influence of weld stiffness on buckling strength of laser-welded web-core sandwich plates, J. Construct. Steel Res. 77 (2012) 12–18, http://dx.doi.org/10.1016/j.jcsr.2012.05.001.

[18] J. Jelovica, J. Romanoff, Load-carrying behaviour of web-core sandwich plates in compression, Thin-Walled Struct. 73 (2013) 264–272, http://dx.doi.org/10.1016/j.tws.2013.08.012.

[19] J. Jelovica, J. Romanoff, Buckling of sandwich panels with transversely flexible core: Correction of the equivalent single-layer model using thick-faces effect, J. Sandw. Struct. Mater. 22 (5) (2020) 1612–1634, http://dx.doi.org/10.1177/1099636218789604.

[20] E. Avi, A. Laakso, J. Romanoff, H. Remes, I. Lillemäe-Avi, Coarse mesh finite element model for cruise ship global and local vibration analysis, Mar. Struct. 79 (2021) 103053, http://dx.doi.org/10.1016/J.MARSTRUC.2021.103053.

[21] A. Laakso, E. Avi, J. Romanoff, Correction of local deformations in free vibration analysis of ship deck structures by equivalent single layer elements, Ships Offshore Struct. 14 (sup1) (2019) 135–147, http://dx.doi.org/10.1080/17445302.2018.1561173.

[22] J. Jelovica, J. Romanoff, Influence of shear-induced secondary bending on buckling of web-core sandwich panels, in: Proc. 5th MARSTRUCT Conference, Southampton, UK, 2015.

[23] E. Byklum, J. Amdahl, A simplified method for elastic large deflection analysis of plates and stiffened panels due to local buckling, Thin-Walled Struct. 40 (11) (2002) 925–953, http://dx.doi.org/10.1016/S0263-8231(02)00042-3.

[24] E. Byklum, E. Steen, J. Amdahl, A semi-analytical model for global buckling and postbuckling analysis of stiffened panels, Thin-Walled Struct. 42 (5) (2004) 701–717, http://dx.doi.org/10.1016/j.tws.2003.12.006.

[25] B. Reinaldo Goncalves, J. Jelovica, J. Romanoff, A homogenization method for geometric nonlinear analysis of sandwich structures with initial imperfections, Int. J. Solids Struct. 87 (2016) 194–205, http://dx.doi.org/10.1016/j.ijsolstr.2016.02.009.

[26] M. Kõrgesaar, J. Romanoff, H. Remes, P. Palokangas, Experimental and numerical penetration response of laser-welded stiffened panels, Int. J. Impact Eng. 114 (2018) 78–92, http://dx.doi.org/10.1016/j.ijimpeng.2017.12.014.

[27] T. Putranto, M. Kõrgesaar, J. Jelovica, K. Tabri, H. Naar, Ultimate strength assessment of stiffened panel under uni-axial compression with non-linear equivalent single layer approach, Mar. Struct. 78 (2021) http://dx.doi.org/10.1016/J.MARSTRUC.2021.103004.

[28] J.N. Reddy, An evaluation of equivalent-single-layer and layerwise theories of composite laminates, Compos. Struct. 25 (1–4) (1993) 21–35, http://dx.doi.org/10.1016/0263-8223(93)90147-I.

[29] E. Barbero, Introduction to Composite Materials Design, second ed., in: Composite Materials, Taylor & Francis, 2010, URL https://books.google.ee/books?id=fZSan7b5z0IC.

[30] D. Garoz, F. Gilabert, R. Sevenois, S. Spronk, W. Van Paepegem, Consistent application of periodic boundary conditions in implicit and explicit finite element simulations of damage in composites, Composites B 168 (2019) 254–266, http://dx.doi.org/10.1016/j.compositesb.2018.12.023, URL https://www.sciencedirect.com/science/article/pii/S1359836818337776.

[31] H.C. Chang, B.F. Chen, Mechanical behavior of submarine cable under coupled tension, torsion and compressive loads, Ocean Eng. 189 (2019) 106272, http://dx.doi.org/10.1016/J.OCEANENG.2019.106272.

[32] J. Loughlan, N. Hussain, The in-plane shear failure of transversely stiffened thin plates, Thin-Walled Struct. 81 (2014) 225–235, http://dx.doi.org/10.1016/J.TWS.2014.02.027.

[33] D. Faulkner, A review of effective plating for use in the analysis of stiffened plating in bending and compression, J. Ship Res. 19 (01) (1975) 1–17.

[34] G. DNV, Rules for classification: Ships, in: Ships for Navigation in Ice. Det Norske, Vol. 726, 2016.

[35] S. Li, D.G. Georgiadis, D.K. Kim, M.S. Samuelides, A comparison of geometric imperfection models for collapse analysis of ship-type stiffened plated grillages, Eng. Struct. 250 (2022) 113480, http://dx.doi.org/10.1016/J.ENGSTRUCT.2021.113480.

[36] D.C. Moreira, L.C. Nunes, Comparison of simple and pure shear for an incompressible isotropic hyperelastic material under large deformation, Polym. Test. 32 (2) (2013) 240–248, http://dx.doi.org/10.1016/J.POLYMERTESTING.2012.11.005.

[37] R. Bai, Z. Lei, X. Wei, W. Tao, C. Yan, Numerical and experimental study of dynamic buckling behavior of a J-stiffened composite panel under in-plane shear, Compos. Struct. 166 (2017) 96–103, http://dx.doi.org/10.1016/J.COMPSTRUCT.2017.01.022.

[38] M.C. Xu, C.G. Soares, Comparisons of calculations with experiments on the ultimate strength of wide stiffened panels, Mar. Struct. 31 (2013) 82–101, http://dx.doi.org/10.1016/J.MARSTRUC.2013.01.003.

[39] J.K. Paik, D.H. Lee, S.H. Noh, D.K. Park, J.W. Ringsberg, Full-scale collapse testing of a steel stiffened plate structure under cyclic axial-compressive loading, Structures 26 (2020) 996–1009, http://dx.doi.org/10.1016/J.ISTRUC.2020.05.026.

[40] C.G. Daley, K.H. Daley, J. Dolny, B.W. Quinton, Overload response of flatbar frames to ice loads, Ships Offshore Struct. 12 (sup1) (2017) S68–S81, http://dx.doi.org/10.1080/17445302.2016.1254520.

[41] Buckling and ultimate strength of plate–stiffener combinations, in: Ultimate Limit State Analysis and Design of Plated Structures, John Wiley & Sons, Ltd, 2018, pp. 79–133, http://dx.doi.org/10.1002/9781119367758.ch2, Chapter 2.

[42] A. Ayensa, E. Oller, B. Beltrán, E. Ibarz, A. Marí, L. Gracia, Influence of the flanges width and thickness on the shear strength of reinforced concrete beams with T-shaped cross section, Eng. Struct. 188 (2019) 506–518, http://dx.doi.org/10.1016/J.ENGSTRUCT.2019.03.057.

[43] E. Avi, I. Lillemäe, J. Romanoff, A. Niemelä, Equivalent shell element for ship structural design, Ships Offshore Struct. 10 (3) (2015) 239–255, http://dx.doi.org/10.1080/17445302.2013.819689.

Appendix 3

III

T. Putranto, M. Kõrgesaar, and K. Tabri. Application of equivalent single layer approach for ultimate strength analyses of ship hull girder, *Journal of Marine Science and Engineering*, 10(10):1–20, 2022

Article

Application of Equivalent Single Layer Approach for Ultimate Strength Analyses of Ship Hull Girder

Teguh Putranto [1,*](ID), Mihkel Kõrgesaar [1](ID) and Kristjan Tabri [1,2](ID)

1   Department of Civil Engineering and Architecture, Kuressaare College, Tallinn University of Technology, Tallinna 19, 93819 Kuressaare, Estonia

2   Department of Civil Engineering and Architecture, School of Engineering, Tallinn University of Technology, Ehitajate tee 5, 19086 Tallinn, Estonia

*   Correspondence: teguh.putranto@taltech.ee

Abstract: The objective of this paper is to present the application of equivalent single layer (ESL) approach for the ultimate strength assessment of ship hull girder in the context of numerical finite element (FE) simulations. In the ESL approach, the stiffened panel is replaced with a single plate, which has the equivalent stiffness of the original panel. Removal of tertiary stiffening elements from the numerical model facilitates time-savings in pre-processing and FE analysis stage. The applicability of ESL approach is demonstrated with two case studies, one compartment model and full-sized double hull tanker model in intact and damaged conditions. The damage extents are determined based on the international association of classification societies from common structural rules (IACS-CSR) for oil tanker. Ship hull girder is exposed to distributed pressure with the sinusoidal shape that bends the hull girder. This pressure load is applied separately to bottom and side structures to obtain the vertical and horizontal bending moments of the hull girder, respectively. Ultimate strength predictions obtained from ESL approach are compared to full three-dimensional finite element method (3D FEM) and IACS incremental-iterative method. The comparison between different methods is provided in terms of longitudinal bending moment and cross sectional stress distribution. Overall, ESL approach yields good agreement compared to the 3D FEM results in predicting the ultimate strength of ship hull girder while providing up to 3 times computational efficiency and ease of modeling.

Keywords: equivalent single layer; ultimate strength; hull girder; finite element method

1. Introduction

Due to extreme and accidental loads, a ship's hull girder can reach its ultimate load-carrying capacity. One of the fatal consequences of structural failure is that the ship may suffer progressive collapse due to internal and external loads during seafaring. To minimize the risk of such accidents, rules stipulate longitudinal strength assessment for all ships [1,2]. The objective of this assessment is to determine the ultimate strength capacity of ship hull girder when the ship is subjected to bending loads. In case of ship grounding or collision, damaged hull section reduces the bending strength further. Therefore, the ultimate strength assessment must be performed both in intact and damaged conditions to ensure that hull girder has sufficient strength reserve.

Several studies have been conducted to evaluate the ultimate strength of ship hull girder using simplified methods and are currently applied in the classification society and commercial software. Caldwell [3] proposed an equivalent thickness approach to replace stiffened panel and used strength reduction coefficients to consider buckling. Smith [4,5] further refined the strength reduction coefficient method and considered that the ultimate strength of a hull girder is dependent on the strength of individual elements reaching their limit at different times. The Smith's method has been adopted in the Common

Structural Rules for Bulk Carrier and Oil Tanker, but the loading is limited to the vertical bending moment. In parallel, Ueda and Rashed [6] proposed the idealized structural unit method (ISUM) which considers more loading scenarios. For example, ISUM can model the buckling response due to all possible hull girder sectional load components (i.e., vertical bending, horizontal bending, vertical shearing force, horizontal shearing force, and torsion). Several advanced applications of ISUM approach have been developed by Ueda et al. [7], Masaoka et al. [8], Fujikubo et al. [9], Paik et al. [10], as well as Lindemann and Kaeding [11] for ultimate strength analyses of stiffened panel structures in different loading conditions.

The ISUM is recognized as one of the most time efficient methods for progressive collapse analysis of ship hull girder [12]. The method has been implemented in the ALPS/HULL program within the MAESTRO FEM analysis code. The ISUM can deal with interaction between local and global failures [13] for a short section of the ship structure. However, larger models offer a number of advantages. To capture the compartment level buckling relevant for lightweight ship structures [14], a large-scale ship model should be considered. Larger models permit inclusion of actual pressure distributions and various load combinations. Additionally, the model length influences the post-buckling behavior, which ultimately determines the bending moment capacity [15]. Furthermore, full ship model are advocated in [16,17] to minimize the boundary effect which often lead to more conservative, heavier scantlings.

The full three-dimensional finite element method (3D FEM) is an effective tool used for performing progressive collapse analysis to obtain structural strength capacity of ship hull girder. The analysis can reflect the local failure of structural members, e.g., local plate buckling and stiffener tripping, if they are modeled in detail. However, the 3D FE simulation of entire ship structure requires enormous modeling and computational effort. To reduce these while maintaining the accuracy of 3D FEM, we propose the use of equivalent single layer (ESL) approach. In the context of ship structures, ESL has been used for analysis of buckling response of panels [18,19], vibration response of sandwich panels [20,21], and ultimate strength of stiffened panels [22,23]. However, the application examples for entire hull girder analysis are missing which this paper aims to fulfill. In the traditional FE modeling, a stiffened panel is modeled in detail composed of longitudinal stiffeners with its attached plating. Using ESL methodology, a stiffened panel is modeled as a plate without the stiffeners, but with the same stiffness as the original panel. Consequently, simplification of stiffened panels enables consideration of design alternatives without changing the FE mesh, and thus more efficient exploration of design space. Therefore, the main benefits of the ESL approach compared with 3D FE analysis are: (1) reduced modeling effort, (2) reduction in degree of freedom (DOF), and (3) reduced computational effort.

This paper presents the application of ESL approach for the ultimate strength assessment of ship hull girder and one compartment models. In the ESL model, the stiffeners are removed and shell properties are defined with equivalent stiffnesses composed of 6×6 membrane and bending stiffness matrices. The stiffness matrices are calculated by the first derivative of membrane force and bending moment obtained from a unit cell under six loading conditions. Two different ship-scale case studies are presented, first focusing on the compartment level analysis (Benson et al. [14]) and second, the full-scale analysis of ship hull girder including structural damage (Tabri et al. [24]). The ultimate strength of ship hull girder is analyzed in intact and damaged conditions due to grounding or collision. For the damage conditions, the damage extents are determined from the IACS-CSR and the structural members located in the damage extent area are removed. The distributed pressures are applied separately along the bottom and side structures of the ship to obtain the vertical and horizontal bending moment curves, respectively. For comparative purposes, analysis are also conducted with the incremental-iterative method from the IACS-CSR. The ultimate strength analysis are validated with the detailed 3D FE simulations.

2. Methods

In this paper, the ESL approach is used to predict the ultimate strength of hull girder. The theoretical framework and assumptions used in the ESL approach are explained in the following section.

2.1. Overview of the ESL Approach

The ESL approach employs the first-order shear deformation theory (FSDT) in which the Kirchhoff hypothesis is relaxed by removing the assumption of transverse normal. In the FSDT, the transverse normals do not remain perpendicular to the middle of the surface after plate is deformed, as can be seen in Figure 1. In this manner, transverse shear strains (γ_{xz}) are considered in the FSDT. Additionally, the rotation in the z direction is assumed to be zero. In the deformed plates, the transverse normals are displaced by u_0 and are rotated by ϕ_x from the undeformed position. Under the assumptions and restrictions used in the FSDT, the non-linear strains are expressed in Equation (1):
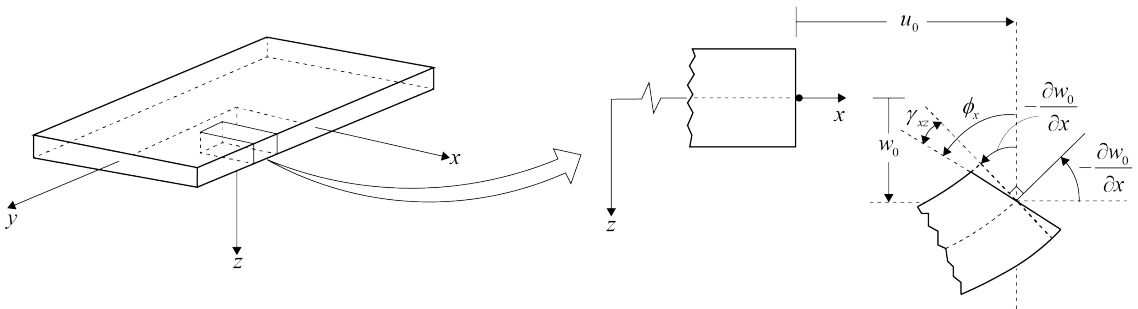
Figure 1. Undeformed and deformed geometries of an edge of a plate under the assumption of the first-order shear deformation theory (FSDT).

$$\begin{Bmatrix} \varepsilon_{xx} \\ \varepsilon_{yy} \\ \gamma_{yz} \\ \gamma_{xz} \\ \gamma_{xy} \end{Bmatrix} = \begin{Bmatrix} \varepsilon_{xx}^0 \\ \varepsilon_{yy}^0 \\ \gamma_{yz}^0 \\ \gamma_{xz}^0 \\ \gamma_{xy}^0 \end{Bmatrix} + z \begin{Bmatrix} \varepsilon_{xx}^1 \\ \varepsilon_{yy}^1 \\ \gamma_{yz}^1 \\ \gamma_{xz}^1 \\ \gamma_{xy}^1 \end{Bmatrix}, \tag{1}$$

where

$$\{\varepsilon^0\} = \begin{Bmatrix} \varepsilon_{xx}^0 \\ \varepsilon_{yy}^0 \\ \gamma_{yz}^0 \\ \gamma_{xz}^0 \\ \gamma_{xy}^0 \end{Bmatrix} = \begin{Bmatrix} \frac{\partial u_0}{\partial x} + \frac{1}{2}\left(\frac{\partial w_0}{\partial x}\right)^2 \\ \frac{\partial v_0}{\partial y} + \frac{1}{2}\left(\frac{\partial w_0}{\partial y}\right)^2 \\ \frac{\partial w_0}{\partial y} + \phi_y \\ \frac{\partial w_0}{\partial x} + \phi_x \\ \frac{\partial u_0}{\partial y} + \frac{\partial v_0}{\partial x} + \frac{\partial w_0}{\partial x}\frac{\partial w_0}{\partial y} \end{Bmatrix}, \tag{2}$$

$$\{\varepsilon^1\} = \begin{Bmatrix} \varepsilon_{xx}^1 \\ \varepsilon_{yy}^1 \\ \gamma_{yz}^1 \\ \gamma_{xz}^1 \\ \gamma_{xy}^1 \end{Bmatrix} = \begin{Bmatrix} \frac{\partial \phi_x}{\partial x} \\ \frac{\partial \phi_y}{\partial y} \\ 0 \\ 0 \\ \frac{\partial \phi_x}{\partial y} + \frac{\partial \phi_y}{\partial x} \end{Bmatrix}. \tag{3}$$

Note that the strains ($\varepsilon_{xx}, \varepsilon_{yy}, \gamma_{xy}$) are linear through the thickness, while the transverse shear strains (γ_{xz}, γ_{yz}) are constant through the thickness based on the FSDT. The strains (ε)

are composed of membrane (ε^0) and bending (ε^1) parts. Thus, the constitutive equations for the FSDT are obtained using the following relations:

$$
\begin{Bmatrix} N_{xx} \\ N_{yy} \\ N_{xy} \\ M_{xx} \\ M_{yy} \\ M_{xy} \end{Bmatrix} =
\begin{bmatrix}
A_{11} & A_{12} & A_{13} & B_{11} & B_{12} & 0 \\
A_{21} & A_{22} & 0 & B_{21} & B_{22} & 0 \\
A_{31} & 0 & A_{33} & 0 & 0 & B_{33} \\
C_{11} & C_{12} & 0 & D_{11} & D_{12} & 0 \\
C_{21} & C_{22} & 0 & D_{21} & D_{22} & 0 \\
0 & 0 & C_{33} & 0 & 0 & D_{33}
\end{bmatrix}
\begin{Bmatrix} \varepsilon^0_{xx} \\ \varepsilon^0_{yy} \\ \gamma^0_{xy} \\ \varepsilon^1_{xx} \\ \varepsilon^1_{yy} \\ \gamma^1_{xy} \end{Bmatrix},
\tag{4}
$$

where N_{xx}, N_{yy} are the membrane forces, N_{xy} is the shear force, M_{xx}, M_{yy} are the bending moments, M_{xy} is the torsion, $\varepsilon^0_{xx}, \varepsilon^0_{yy}, \gamma^0_{xy}$ are the membrane strains, and $\varepsilon^1_{xx}, \varepsilon^1_{yy}, \gamma^1_{xy}$ are the curvatures. The **ABCD** stiffness matrices are obtained from the first derivative of membrane forces and bending moments of the unit cell (UC) simulations under six loading conditions, as can be seen in Figure 2. Compared to full 3D FEM, the generation of stiffness matrices requires an additional modeling and computational effort, which however can be made fairly automatic using programming.
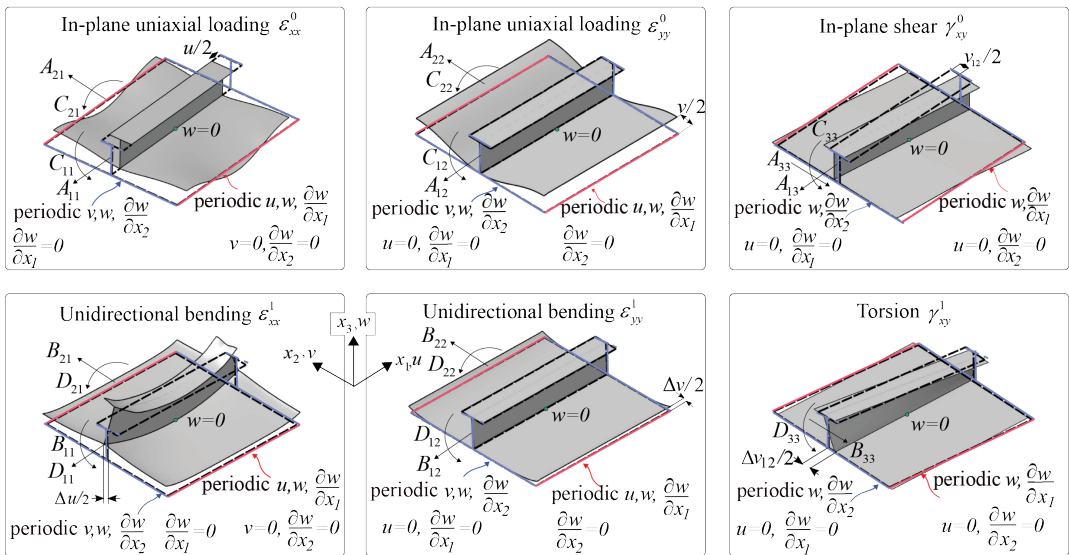
Figure 2. Six different unit cell (UC) configurations with boundary conditions needed for ABCD stiffness matrix definition. Forces and moments shown with arrows are associated with respective stiffness components. Boundary conditions for edges with the same color are identical.

The assumed UC is a periodic constituent of the full panel, thus periodic boundary conditions are imposed on UC, see Figure 2. The details of performing UC simulations are given in the previous papers by the authors [22,23]. Essentially, the same procedure was applied for each of the stiffened panel in case study analyses. Representative unit cell model was created for each panel with different topology (plate thickness and stiffener type) and 3D FE analyses were performed to obtain ABCD stiffness matrices. Compartment model (first case study) consisted only 1 stiffened panel configuration that was replaced by ESL. In a full ship hull (second case study), there were 45 different panel configurations, giving total of 270 (6 × 45) UC simulations. The entire procedure of UC analysis (pre- and post-processing) was made automatic using python scripts, which read the structural details from text file, prepare the models, and extract ABCD stiffness matrices.

Additionally, transverse shear strains are assumed to be constant based on the FSDT. The transverse shear force resultants (Q_x,Q_y) are calculated by multiplying the transverse

shear stiffnesses (D_{Q_x}, D_{Q_y}) and transverse shear strains (γ_{xz}, γ_{yz}), as expressed in the following equation:

$$\begin{Bmatrix} Q_x \\ Q_y \end{Bmatrix} = \begin{bmatrix} D_{Q_x} & 0 \\ 0 & D_{Q_y} \end{bmatrix} \begin{Bmatrix} \gamma_{xz} \\ \gamma_{yz} \end{Bmatrix} \tag{5}$$

$$D_{Q_x} = k_{xz}\left(G_p t_p + G_w h_w + G_f h_f \right) \tag{6}$$

$$D_{Q_y} = k_{yz} G_p t_p \tag{7}$$

where k_{xz} is the longitudinal shear correction factor calculated by dividing the average shear stress ($\tau_{xz(avg)}$) to the maximum shear stress ($\tau_{xz(max)}$), k_{yz} is the transverse shear correction factor as $5/6$. The shear moduli of the web (G_w) and flange (G_f) are the function of plate (G_p), web thickness (t_w), flange width (b_f), and stiffener spacing (s):

$$G_w = G_p(t_w/s) \tag{8}$$

$$G_f = G_p\left(b_f/s \right) \tag{9}$$

2.2. Implementation of ESL in Abaqus

In ESL approach, stiffened panels are replaced by a single plate. An example is shown in Figure 3, where ship hull girder composed of stiffened panels is modeled using ESL approach. ESL properties are composed of 6 × 6 matrix considering membrane and bending stiffness components. In Abaqus software these ESL properties are given to elements by using shell general section option. This option allows reference to external Fortran-based VUGENS subroutine where the non-linear stiffness of ESL is calculated specific to loading stage. VUGENS subroutine is available starting from Abaqus 2022 and suitable for explicit analysis. To the best of authors knowledge, the analyses reported here are the first attempt to use VUGENS subroutine since in earlier versions of Abaqus only implicit version of shell general section definition could be used (UGENS). Note that in combination with explicit integration scheme the ESL approach could be potentially used in ship collision or grounding analysis. In non-ESL elements (frames, bracket, and other plates), standard isotropic properties are used by defining Young's modulus, Poisson's ratio, and material stress–strain curve.
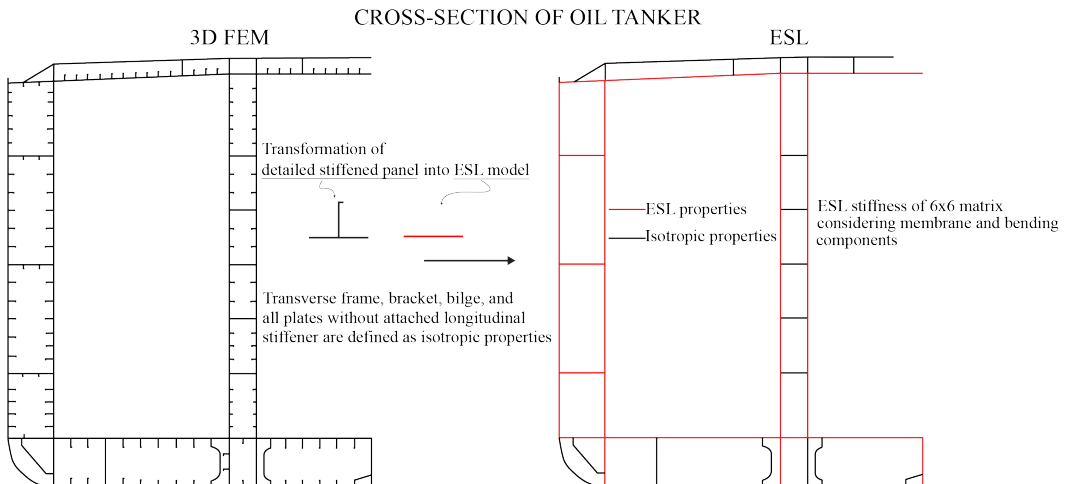

Figure 3. Application of ESL in a ship's hull girder.

3. Case Study of One Compartment Aluminium Box Girder

This paper examines the application of ESL to analysis of compartment level collapse, for details see Benson et al. [14]. The ultimate strength of one compartment box girder was analyzed and characterized by the bending moment versus curvature curve. The analyses were performed using the detailed 3D FEM and ESL approach. The detailed 3D FE analysis utilizes conventional modeling techniques with explicit modeling of stiffened plates further strengthened with larger transverse webframes with all parts given isotropic material properties. In the ESL model, longitudinally stiffened panels were represented with equivalent single layer plates having the same stiffness as the original plate with stiffeners while webframes were still explicitly modeled.

Modeled box girder with a 8.4 m length had a square cross section, stiffened on each side by 20 longitudinals spaced 400 mm apart. The panel configuration M1 was selected for analyses, see [14]. The longitudinal T-stiffeners had the web and flange dimensions of 120 × 55 mm and 55 × 7.7 mm, respectively. The transverse webframes were flat bars with the size of 180 × 10 mm spaced 1200 mm apart. There were six webframes between transverse bulkheads, which is sufficient to demonstrate buckling characteristics at the compartment level. To maintain the straightness of the compartment ends during bending, the bulkheads were modeled with a very large thickness. The mesh size used was 50 × 50 mm, which was determined by Benson et al. [14] through the mesh convergence analysis. The mesh size sensitivity study of ESL was performed using element sizes of 50 × 50 mm, 300 × 300 mm and 600 × 600 mm which are consisted of 24, 4 and 2 elements between webframes, respectively. The box girder was given aluminium 5083 properties with an elastic modulus of 70 GPa and a yield stress of 302 MPa. The non-linear stress–strain response of this material was characterized by the Ramberg–Osgood relationship, as expressed in the following equation:

$$\varepsilon = \frac{\sigma}{E} + 0.002 \left(\frac{\sigma}{\sigma_{0.2}} \right)^n \tag{10}$$

where ε is the strain, σ is the applied stress, E is the elastic modulus, $\sigma_{0.2}$ is the 0.2% offset proof stress, n is the exponent.

Boundary conditions applied in the box girder are explained in Figure 4. At the reference point, a moment to the z-axis was applied resulting in compression on the top panel and tension on the bottom panel. This reference point was connected to the nodes at the boundary using kinematic coupling so that the section remained flat during rotation. At the opposite section, the clamped boundary condition was imposed. Only half of the girder was modeled by imposing symmetry on the center line.

The response of the box girder is compared in terms of bending moment vs. curvature curves and overall deformations obtained at the maximum bending moment, see Figure 5. Current 3D FE analysis gives slightly softer response compared with 3D FE results from Benson et al. [14]. Curvature in current study was determined by tracking the rotation at the reference point. The way curvature was obtained in analysis of Benson was not detailed, which possibly explains the slightly softer response obtained with current 3D FE analysis, while the overall behavior is well captured. Proceeding to analyze differences between current 3D FEM and ESL we also note close agreement in maximum bending moment. Even the coarsest (and stiffest) ESL model of 600 × 600 mm shows the difference of mere 4.57% compared with 3D FEM result. All studied element sizes can capture accurately compartment level (overall) buckling behavior and for overall efficiency we advocate to use the largest mesh of 600 × 600 mm or two elements between webframes. However, the ESL accuracy decreases if the stiffened panel is subjected to local buckling of the stiffener web or plate [22,23]. Therefore, further investigation should be performed what is the suitable element size for such simulations. In the post-ultimate stage, there is a sudden decrease in bending moment due to transition from interframe to overall buckling mode. ESL model cannot accurately trace this structural response at the post-ultimate stage.
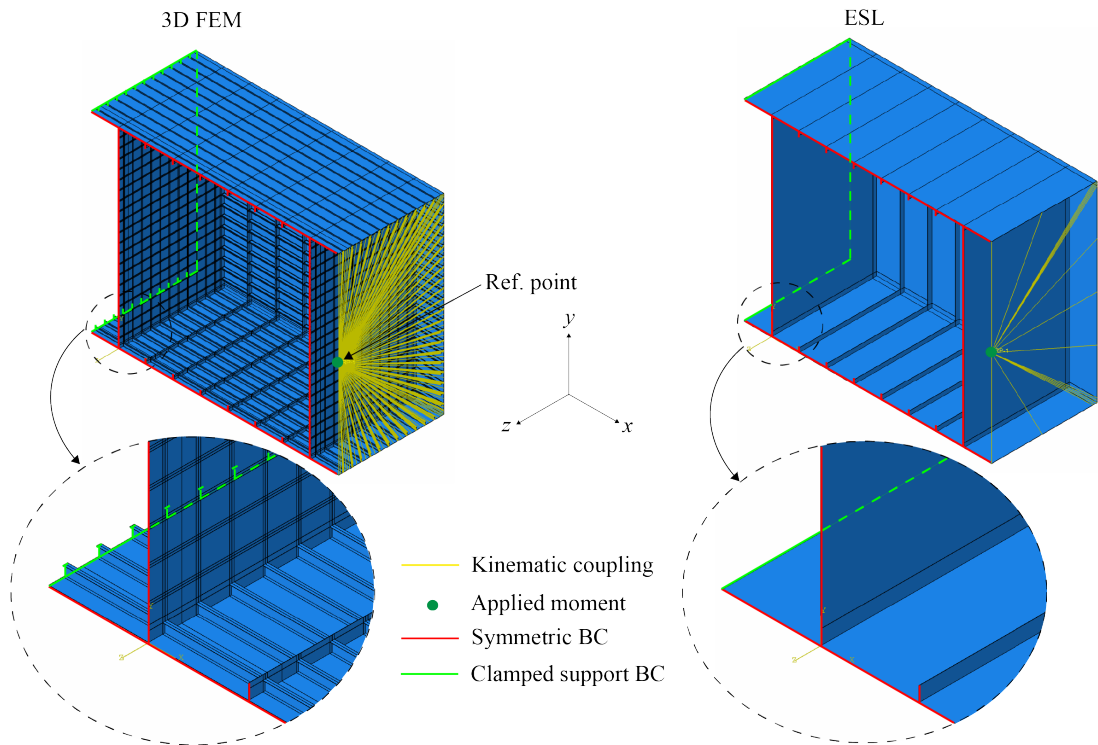
Figure 4. Boundary condition applied in 3D FEM and ESL of box girder.

In addition to providing a high level of accuracy with coarse elements of 600 × 600 mm, ESL approach also provides shorter computation times than 3D FEM. With ESL mesh of 600 × 600 mm the computation time is only 27.7% of full 3D model, see Figure 6. All simulations were ran with processor type of Intel(R) Xeon(R) CPU E5-2690 0 @ 2.90 GHz, 4 cores, 4 domains, and RAM of 24.0 GB.
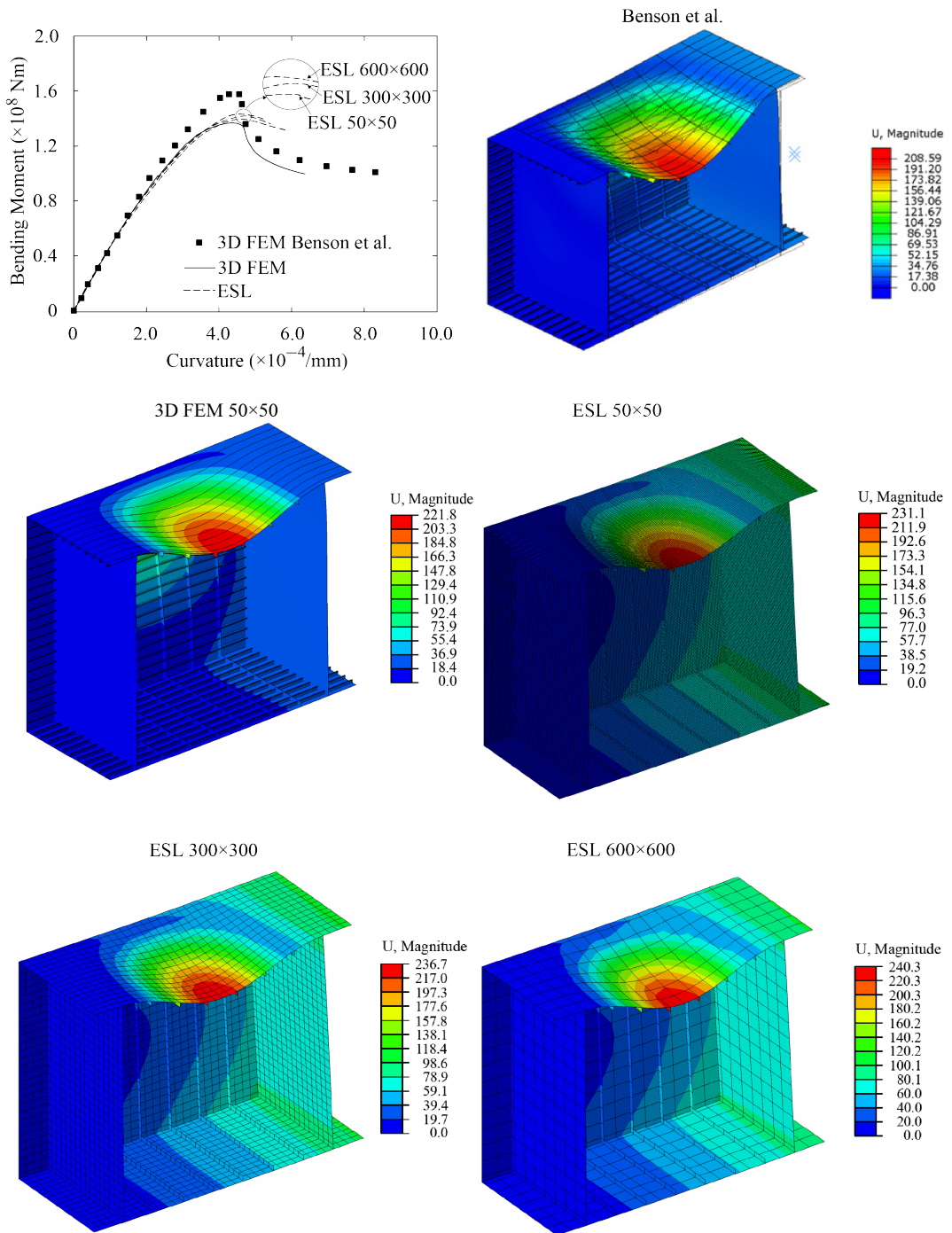
Figure 5. Bending moment–curvature curves and deformation shapes obtained from Benson et al. [14], 3D FEM and ESL models. U is in mm.
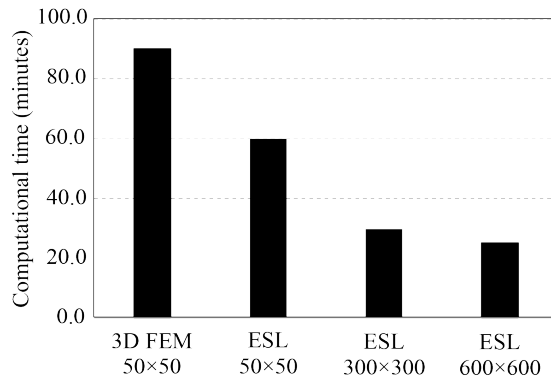
Figure 6. Computational time for 3D FEM and ESL with several mesh sizes.

4. Case Study of Full-Scale Steel Ship Structure

Ultimate strength analyses of ship hull girder in intact and damaged conditions were performed using the ESL approach, full 3D FEM, and incremental-iterative method from the IACS-CSR. A traditional ship hull can be considered as a light-weight thin-walled structure composed of an outer shell that is stiffened with framing members. In other words, ship hull girder is built from stiffened panels. From a design perspective, a detailed modeling of stiffened panel composed of plates and stiffeners is required for 3D FEM. However, ESL simplifies the modeling process as the plate elements are given stiffness properties representative of stiffened panels rendering explicit modeling of stiffeners unnecessary. In the IACS-CSR, ultimate strength is calculated based on a cross-section of hull girder between two adjacent transverse webframes. In Section 2, the theory and implementation of ESL approach was explained. In this section, the full 3D FEM and incremental-iterative method are described.

4.1. Ship Particulars

The case study structure is a chemical product tanker that was previously analyzed in Tabri et al. [24]. The midship section and bulkhead arrangement are given in Figure 7 and the main particulars in Table 1. The ship is designed from high strength steel (AH36) with Young's modulus of $E = 210$ GPa, Poisson ratio of $v = 0.3$, and yield stress of $\sigma_y = 355$ MPa.

Table 1. Main particulars of the chemical tanker.

| Parameter	Symbol	Unit	Value
Overall length	L_{OA}	m	182.2
Length between perpendiculars	L_{PP}	m	175.3
Moulded breadth	B	m	32.2
Depth	H	m	15.0
Design draught	B	m	11.1
Displacement	∇	t	52,298
Double bottom height	H_{DB}	m	2.21

4.2. Loading and Boundary Conditions

Being a flexible thin-walled beam, the hull girder of the ship flexes globally when exposed to loads. The load components that act on the ship hull girder are the weight of the ship, its cargo, and the hydrostatic and hydrodynamic pressures (external load). The resultant of these load components can be treated with longitudinally distributed load applied on the hull girder, which can increase only by the external pressure due to waves. Therefore, global bending of the ship hull was achieved with longitudinally distributed

pressure, which amplitude was gradually increased until ultimate strength was reached. The distributed pressure was applied either on ship bottom or side, depending on whether vertical or horizontal bending moment was determined, respectively. The sinusoidal shape of distributed pressure was kept unchanged during loading, as shown in Figure 8b. Although, in realistic situations, the distribution of load can play an important role, here only the simplified sinusoidal shape was considered. The direction of bending was controlled by the sign of the pressure amplitude (*A*), see the Equation in Figure 8b. This resulted in sagging/hogging in vertical bending and starboard/portside bending in horizontal bending. In damaged condition, the pressure was not applied in the damage opening. In Abaqus, the VDLOAD subroutine was invoked to apply the distributed pressure.
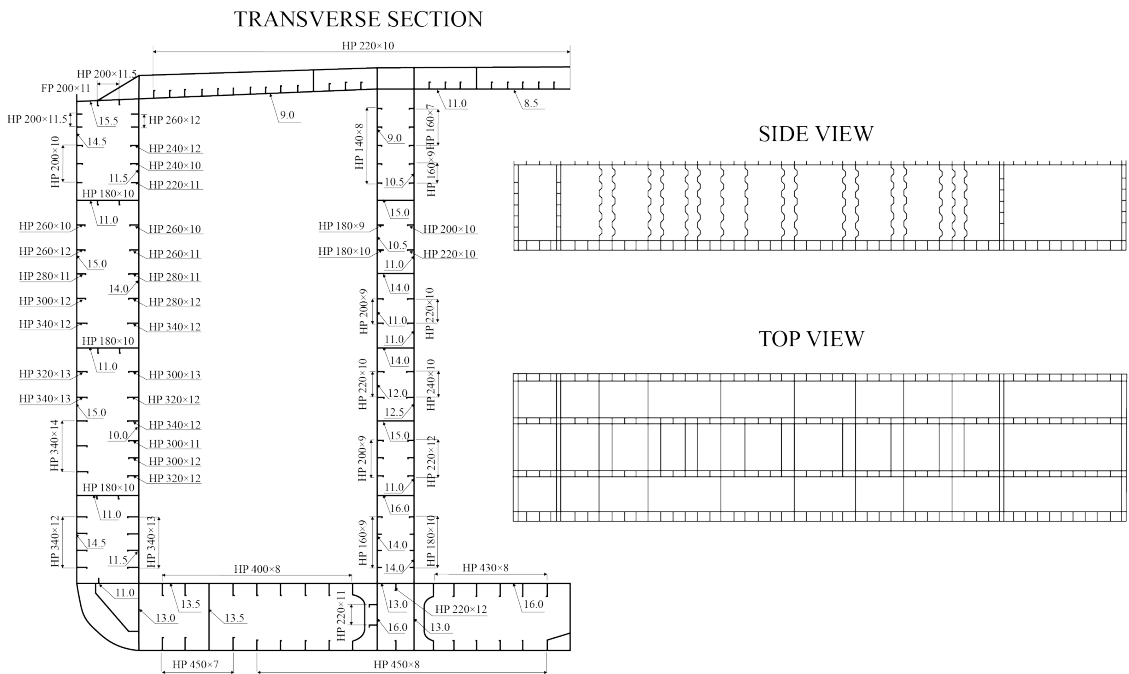
Figure 7. Design of hull structure for case study: midship section (**left**) and side view and top view (**right**).

A simply supported boundary condition was imposed on the ship at the mid nodes marked with •, see Figure 8a. The aft of the ship was pin constrained with all translations fixed while rotations were free. In the fore part, the constraints were the same except translation in longitudinal direction which was free to avoid an excessive stress concentration during deflection. Furthermore, rigid beams were modeled through the constraint nodes to keep the ends of the beam straight under increasing load and, thus, prevent local buckling. The surfaces where pressure was applied were specified with rectangles ABCD (for vertical bending moment) and EFGH (for horizontal bending moment), see Figure 8a. The reaction forces on the support is assumed to be very small since the distributed pressures produce the resultant forces of zero.

$$P(x_1) = A\cos(2\pi x_1 / L)$$
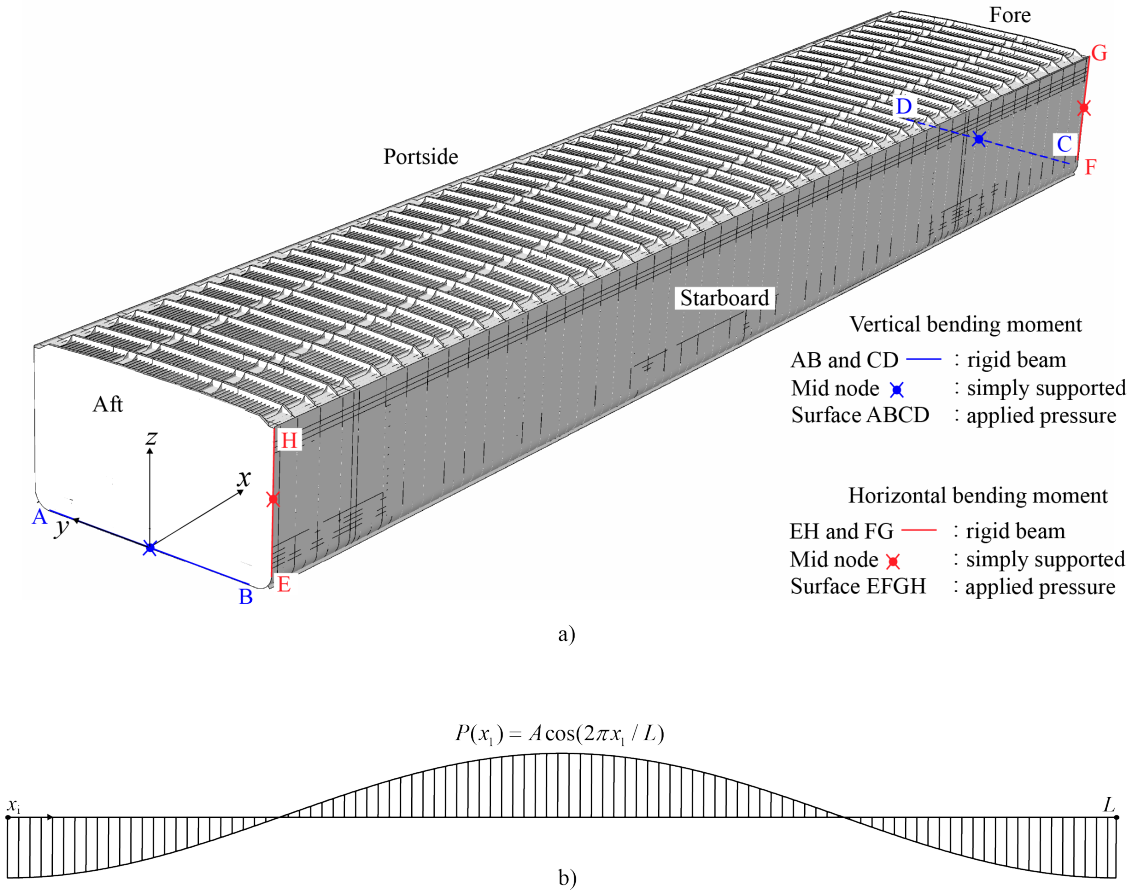
Figure 8. (**a**) Boundary condition applied in the tanker under vertical and horizontal bending moments. (**b**) Distributed pressure applied on the surface.

4.3. Damage Scenario

For post-accidental strength assessment of ship structure, both grounding and collision scenarios were considered. The extent of damage was determined based on the definition provided by the IACS-CSR. The damage was modeled by removing the plates, stiffeners, and frames that fall within the specified damage extent. The selected length of damage was 10 m with its center in the middle of the ship. This position was chosen since it significantly reduces the longitudinal bending strength of the ship. In case of collision damage, the transverse damage extent was equal to $B/16$ where B is the breadth of the ship. Therefore, respective structural elements in the parts of inner and outer skin and main deck were removed. The vertical damage extent was taken as $0.6D$ measured from the main deck, where D is the depth of the ship.

In case of grounding damage, the transverse damage extent was taken as $0.6B$, which is symmetric with respect to the centerline. The damage penetration height was equal to the depth of the double bottom (H_{DB}). Figure 9 shows the damage extents of the double hull oil tanker for grounding and collision scenario.
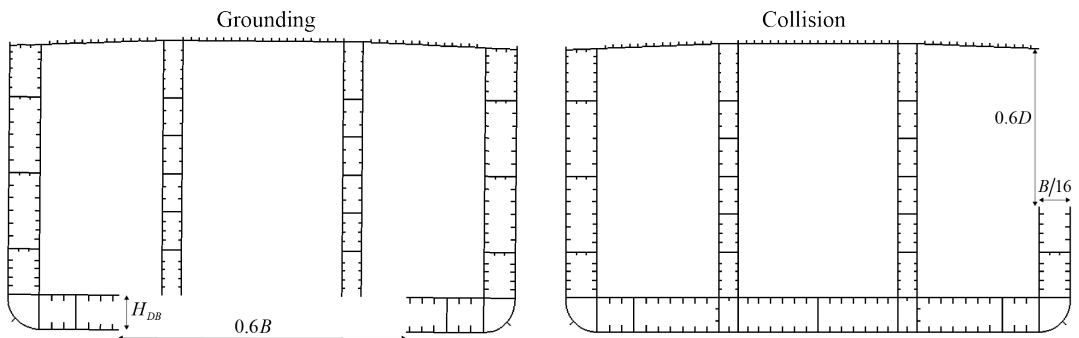
Figure 9. Assumed grounding and collision damage extents in tanker.

4.4. Full 3D Finite Element (3D FE) Model

Non-linear finite element method (NLFEM) is a sophisticated tool to solve the solid mechanics problem of complex engineering structures. Using NLFEM, the effect of material and geometrical non-linearities during progressive collapse of hull girder can be taken into account. A chemical tanker was modeled using Abaqus/Explicit software. All models were meshed using four-node shell elements (S4R), including plates, stiffener webs, frames, and girders. Stiffening was achieved with HP bulb profiles where the flanges were modeled using beam elements (B21). Stiffener webs were modeled using shell elements to capture the collapse mode, e.g., local buckling of stiffener web or stiffener tripping, expected during the progressive collapse of the hull girder. The mesh convergence study was conducted by Tabri et al. [24] to obtain the balance between numerical accuracy and simulation cost. Thus, the mesh density in the one compartment is illustrated in Figure 10 and can be summarized as follows: (1) plates between longitudinal stiffeners, 4 × 16 shells; (2) stiffener web plates, 1 × 16 (web height < 300 mm) shells and 2 × 16 (web height > 300 mm) shells; (3) side stringers and girders, 12 × 16 shells; and (4) corrugated bulkhead plates, 6 × 40 and 5 × 60 shells. The 3D FE model consisted of 3,160,000 nodes and 2,800,000 elements from which 2.5 M were shell and 0.3 M were beam elements. In the ESL model, stiffeners (shell elements related to web and beam element for flange) were removed so the total number of elements was reduced by 25% to 2,120,000 compared with the full 3D FE model.

4.5. Incremental-Iterative Method

The IACS-CSR provides the incremental-iterative method to calculate the ultimate strength of hull girder. Details of the method are given in CSR, which are briefly summarized here for entirety. The assumption is that hull girder collapse occurs in between two adjacent transverse webs. Accordingly, two-dimensional (2D) cross-section of the ship hull structure is divided into a series of structural elements, such as stiffeners, plates, and hard corners. The response of each of those elements is described with load-end-shortening curve compliant with prevalent collapse mode. Under compression, the stiffener element may experience the specific collapse mode, such as beam-column buckling, torsional buckling, or web buckling. For the plating element, the collapse mode of plate buckling may occur. Other element types under compression or tension may experience idealized elastic-plastic failure. Accordingly, the load-end-shortening curves for each structural element were obtained.

The calculation procedure of ultimate strength starts with estimation of neutral axis (NA) position. The iterative approach involves increasing the assumed curvature of the hull girder and calculating the new position of NA based on the moment equilibrium. Bending moment is obtained by integrating the load over the cross-section, while the load for each element is obtained from the load-end-shortening curves used as input. Once the updated

location of the NA is obtained, the curvature is further increased and procedure is repeated until the maximum bending moment is achieved.
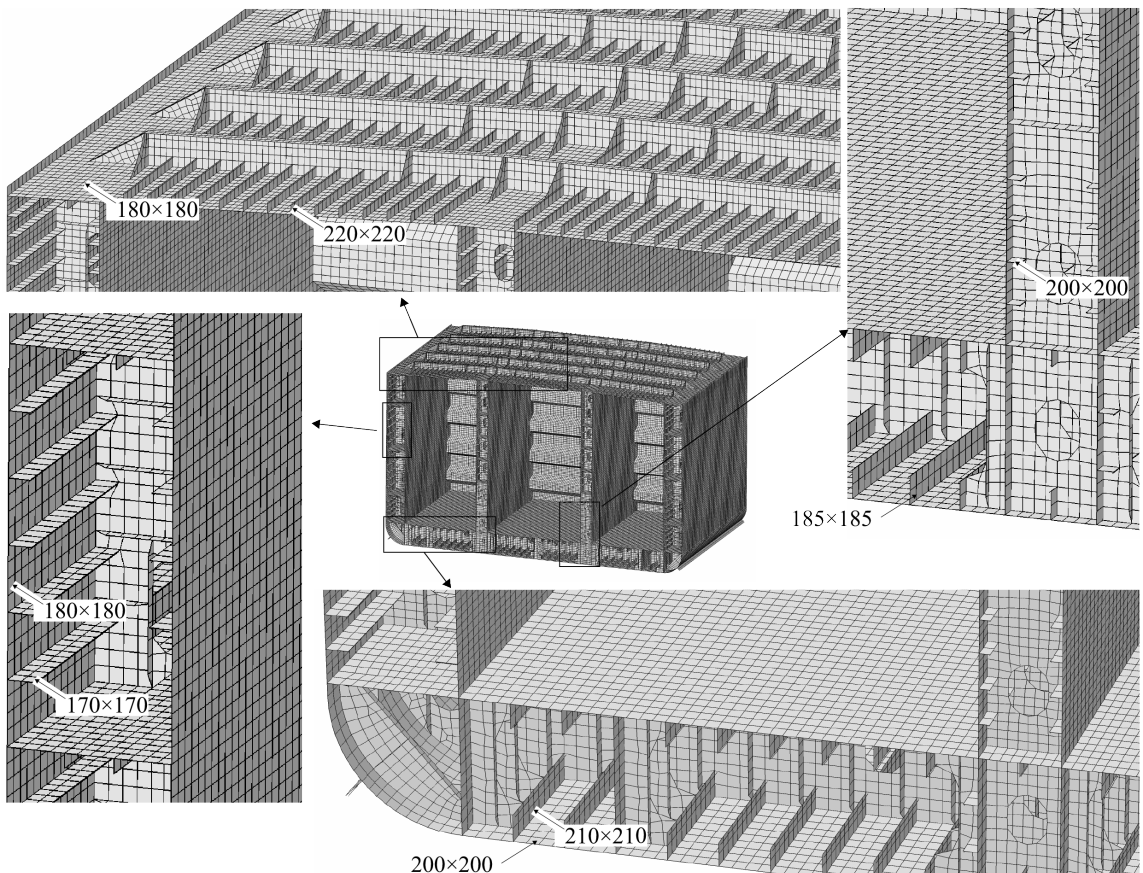
Figure 10. Mesh of the one compartment in the FE-model of chemical tanker.

5. Ultimate Strength Analysis

Ultimate strength of a chemical tanker was analyzed under vertical and horizontal bending moments. The results obtained from the ESL approach, 3D FEM, and incremental-iterative method are presented.

5.1. Vertical Bending Moment

Figure 11 shows the vertical deflection of intact chemical tanker along its length under hogging and sagging conditions. The horizontal bending moment is discussed in the next section. The deflections at the aft and fore are zero since the vertical translation of those parts is constrained. The maximum deflection occurs in the middle of the ship where the distributed pressure has maximum amplitude. In general, ESL deflection correlates well with the 3D FEM results.
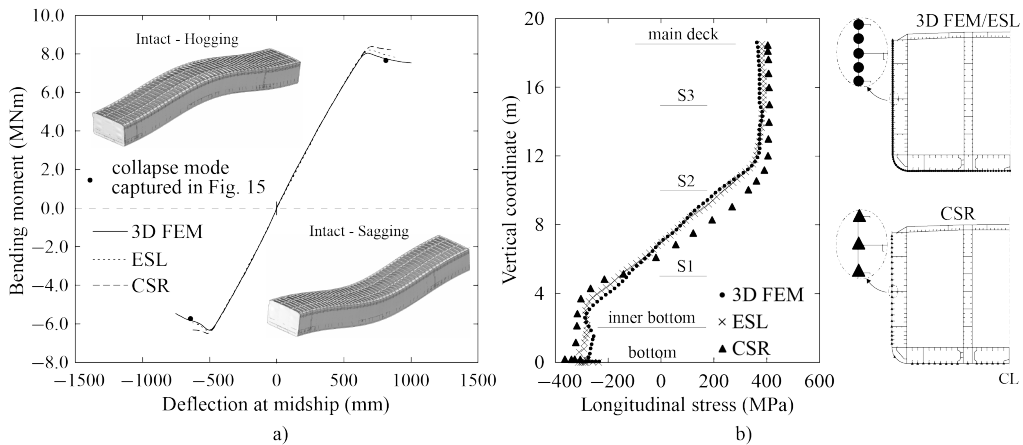
The bending moment–deflection curves for 3D FEM, ESL, and incremental-iterative approach (hereinafter referred to as CSR method) for intact ship are presented in Figure 12a. The entire curve until maximum bending moment is accurately predicted by both, ESL and CSR method. Therefore, benefits of performing computationally more demanding ESL analyses are missing until more detailed information is desired. For instance, Figure 12b shows the longitudinal stress in vertical coordinate at the ship midsection under hogging

condition. The constant tensile stresses in the upper decks (above side stringer S2) indicate to fully plastic condition. In the compressive side below the NA (slightly above side stringer S1) stress distribution is more complex due to non-linear buckling of structural elements. The stress provided by ESL approach has better agreement with the 3D FEM than CSR method. Furthermore, with 3D FE model available, similar stress distributions could be obtained in different cross-sections along the length, which is not possible with CSR.
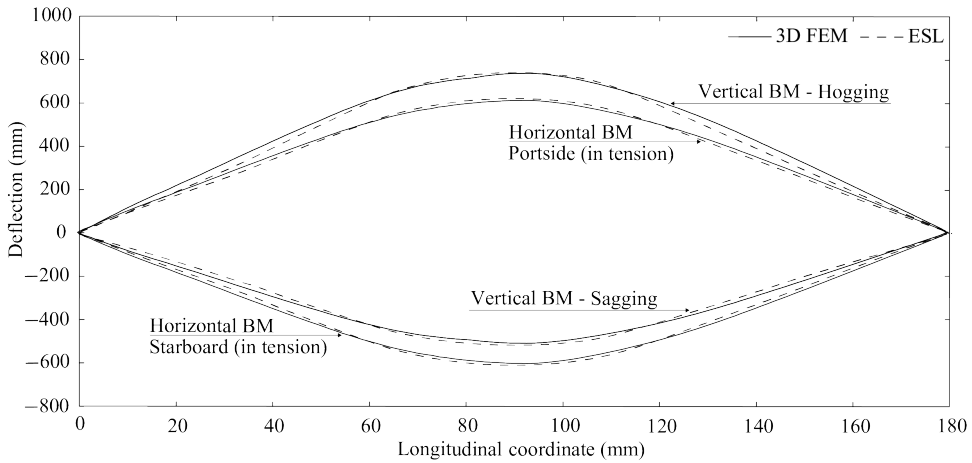

Figure 11. Deflection of ship's hull along its length at the ultimate stage under vertical and horizontal bending moments.

In the case of ship grounding, the bending moment–deflection curve is presented in Figure 13a. The initial stiffness is the same for all three curves. The bending moment increases linearly until gradual buckling of structural elements. The moment reduction under hogging condition is more significant since compressive loads are carried by damaged double bottom structure. The comparison of longitudinal stress distributions in Figure 13b shows that while ESL accuracy decreases compared with intact analyses, the stresses are still more accurately predicted compared with CSR.
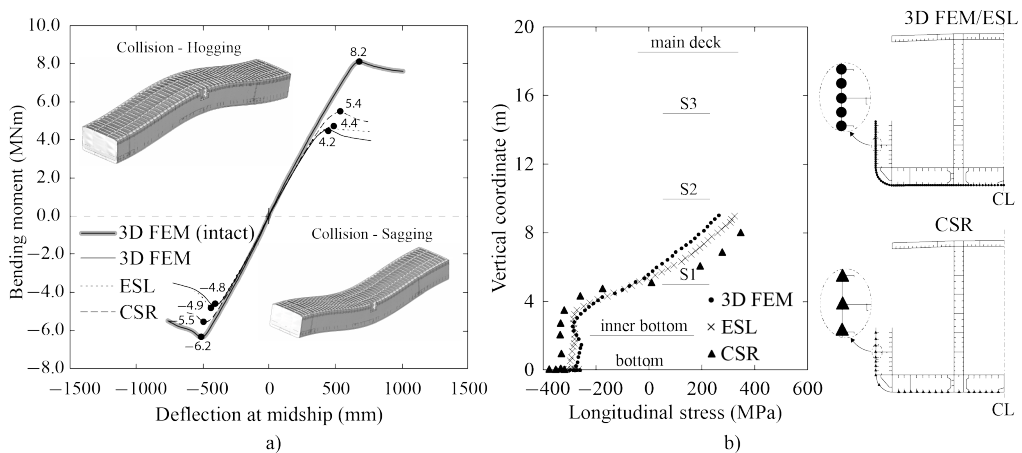

Figure 12. Response of intact ship under vertical bending moment. (**a**) Bending moment–deflection curves. (**b**) Longitudinal stress distribution to vertical coordinate at the midship under hogging condition.
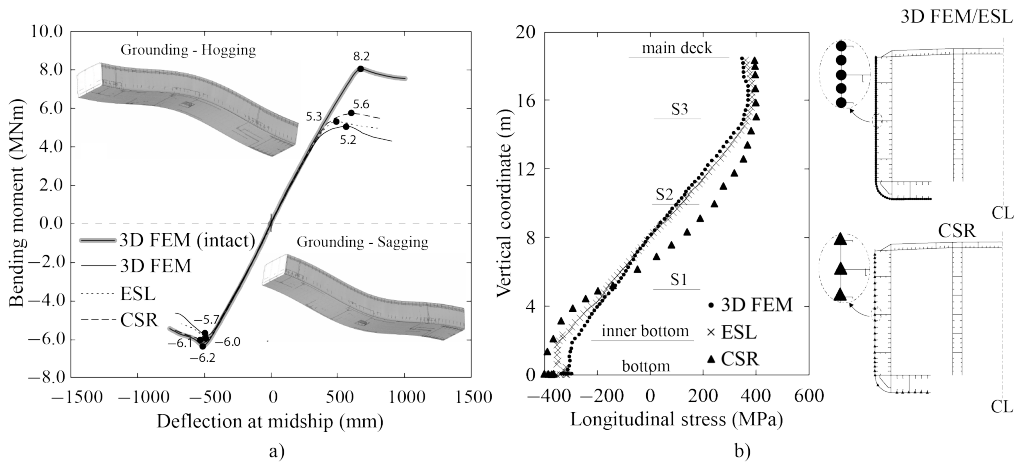
Figure 13. Response of ship grounding under vertical bending moment. (**a**) Bending moment–deflection curves. The maximum bending moments are used in calculating the histogram of moment reduction ratio. (**b**) Longitudinal stress distribution to vertical coordinate at the midship under hogging condition.

In the case of collision damage, the relationship between bending moment and deflection under sagging/hogging conditions is presented in Figure 14a. The longitudinal structure, especially the deck-side corner, greatly contributes to longitudinal strength. By removing the damaged side and deck structure, the ultimate bending moment decreases more than in case of grounding damage. However, this decrease in maximum bending moment is well captured by the ESL method which shows improved predictions compared with CSR. The reduced accuracy of CSR is explained by the effect of the removed deck-side corner. With respect to the longitudinal stresses in Figure 14b, the ESL method has similar accuracy as in grounding case, while maintaining the advantage over CSR.


Figure 14. Response of ship collision under vertical bending moment. (**a**) The bending moment–deflection curves. The maximum bending moments are used in calculating the histogram of moment reduction ratio. (**b**) The longitudinal stress distribution to vertical coordinate at the midship under hogging condition.

The ESL approach captures the bending moment until ultimate stage with very good accuracy. In the post-ultimate stage bending moment is captured accurately under sagging, but not under hogging. Under hogging condition ESL fails to capture the local stiffener web buckling collapse in bottom structure as shown in Figure 15. It was also shown in analysis of [22,23] that beyond certain threshold slenderness ($\beta = 1.96$) the collapse mode becomes local which is not captured by ESL. In current analysis the plate slenderness in bottom structure is 2.12, while in deck structure slenderness is 1.55. In contrast, the slenderness of deck plates is much lower circumventing the local collapse under sagging condition, which ultimately leads to very good accuracy also in post-ultimate bending moment prediction, see Figure 14a.

The bending moment reduction with respect to intact condition obtained with each method (3D FEM, ESL, and CSR) are summarized in Figure 16. This reduction is calculated by dividing the maximum bending moment at damaged condition with the corresponding maximum from intact condition for each method concerned. Furthermore, the error in moment reduction obtained with ESL and CSR is calculated with respect to 3D FEM results and shown in the figure. The overall accuracy of ESL is excellent remaining in 5% in all cases. The compromise between accuracy and overall analyses cost favor CSR over ESL in grounding analyses, while accuracy of CSR reduces in collision analyses.
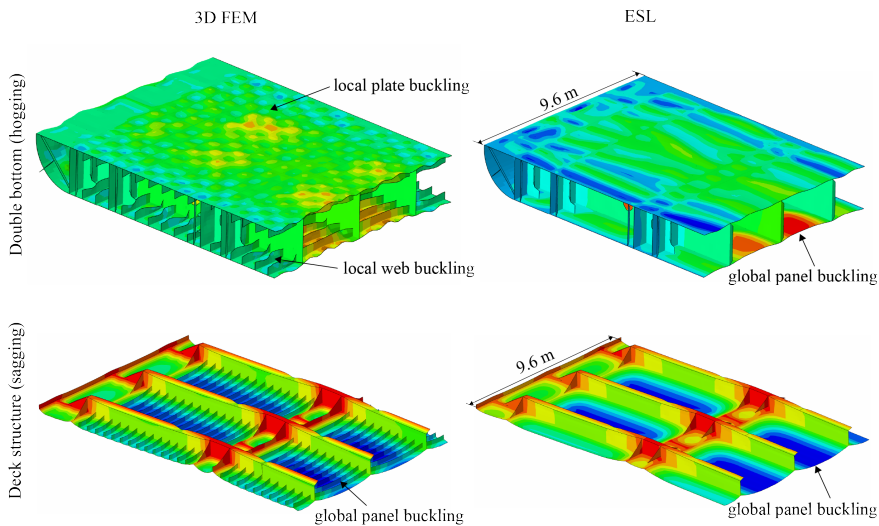
Figure 15. Collapse mode in double bottom and main deck structures under hogging and sagging conditions in post-ultimate stage, respectively. Deformation scaling factor is 5×.
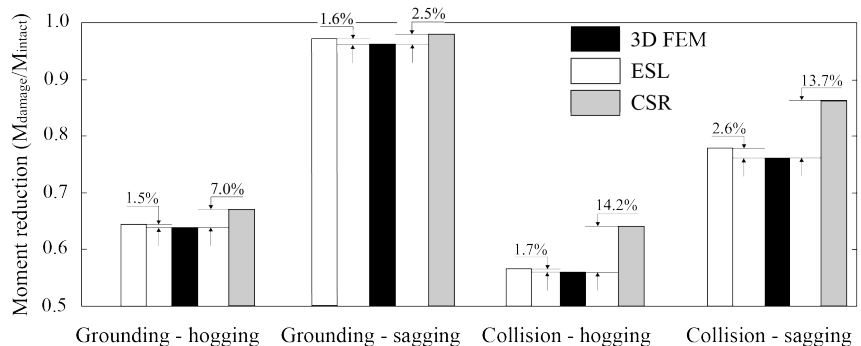

Figure 16. The moment reduction ratio under grounding and collision damage in the hogging and sagging conditions using the 3D FEM, ESL, and CSR methods.
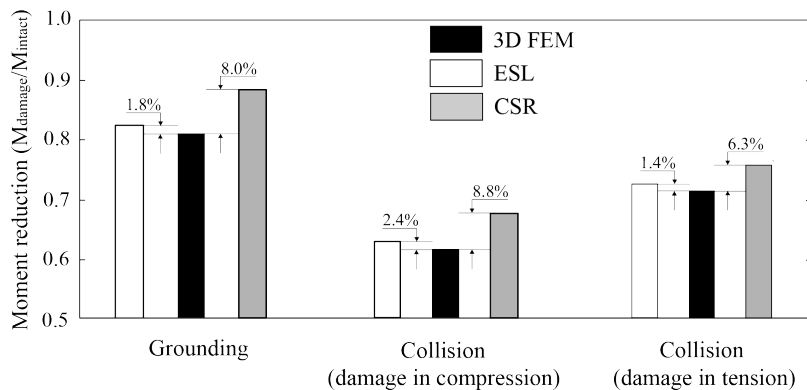
5.2. Horizontal Bending Moment

The horizontal bending moment–deflection at midship curves are presented in Figure 17a–d for intact and damaged ship. Overall, a close agreement exists between the bending moment resulted by the ESL and 3D FEM until the ultimate stage. Since hull girder has greater depth than breadth, the ultimate horizontal bending moment is greater than vertical bending moment. For intact and grounding model, the cross-section of the ship is symmetric to the centerline so that the bending moment is independent whether the loading comes from port or starboard side. However, for collision model, the bending moment is dependent on the loading direction. For these cases, the ESL model can accurately capture the reduction in bending moment until the ultimate condition.

The moment reduction ratio under horizontal bending moment for the three methods are shown in Figure 18. The error percentage represents the difference between the analyzed method and 3D FEM. In all cases, the ESL results are consistently close to the 3D FEM.
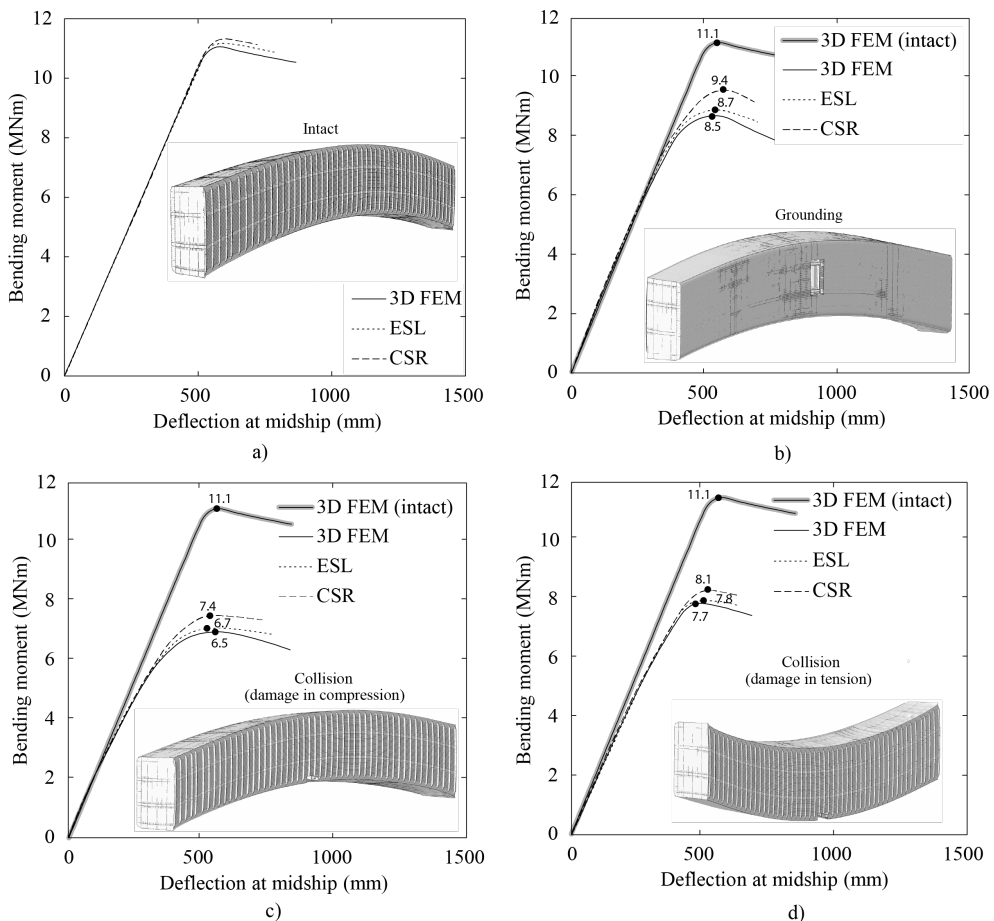
Figure 17. Horizontal bending moment-deflection relationships of tanker in the condition of (**a**) intact, (**b**) grounding, (**c**) collision with damage in compression, and (**d**) collision with damage in tension. The maximum bending moments are used in calculating the histogram in Figure 18.

Figure 18. The moment reduction ratio of horizontal bending moment in grounding and collision cases for the 3D FEM, ESL, and CSR methods.

6. Conclusions

The ultimate strength analyses are carried out using the one compartment and full-scale ship models. The one compartment model is analyzed under vertical bending moment. The full-scale ship model in intact and damaged conditions is analyzed under vertical and horizontal bending moments. The analyses are performed with three methods, namely 3D FEM, ESL, and CSR. Overall, the ultimate strength predicted by the ESL approach give the results close to 3D FEM for all cases.

The ESL approach provides a more time-efficient way to analyze the ultimate strength compared to the detailed 3D FEM. In the ESL approach, plate with stiffeners is represented with an equivalent plate with equal stiffness so that stiffeners are not explicitly modeled. This reduces modeling effort as well as computational time and, thus, could be potentially used with great efficiency in structural optimization, which has seen increased popularity due to the advancements in computing power. Current analysis showed that in case of one compartment model, the analysis time was up to 3 times shorter when using the coarsest possible mesh. Moreover, the computational efficiency does not compromise the accuracy as the ultimate bending moment was captured with less than 5% error compared with 3D FEM in all analyzed cases. In contrast, the CSR results overestimate the collapse moment by up to 14.2% in collision damage scenario under hogging. This overestimation of bending moment obtained with CSR method is consistent with analysis in literature, see [25,26].

In addition to accurately visualizing the full-scale ship deflection, ESL model can capture the load-response of a ship structure until ultimate bending moment with very good accuracy. However, due to the interaction of structural members, the ESL approach cannot accurately account the local stiffener web buckling collapse in the post-ultimate stage. Furthermore, with ESL methodology one cannot visualize stresses in the post-processing stage. Both aspects need to be addressed in future investigations.

Author Contributions: Conceptualization, T.P., M.K. and K.T.; methodology, T.P. and M.K.; software, T.P.; validation, T.P.; formal analysis, T.P. and M.K.; investigation, T.P.; resources, T.P.; data curation, T.P.; writing—original draft preparation, T.P.; writing—review and editing, T.P., M.K. and K.T.; visualization, T.P.; supervision, M.K.; project administration, M.K. and K.T.; funding acquisition, M.K. and K.T. All authors have read and agreed to the published version of the manuscript.

Institutional Review Board Statement: Not applicable.

Informed Consent Statement: Not applicable.

Data Availability Statement: The data presented in this study are available on request from the corresponding author.

Conflicts of Interest: The authors declare no conflict of interest.

References

1. Det Norske Veritas, G.L. Rules for classification: Ships. *Ships Navig. Ice Det Nor.* **2016**, *3*, 351–354.
2. IACS. Background Document—Section 9/1, Design Verification, Hull Girder Ultimate Strength. IACS Common Structural Rules for Double Hull Oil Tankers, January 2006. pp. 321–368. Available online: https://www.classnk.or.jp/hp/pdf/activities/csr/ECSR-T-TB002.pdf (accessed on 20 September 2022).
3. Caldwell, J. Ultimate Longitudinal Strength. *Trans. RINA* **1965**, *10*, 411–430.
4. Smith, C.S. Influence of local compressive failure on ultimate longitudinal strength of a ship's hull. *Trans. PRADS* **1977**, *10*, 73–79.
5. Tatsumi, A.; Iijima, K.; Fujikubo, M. A Study on Progressive Collapse Analysis of a Hull Girder Using Smith's Method—Uncertainty in the Ultimate Strength Prediction. Practical Design of Ships and Other Floating Structures, Singapore, 2021. Available online: https://www.sciencegate.app/document/10.1007/978-981-15-4672-3_7 (accessed on 20 September 2022).
6. Yukio, U.; Rashed, S.M.H. The idealized structural unit method and its application to deep girder structures. *Comput. Struct.* **1984**, *18*, 277–293. [CrossRef]
7. Ueda, Y.; Rashed, S.M.H.; Abdel-Nasser, Y. An improved ISUM rectangular plate element taking account of post-ultimate strength behavior. *Mar. Struct.* **1994**, *7*, 139–172. [CrossRef]
8. Masaoka, K.; Okada, H.; Ueda, Y. A rectangular plate element for ultimate strength analysis. In Proceedings of the 2nd International Conference on Thin-Walled Structures, Singapore, 2–4 December, 1998.
9. Fujikubo, M.; Kaeding, P.; Olaru, D.; Pei, Z. Development of ISUM Plate Element Considering Lateral Pressure Effects and Its Application to Stiffened Plate. Transactions of The West-Japan Society of Naval Architects The 109th West-Japan Society of Naval Architects Meeting (Joint Autumn Meeting of Three Societies of Naval Architects in Japan, 2004) (Transactions of The West-Japan Society of Naval Architects No. 109, Japan, 2005. Available online: https://www.jstage.jst.go.jp/article/jjasnaoe/3/0/3_0_285/_article (accessed on 20 September 2022).
10. Paik, J.K.; Seo, J.K.; Kim, D.M. Idealized structural unit method and its application to progressive hull girder collapse analysis of ships. *Ships Offshore Struct.* **2006**, *1*, 235–247. [CrossRef]
11. Lindemann, T.; Kaeding, P. Application of the idealized structural unit method for ultimate strength analyses of stiffened plate structures. *Ship Technol. Res.* **2017**, *1*, 15–29. [CrossRef]
12. Paik, J.K.; Thayamballi, A.K. *Ship-Shaped Offshore Installations: Design, Building, and Operation*; Cambridge University Press: Cambridge, UK, 2007.
13. Kim, D.K.; Kim, H.B.; Mohd, M.H.; Paik, J.K. Comparison of residual strength-grounding damage index diagrams for tankers produced by the ALPS/HULL ISFEM and design formula method. *Int. J. Nav. Archit. Ocean Eng.* **2013**, *5*, 47–61. [CrossRef]
14. Benson, S.; Downes, J.; Dow, R.S. Compartment level progressive collapse analysis of lightweight ship structures. *Mar. Struct.* **2013**, *31*, 44–62. [CrossRef]
15. Tekgoz, M.; Garbatov, Y.; Soares, C.G. Strength assessment of an intact and damaged container ship subjected to asymmetrical bending loadings. *Mar. Struct.* **2018**, *58*, 172–198. [CrossRef]
16. Yoshikawa, T.; Bayatfar, A.; Kim, B.J.; Chen, C.P.; Wang, D.; Boulares, J.; Gordo, J.M.; Josefson, L.; Smith, M.; Kaeding, P. Report of ISSC 2015 Committee III. 1 Ultimate Strength. In Proceedings of the 19th International Ship and Offshore Structures Congress, Lisbon, Portugal, 7–10 September 2015.
17. Mohammed, E.A.; Benson, S.D.; Hirdaris, S.E.; Dow, R.S. Design safety margin of a 10,000 TEU container ship through ultimate hull girder load combination analysis. *Mar. Struct.* **2016**, *46*, 78–101. [CrossRef]
18. Nordstrand, T. On buckling loads for edge-loaded orthotropic plates including transverse shear. *Compos. Struct.* **2004**, *46*, 1–6. [CrossRef]
19. Jelovica, J.; Romanoff, J.; Ehlers, S.; Varsta, P. Influence of weld stiffness on buckling strength of laser-welded web-core sandwich plates. *J. Constr. Steel Res.* **2012**, *77*, 12–18. [CrossRef]
20. Lok, T.S.; Cheng, Q.H. Free vibration of clamped orthotropic sandwich panel. *J. Sound Vib.* **2000**, *229*, 311–327. [CrossRef]
21. Jelovica, J.; Romanoff, J.; Klein, R. Eigenfrequency analyses of laser-welded web-core sandwich panels. *Thin-Walled Struct.* **2016**, *101*, 120–128. [CrossRef]
22. Putranto, T.; Kõrgesaar, M.; Jelovica, J.; Tabri, K.; Naar, H. Ultimate strength assessment of stiffened panel under uni-axial compression with non-linear equivalent single layer approach. *Mar. Struct.* **2021**, *78*, 103004. [CrossRef]
23. Putranto, T.; Kõrgesaar, M.; Jelovica, J. Ultimate strength assessment of stiffened panels using Equivalent Single Layer approach under combined in-plane compression and shear. *Thin-Walled Struct.* **2022**, *180*, 109943. [CrossRef]
24. Tabri, K.; Naar, H.; Kõrgesaar, M. Ultimate strength of ship hull girder with grounding damage. *Ships Offshore Struct.* **2020**, *15*, 161–175. [CrossRef]

25.   Shen, L.; Kyun, D.K. A comparison of numerical methods for damage index based residual ultimate limit state assessment of
        grounded ship hulls. *Thin-Walled Struct.* **2022**, *172*, 108854.
26.   Paik, J.K.; Kim, D.K.; Park, D.H.; Kim, H.B.; Mansour, A.E.; Caldwell, J.B. Modified Paik-Mansour formula for ultimate strength
        calculations of ship hulls. *Ships Offshore Struct.* **2013**, *8*, 245–260. [CrossRef]

Curriculum Vitae

1. Personal data

Name	Teguh Putranto
Date and place of birth	13.05.1990, Jember, Indonesia
Nationality	Indonesian

2. Contact information

Address	Tallinn University of Technology, School of Engineering, Kuressaare College, Tallinna 19, 93819 Kuressaare, Estonia
Phone	+372 57806889
E-mail	teguh.putranto@taltech.ee

3. Education

2018–…	Tallinn University of Technology, School of Engineering, Coastal and Marine Engineering, Ph.D. studies
2012–2013	Institut Teknologi Sepuluh Nopember, Faculty of Marine Technology, Marine Production and Material Engineering, M.Eng. *cum laude*
2008–2012	Institut Teknologi Sepuluh Nopember, Faculty of Marine Technology, Naval Architecture, B.Eng.

4. Language competence

Indonesian	native
English	fluent

5. Professional employment

2018–…	Tallinn University Technology, Doctoral student – junior researcher
2014–…	Institut Teknologi Sepuluh Nopember (ITS), Lecturer
2012–2014	Laboratory of Ship Design ITS, Structural Engineer

6. Voluntary work

2022–…	Thin-Walled Structures, Elsevier (Reviewer)
2021–…	Journal of the Mechanical Behavior of Materials, De Gruyter (Reviewer)
2021–…	Journal of Marine Science and Engineering, MDPI (Reviewer)

7. Computer skills

- Document preparation: Microsoft Office

- Programming languages: Python, Fortran, Matlab

- Scientific packages: Abaqus FEA (CAE, Standard, Explicit), Ansys Mechanical APDL

8. Honours and awards

- 2018, awarded an European Regional Development Fund for doctoral program scholarship, Tallinn University of Technology, Estonia

- 2011, awarded a master program scholarship fund through Fast-track scheme, Institut Teknologi Sepuluh Nopember, Indonesia

9. Defended theses

- 2013, Ship collision analyses using finite element method for non-linear dynamic response , M.Eng. degree, supervisor Wasis Dwi Aryawan, Ph.D. and Prof. Achmad Zubaydi, Faculty of Marine Technology, Institut Teknologi Sepuluh Nopember, Indonesia

- 2012, Strength analysis of stiffened panel using finite element and finite different methods, B.Eng. degree, supervisor Asjhar Imron, PED., Faculty of Marine Technology, Institut Teknologi Sepuluh Nopember, Indonesia

10. Field of research

- Finite element method

- Equivalent single layer

- Ultimate strength analysis

11. Scientific work
Scientific articles

1. T. Putranto, M. Kõrgesaar, J. Jelovica, K. Tabri, and H. Naar. Ultimate strength assessment of stiffened panel under uni-axial compression with non-linear equivalent single layer approach, *Marine Structures*, 78:103004, 2021

2. T. Putranto, M. Kõrgesaar, and J. Jelovica. Ultimate strength assessment of stiffened panels using equivalent single layer approach under combined in-plane compression and shear, *Thin-Walled Structures*, 180:109943, 2022

3. T. Putranto, M. Kõrgesaar, and K. Tabri. Application of equivalent single layer approach for ultimate strength analyses of ship hull girder, *Journal of Marine Science and Engineering*, 10(10):1–20, 2022

4. R. Ridwan, A.R. Prabowo, N. Muhayat, T. Putranto, and J.M. Sohn. Tensile analysis and assessment of carbon and alloy steels using FE approach as an idealization of material fractures under collision and grounding, *Curved and Layered Structures*, 188–198, 2020

5. A.R. Prabowo, T. Putranto and J.M. Sohn. Crashworthiness performance of stiffened bottom tank structure subjected to impact loading conditions: ship-rock interaction, *Journal of Marine Science and Engineering*, 1–15, 2019

Conference presentations

1. T. Putranto and M. Kõrgesaar. *Numerical study on the structural behavior of intact and damaged box beams under four-point bending load*, the 8th International Conference on Collision and Grounding of Ships and Offshore Structures (ICCGS 2019): 21–23 October 2019, Lisbon, Portugal

2. T. Putranto and M. Kõrgesaar. *Numerical investigation on the buckling response of stiffened panel subjected to axial compression with non-linear equivalent single layer approach*, the International Offshore and Polar Engineering Conference, 20–25 June 2021, Rhodes, Greece

Elulookirjeldus

1. Isikuandmed

Nimi	Teguh Putranto
Sünniaeg ja -koht	13.05.1990, Jember, Indonesia
Kodakondsus	Indoneesia

2. Kontaktandmed

Aadress	Tallinna Tehnikaülikool, Kuressaare Kolledž, Tallinna 19, 93819 Kuressaare, Eesti
Telefon	+372 57806889
E-post	teguh.putranto@taltech.ee

3. Haridus

2018–…	Tallinna Tehnikaülikool, Inseneriteaduskond, Ranniku- ja meretehnika, doktoriõpe
2012–2013	Insitut Teknologi Sepuluh Nopember, Meretehnoloogia teaduskond, Meretootmine ja materjalitehnika, M.Eng. *cum laude*
2008–2012	Insitut Teknologi Sepuluh Nopember, Meretehnoloogia teaduskond, Mereväe arhitektuur, B.Eng.

4. Keelteoskus

Indoneesia keel	emakeel
Inglise keel	kõrgtase

5. Teenistuskäik

2018–…	Tallinna Tehnikaülikool, Doktorant-nooremteadur
2014–…	Institut Teknologi Sepuluh Nopember (ITS), Dotsent
2012–2014	Laevadisaini ITS labor, Ehitusinsener

6. Vabatahtlik töö

2022–…	Thin-Walled Structures, Elsevier (Reviewer)
2021–…	Journal of the Mechanical Behavior of Materials, De Gruyter (Reviewer)
2021–…	Journal of Marine Science and Engineering, MDPI (Reviewer)

7. Computer skills

- Operatsioonisüsteemid: Windows 10

- Kontoritarkvara: Microsoft Office

- Programmeerimiskeeled: Python, Fortran, Matlab

- Teadustarkvara paketid: Abaqus FEA (CAE, Standard, Explicit), Ansys Mechanical APDL

8. Autasud

- 2018, pälvis Euroopa Regionaalarengu Fondi doktoriprogrammi stipendiumi saamiseks, Tallinna Tehnikaülikool

- 2011, pälvis magistriprogrammi stipendiumifondi Fast-track skeemi kaudu, Institut Teknologi Sepuluh Nopember

9. Kaitstud lõputööd

- 2013, Laeva kokkupõrke analüüsid mittelineaarse dünaamilise reaktsiooni jaoks lõplike elementide meetodil, M.Eng., juhendaja Wasis Dwi Aryawan, Ph.D. ja Prof. Achmad Zubaydi, Institut Teknologi Sepuluh Nopember, Meretehnoloogia teaduskond

- 2012, Jäigastatud paneeli tugevusanalüüs lõplike elementide ja lõplike erinevate meetodite abil, B.Eng., juhendaja Asjhar Imron, PED, Institut Teknologi Sepuluh Nopember, Meretehnoloogia teaduskond

10. Teadustöö põhisuunad

- Lõplike elementide meetod

- Samaväärne ühekihiline

- Ülim tugevusanalüüs

11. Teadustegevus
Teadusartikleid

1. T. Putranto, M. Kõrgesaar, J. Jelovica, K. Tabri, and H. Naar. Ultimate strength assessment of stiffened panel under uni-axial compression with non-linear equivalent single layer approach, *Marine Structures*, 78:103004, 2021

2. T. Putranto, M. Kõrgesaar, and J. Jelovica. Ultimate strength assessment of stiffened panels using equivalent single layer approach under combined in-plane compression and shear, *Thin-Walled Structures*, 180:109943, 2022

3. T. Putranto, M. Kõrgesaar, and K. Tabri. Application of equivalent single layer approach for ultimate strength analyses of ship hull girder, *Journal of Marine Science and Engineering*, 10(10):1–20, 2022

4. R. Ridwan, A.R. Prabowo, N. Muhayat, T. Putranto, and J.M. Sohn. Tensile analysis and assessment of carbon and alloy steels using FE approach as an idealization of material fractures under collision and grounding, *Curved and Layered Structures*, 188–198, 2020

5. A.R. Prabowo, T. Putranto and J.M. Sohn. Crashworthiness performance of stiffened bottom tank structure subjected to impact loading conditions: ship-rock interaction, *Journal of Marine Science and Engineering*, 1–15, 2019

Konverentsi ettekanded

1. T. Putranto and M. Kõrgesaar. *Numerical study on the structural behavior of intact and damaged box beams under four-point bending load*, the 8th International Conference on Collision and Grounding of Ships and Offshore Structures (ICCGS 2019): 21–23 October 2019, Lisbon, Portugal

2. T. Putranto and M. Kõrgesaar. *Numerical investigation on the buckling response of stiffened panel subjected to axial compression with non-linear equivalent single layer approach*, the International Offshore and Polar Engineering Conference, 20–25 June 2021, Rhodes, Greece